

Aus dem Veterinärwissenschaftlichen Department der Tierärztlichen
Fakultät der Ludwig-Maximilians-Universität München

Arbeit angefertigt unter der Leitung von
PD Dr. Marlon R. Schneider

Effects of *Dro1* loss on colorectal carcinogenesis
and body growth in a constitutive
knockout mouse model

Inaugural-Dissertation zur Erlangung der tiermedizinischen Doktorwürde
der Tierärztlichen Fakultät
der Ludwig-Maximilians-Universität München

Von Jessica Isabel Grill

aus Augsburg

München 2012

Aus dem Veterinärwissenschaftlichen Department der Tierärztlichen
Fakultät der Ludwig-Maximilians-Universität München

Arbeit angefertigt unter der Leitung von
PD Dr. Marlon R. Schneider

Auswirkungen des Verlustes von *Dro1* auf die kolorektale
Karzinogenese und das Körperwachstum in einem
konstitutiven Knockout-Mausmodell

Inaugural-Dissertation zur Erlangung der tiermedizinischen Doktorwürde
der Tierärztlichen Fakultät
der Ludwig-Maximilians-Universität München

Von Jessica Isabel Grill

aus Augsburg

München 2012

Gedruckt mit der Genehmigung der Tierärztlichen Fakultät
der Ludwig-Maximilians-Universität München

Dekan: Univ.-Prof. Dr. Braun

Berichterstatter: Priv.-Doz. Dr. Schneider

1. Korreferent: Univ.-Prof. Dr. Göbel
2. Korreferent: Univ.-Prof. Dr. Aigner
3. Korreferent: Univ.-Prof. Dr. Wanke
4. Korreferent: Univ.-Prof. Dr. Hirschberger

Tag der Promotion: 21. Juli 2012

Meiner Familie

Die Nager [...] sind [...] höchst merkwürdig gebildet. Scharfes, aber geringes Erfassen, eilige Sättigung, auch nachher wiederholtes Abraspeln der Gegenstände, fortgesetztes, fast leidenschaftliches, absichtslos zerstörendes Knuspern, welches dann wieder in den Zweck, sich Lager und Wohnungen aufzubauen und einzurichten, unmittelbar eingreift und sich dadurch abermals bewährt: daß im organischen Leben selbst das Unnütze, ja das Schädliche selbst, in den notwendigen Kreis des Daseyns aufgenommen, ins Ganze zu wirken und als wesentliches Bindemittel disperater Einzelheiten gefordert wird.

– Johann Wolfgang von Goethe: Die Skelette der Nagetiere –

Contents

1. Introduction and objectives	1
2. Review of the literature	3
1.1 Down-regulated by oncogenes 1 (<i>DRO1/Dro1</i>)	3
1.1.1 Overview	3
1.1.2 The putative tumor suppressor role	4
1.1.3 Putative functions in adipose tissue	5
1.2 Intestine	6
1.2.1 Overview	6
1.2.2 Small intestine	7
1.2.3 Large intestine	9
1.2.4 Genetics of colorectal cancer	9
1.3 Adipose tissue	11
1.3.1 Overview	11
1.3.2 White adipose tissue	12
1.3.3 Brown adipose tissue	13
1.3.4 Obesity	14
3. Animals, Materials and Methods	17
3.1 Animals	17
3.1.1 <i>Dro1</i> constitutive knockout mice (<i>Dro1</i> ^{-/-})	17
3.1.2 B6.C-Tg(CMV-cre)1Cgn/J mice	18
3.1.3 C57BL/6J- <i>Apc</i> ^{Min} /J mice	18
3.1.4 Animal maintenance	20
3.2 Materials and Methods	21
3.2.1 Mouse Genotyping	21
3.2.1.1 Sample collection	21
3.2.1.2 Extraction of DNA from mouse tail tips	21
3.2.1.3 PCR analysis	22
3.2.2 Identification of knockout mice by non-radioactive Southern blot	23
3.2.2.1 Digest, electrophoresis and transfer of DNA	23
3.2.2.2 Non-radioactive probe labeling	24
3.2.2.3 Hybridization, washing and detection	25
3.2.3 Evaluation of gene expression at the RNA level	26

3.2.3.1	Extraction of RNA from tissues.....	26
3.2.3.2	cDNA synthesis	27
3.2.3.3	Quantitative real-time PCR.....	28
3.2.4	Evaluation of gene expression at the protein level	30
3.2.4.1	Extraction of proteins from tissues	30
3.2.4.2	Determination of protein concentration	30
3.2.4.3	SDS-Polyacrylamide gel electrophoresis (SDS-PAGE).....	31
3.2.4.4	Blotting	32
3.2.4.5	Detection.....	33
3.2.5	Histological analysis	34
3.2.5.1	Hematoxylin and eosin (H&E) staining	34
3.2.5.2	Periodic acid Schiff (PAS) staining.....	35
3.2.5.3	Elastic van Gieson (EvG) staining.....	35
3.2.6	Immunohistochemistry	35
3.2.6.1	Bromodeoxyuridine (BrdU) staining	35
3.2.6.2	Matrix metalloproteinase-7 (MMP-7) staining.....	36
3.2.6.3	Cleaved caspase-3 staining	37
3.2.6.4	β -catenin staining.....	38
3.2.6.5	Ki-67 staining	38
3.2.7	Analysis of body and organ growth.....	38
3.2.8	Analysis of adipose tissue parameters	39
3.2.8.1	Total body fat content	39
3.2.8.2	Fat pad weight.....	39
3.2.9	Analysis of liver triglyceride content.....	39
3.2.10	Evaluation of serum parameters	40
3.2.10.1	Blood collection.....	40
3.2.10.2	Serum free fatty acids	40
3.2.10.3	Serum triglycerides	40
3.2.11	Analysis of glucose tolerance and insulin tolerance.....	40
3.2.12	Evaluation of preadipocyte differentiation in primary cell culture.....	41
3.2.12.1	Isolation of SV cells.....	41
3.2.12.2	Maintenance and differentiation of SV cells	42
3.2.12.3	Oil red O staining.....	42
3.2.12.4	Differentiation scoring.....	43

3.2.13	Analysis of aberrant crypt foci (ACF)	44
3.2.13.1	Tissue collection	44
3.2.13.2	Methylene blue staining.....	44
3.2.13.3	ACF scoring.....	45
3.2.14	Analysis of weight and length of the intestine.....	45
3.2.15	Analysis of intestinal neoplastic lesions	45
3.2.15.1	Tissue collection	45
3.2.15.2	Tumor scoring.....	45
3.2.16	Statistical analysis.....	46
3.2.17	Primer sequences	46
3.2.18	Materials	47
3.2.18.1	Machines	47
3.2.18.2	Consumables	48
3.2.18.3	Chemicals.....	49
3.2.18.4	Drugs.....	53
4.	Results	54
4.1	Generation of <i>Dro1</i> ^{-/-} mice.....	54
4.1.1	Establishment of <i>Dro1</i> ^{-/-} mice	54
4.1.2	Analysis of genomic recombination	55
4.1.3	Expression analysis.....	56
4.1.4	Protein analysis	57
4.2	Effects of <i>Dro1</i> loss on intestinal tumor formation	58
4.2.1	Anatomy and histology of the intestine	58
4.2.1.1	Weight and length of the intestine	58
4.2.1.2	Intestinal epithelium	59
4.2.2	Spontaneous intestinal tumor formation	62
4.2.3	Intestinal tumor formation in <i>Apc</i> ^{+/<i>Min</i>} mice	62
4.2.3.1	Morbidity and mortality.....	63
4.2.3.2	Intestinal tumor number and size.....	64
4.2.3.3	Tumor histology.....	68
4.2.3.4	Tumor proliferation rate.....	71
4.2.3.5	Nuclear β -catenin accumulation	73
4.2.3.6	ACF formation.....	75
4.2.3.7	<i>Mom1</i> status	75

4.3 Effects of <i>Dro1</i> loss on body growth.....	77
4.3.1 Standard feeding conditions.....	77
4.3.1.1 Body weight.....	77
4.3.1.2 Longitudinal growth	78
4.3.1.3 Organ growth	78
4.3.1.4 Total body fat and lean mass	81
4.3.1.5 Fat pad growth	81
4.3.1.6 Glucose metabolism.....	83
4.3.1.7 Serum triglycerides and free fatty acids	83
4.3.2 High-fat diet feeding conditions	84
4.3.2.1 Body weight, body fat and lean mass	84
4.3.2.2 Glucose metabolism.....	87
4.3.2.3 Organ growth	88
4.3.2.4 Fat pad growth	90
4.3.2.5 Liver histology.....	91
4.3.2.6 Serum triglycerides and free fatty acids	93
4.3.3 Analysis of adipogenesis in SV cells.....	93
5. Discussion	95
5.1 Generation of <i>Dro1</i> ^{-/-} mice.....	95
5.2 Effects of <i>Dro1</i> loss on intestinal tumor formation	96
5.3 Effects of <i>Dro1</i> loss on body growth.....	100
5.4 Final considerations	105
6. Summary	107
7. Zusammenfassung	109
8. Bibliography	112
9. Acknowledgements	125
10. Curriculum vitae	126

Abbreviations

µg	microgram
µl	microliter
µm	micrometer
µM	micromol
ACF	aberrant crypt foci
AIB1	amplified in breast cancer 1
am	<i>ante meridiem</i>
APC/Apc	adenomatous polyposis coli
apoC-II	apolipoprotein C-II
AZ	Aktenzeichen
BCA	bicinchoninic acid
BCLAF1	B-cell lymphoma 2-associated transcription factor 1
BMI	body mass index
bp	base pairs
BRAF	v-raf murine sarcoma viral oncogene homolog B1
BrdU	bromodeoxyuridine
BSA	bovine serum albumin
C/EBPα	CCAAT/enhancer binding protein alpha
Ccdc80	coiled-coil domain containing 80
cDNA	complementary deoxyribonucleic acid
cm	centimeter
cm ²	square centimeter
CMV	cytomegalovirus
Cre	causes recombination
CuSO ₄	cupric sulphate
d	day
DCC	deleted in colorectal cancer
DEPC	diethylpyrocarbonate
DIG	digoxigenin
dl	deciliter
DMEM	Dulbecco's modified Eagle's medium
DNA	deoxyribonucleic acid
dNTPs	deoxynucleotides

DRO1/Dro1	down-regulated by oncogenes 1
DTT	dithiothreitol
e.g.	<i>exempli gratia</i>
E14	embryonic day 14
EDTA	ethylenediaminetetraacetic acid
EvG	elastic van Gieson
FAP	familial adenomatous polyposis
FBS	fetal bovine serum
FFA	free fatty acids
Fig.	figure
FW	forward
g	gram
GALT	gut-associated lymphatic tissue
Gapdh	glyceraldehydes-3-phosphate dehydrogenase
GLI	glioma-associated oncogene
GLUT-4	glucose transporter type 4
GSK-3	glycogen synthase kinase-3
h	hour
H&E	hematoxin and eosin
H ⁺	hydrogen ion
H ₂ O	water
H ₂ O ₂	hydrogen peroxide
HCl	hydrochloric acid
HEK293T	human embryonic kidney 293T
HEPES	4-(2-hydroxyethyl)-1-piperazineethanesulfonic acid
HRAS	Harvey rat sarcoma virus oncogene 1
HSV-TK	herpes simplex virus thymidine kinase
i.e.	<i>id est</i>
IBMX	3-isobutyl-1-methylxanthine
IEN	intraepithelial neoplasia
IL-6	interleukin-6
ipGTT	intraperitoneal glucose tolerance test
ipITT	intraperitoneal insulin tolerance test
J	joule

kb	kilobase
KCl	potassium chloride
kDa	kilo Dalton
kg	kilogram
KH ₂ PO ₄	monopotassium phosphate
KRAS	v-Ki-ras2 Kirsten rat sarcoma viral oncogene homolog
l	liter
LOH	loss of heterozygosity
loxP	locus of crossing-over
M	molar
mA	milliampere
MCF-7	Michigan Cancer Foundation-7
MCP-1	monocyte chemotactic protein-1
mg	milligram
MgCl ₂	magnesium chloride
min	minute
Min	multiple intestinal neoplasia
ml	milliliter
mm	millimeter
mM	millimolar
MMP-7	matrix metalloproteinase-7
Mom	modifiers of <i>Min</i>
Mom1	modifier of <i>Min</i> 1
MRI	magnetic resonance imaging
mRNA	messenger ribonucleic acid
N	normal
Na ₂ HPO ₄	sodium dihydrogen phosphate
NaCl	sodium chloride
NaOH	sodium hydroxide
ng	nanogram
nm	nanometer
nmol	nanomole
NRL	nose-rump-length
pm	<i>post meridiem</i>

p53	protein p53
PAS	periodic acid Schiff staining
PBS	phosphate buffered saline
PCR	polymerase chain reaction
PGK-neo	phosphoglycerine kinase neomycin resistance cassette
PPAR γ	peroxisome proliferator activated receptor gamma
PVDF	polyvinylidene fluoride
RNA	ribonucleic acid
RNRL	relative nose-rump-length
rpm	revolutions per minute
RT-PCR	real-time polymerase chain reaction
RV	reverse
s	second
siRNA	small interfering ribonucleic acid
SDS	sodium dodecyl sulfate
SDS-PAGE	sodium dodecyl sulfate polyacrylamide gel electrophoresis
SMAD2	mothers against decapentaplegic homolog 2
SMAD4	mothers against decapentaplegic homolog 4
SRPX	sushi repeat-containing protein, X chromosome
SSC	saline sodium citrate
SSG1	steroid-sensitive gene 1
SV	stromal vascular
TAE	Tris-acetate-EDTA buffer
Taq	thermus aquaticus
TBS	Tris buffered saline
TBST	Tris buffered saline Tween20
TCF/LEF	T-cell factor/lymphoid enhancing factor
TNF- α	tumor necrosis factor-alpha
Tris	tris-(hydroxymethyl)-aminomethane
U	unit
UCP1	uncoupling protein 1
URB	upregulated in bombesin receptor subtype 3 knockout mouse
V	Volt

WHO

World Health Organization

1. Introduction and objectives

Colorectal cancer constitutes a major cause of tumor-related morbidity and mortality in the industrialized world (Parkin *et al.*, 2005; World Cancer Research Fund, 2007). To our current understanding, colorectal cancer develops from adenomatous precursor lesions by a multistep progress that involves multiple independent mutational events in oncogenes and tumor suppressor genes (Arnold *et al.*, 2005; Fearon, 2011). In most cases of sporadic colon cancers, one allele of certain tumor suppressor genes becomes inactivated by loss of specific chromosomal regions (“loss of heterozygosity”, LOH), with particularly high frequencies on chromosome 17p (*p53*), 18q (*DCC*, *SMAD4*, *SMAD2*) and 5q (*APC*) (Fearon and Vogelstein, 1990; Arnold *et al.*, 2005; Fearon, 2011). The acquirement of an inactivating somatic mutation in the remaining wildtype allele promotes tumor development due to perturbation of critical signaling pathways controlling cellular metabolism, proliferation, differentiation; and survival (Fearon, 2011; Hanahan and Weinberg, 2011).

Previously, down-regulated by oncogenes 1 (*DROI*) was noted to be down-regulated after neoplastic transformation of RK3E cells, in various colorectal and pancreatic cancer cell lines, in several primary colorectal cancer specimens (Bommer *et al.*, 2005) and in thyroid neoplastic cell lines and tissues (Visconti *et al.*, 2003). Moreover, re-expression of *DROI* in several cancer cell lines reduced both colony formation and anchorage-independent growth (Bommer *et al.*, 2005), and induced sensitization to various apoptotic stimuli (Bommer *et al.*, 2005; Ferragud *et al.*, 2011). Thus, *DROI* was proposed to be a putative tumor suppressor gene (Bommer *et al.*, 2005).

Obesity, characterized by excessive body fat accumulation, is known to be a major risk factor for the development of cardiovascular and metabolic disease (WHO, 2011). According to the WHO, obesity is a worldwide epidemic (WHO, 2011). White adipose tissue functions as an endocrine organ, secreting a variety of hormones and cytokines, so called adipokines, implicated in energy homeostasis and body weight regulation (Vazquez-Vela *et al.*, 2008; Singla *et al.*, 2010). Dysregulated production of adipokines, as in obesity, leads to the disruption of whole-body energy homeostasis and contributes to the development of metabolic disorders (Ailhaud *et al.*, 2006; Ahima and Osei, 2008).

DROI/Dro1 is known to be ubiquitously expressed, with highest levels in white adipose tissue (Aoki *et al.*, 2002; Liu *et al.*, 2004; Bommer *et al.*, 2005; Okada *et al.*, 2008;

Tremblay *et al.*, 2009). *Dro1* expression was also substantially decreased in epididymal white adipose tissue of several obese mouse models (Okada *et al.*, 2008). Recent *in vitro* studies reported *Dro1* to be a novel adipocyte-secreted protein that modulates adipocyte differentiation (Tremblay *et al.*, 2009), a process involved in adipose tissue expansion (Hausman *et al.*, 2001; Guilherme *et al.*, 2008;).

The aim of the present study was to elucidate the effects of *Dro1* loss on colorectal carcinogenesis and body growth *in vivo*. We therefore generated the first constitutive *Dro1* knockout mouse model (*Dro1*^{-/-}) using a Cre/loxP strategy. To investigate the effect of *Dro1* loss on colorectal tumorigenesis, *Dro1*^{-/-} mice were crossed into the *Apc*^{+Min} background, a well established intestinal tumor mouse model (Moser *et al.*, 1990). Body weight, total body fat, lean mass, longitudinal growth, organ and fat pad weight as well as glucose and lipid metabolism were investigated under normal diet conditions and when maintained on a high-fat diet to evaluate a possible involvement in body growth. Moreover, the differentiation potential of primary mouse *Dro1*^{-/-} preadipocytes was assessed *in vitro* to clarify the role of *Dro1* in adipogenesis.

2. Review of the literature

2.1 Down-regulated by oncogenes 1 (*DRO1/Dro1*)

2.1.1 Overview

DRO1, also named, steroid-sensitive gene 1 (*SSG1*), up-regulated in bombesin receptor subtype 3 knockout mouse (*URB*), coiled-coil domain containing 80 (*Ccdc80*), *CL2* and *Equarin-L* was first described in 2001 and to date is characterized in man, mouse, rat, chicken and *Xenopus* (Marcantonio *et al.*, 2001; Aoki *et al.*, 2002; Mu *et al.*, 2003; Visconti *et al.*, 2003; Bommer *et al.*, 2005; Tremblay *et al.*, 2009). Mouse *Dro1* comprises 57.744 bp and is encoded by 8 exons (Bommer *et al.*, 2005; <http://genome.ucsc.edu/>). The start codon is located on exon 2 that also encodes most of the protein mass (<http://genome.ucsc.edu/>). *DRO1/Dro1* was found to be ubiquitously expressed, with highest levels in white adipose tissue (Aoki *et al.*, 2002; Liu *et al.*, 2004; Bommer *et al.*, 2005; Okada *et al.*, 2008; Tremblay *et al.*, 2009). In chicken and man, two alternatively spliced transcripts were identified (Mu *et al.*, 2003, Bommer *et al.*, 2005; Cha *et al.*, 2005; Tremblay *et al.*, 2009). Mouse *DRO1* features a single long open reading frame of 949 amino acids, with an apparent molecular mass of 108 kDa (Mu *et al.*, 2003; Liu *et al.*, 2004; Bommer *et al.*, 2005). Mouse, rat, chicken and human *DRO1* show pronounced sequential and structural similarities (Mu *et al.*, 2003; Liu *et al.*, 2004; Bommer *et al.*, 2005; Tremblay *et al.*, 2009). The amino acid sequence exhibits 3 internal repeats which represent the most highly conserved (93 to 97%) regions between mouse, rat, chicken and man (Aoki *et al.*, 2002; Liu *et al.*, 2004; Bommer *et al.*, 2005; Tremblay *et al.*, 2009). Moreover, it shows homology to the putative tumor suppressor sushi repeat-containing protein, X chromosome (SRPX) (Aoki *et al.*, 2002; Visconti *et al.*, 2003; Liu *et al.*, 2004; Bommer *et al.*, 2005; Tremblay *et al.*, 2009). Within the cell, *DRO1* was found to be located in the cytosol (Marcantonio *et al.*, 2001; Bommer *et al.*, 2005), the nucleus/nucleolus (Visconti *et al.*, 2003), the Golgi apparatus and at the cytoplasmic membrane (Ferragud *et al.*, 2011). A hydrophobic N-terminal signal peptide suggests *DRO1* to be a secretory protein (Mu *et al.*, 2003; Visconti *et al.*, 2003; Liu *et al.*, 2004; Bommer *et al.*, 2005). Secretion of full-length forms as well as cleaved fragments was reported for adipose tissue-derived stromal cells (Okada *et al.*, 2008) and several cell lines ectopically expressing *DRO1/Dro1*, namely 3T3-L1 fully differentiated adipocytes (Tremblay *et al.*, 2009), COS7 (Liu *et al.*, 2004), Flp293 (Okada *et al.*, 2008) and MCF-7-TetOn cells (Ferragud

et al., 2011). By contrast, it was not detected to be a secretory protein in transfected HEK293T and COS cells (Bommer *et al.*, 2005). *In vivo* DRO1 was identified to be a secreted cartilage protein since it localized to the extracellular matrix of post-natal mouse femoral head cartilage (Wilson *et al.*, 2011), the hypertrophic cartilage region of facial, axial and appendicular developing mouse skeleton (Liu *et al.*, 2004) and mouse embryonic rib cartilage (Manabe *et al.*, 2008).

In rat mammary tissue *Dro1* expression was identified to be tightly regulated by estrogen and it was proposed that its over-expression is associated with mammary carcinogenesis (Marcantonio *et al.*, 2001). High *DRO1* expression was shown in human bone marrow stromal cells, with a drastically decrease during osteoblastic differentiation. As temporal and spatial expression patterns correlate with the timing and sites of cartilage development in skeleton element formation in mouse embryos, *Dro1* was implicated in skeletogenesis (Liu *et al.*, 2004). Consistently, recent findings suggest a role for *Dro1* within the extracellular matrix during mouse post-natal cartilage development prior to bone formation (Wilson *et al.*, 2011). DRO1 was also identified as an extracellular matrix component that promotes cell attachment and matrix assembly *in vitro* (Manabe *et al.*, 2008). In chicken eye development *Dro1* was demonstrated to be expressed in the lens with a high-dorsal-to-low-ventral gradient at the equatorial region from the early embryonic stage until the postnatal period (Mu *et al.*, 2002). Microinjection of *DRO1* mRNAs into 4-8 cell stage *Xenopus* embryos caused abnormal eye formation, thus it was proposed to play an important role in eye development (Mu *et al.*, 2002). *Dro1* was also implicated in hair development due to the fact that it is over-expressed in hair follicle dermal papilla cells as compared to dermal fibroblasts (Cha *et al.*, 2005). Furthermore, in hair follicle dermal papilla cells *DRO1* expression was found to be androgen responsive (Cha *et al.*, 2005). The putative function of *DRO1* in adipose tissue as well as its proposed tumor suppressor gene role are presented in the following in more detail.

2.1.2 The putative tumor suppressor role

DRO1 was found to be down-regulated in RK3E epithelial cells neoplastically transformed by β -catenin stabilization as well as by various oncogenes. Also, *DRO1* expression is considerably reduced in several colon and pancreatic cancer cell lines, in the majority of primary colorectal cancers samples (Bommer *et al.*, 2005) and in human thyroid neoplastic cell lines and tissues (Visconti *et al.*, 2003). *DRO1* down-regulation

is presumably mediated by transcriptional repression through trans-acting repressors binding to the promoter. Recent findings demonstrated down-regulation of *DRO1* by amplified in breast cancer 1 (*AIB1*) (Ferragud *et al.*, 2011), an oncogene that acts as a transcriptional co-activator in the nucleus and is implicated in cancer development (Gojis *et al.*, 2010). Furthermore, *DRO1* sensitizes cells to different apoptotic stimuli *in vitro* and re-expression in cancer cell lines results in a reduction of their malignant growth properties. *DRO1* was therefore postulated to be a candidate tumor suppressor gene that may play a crucial role in both intestinal tissue homeostasis and carcinogenesis (Bommer *et al.*, 2005). Repression of *DRO1* by the *AIB1* oncogene contributes to inhibition of apoptosis, confirming the role of *DRO1* in facilitating the apoptotic cascade (Ferragud *et al.*, 2011).

2.1.3 Putative functions in adipose tissue

DRO1/Dro1 is a gene predominantly expressed in white adipose tissue with considerably lower levels in other tissues (Aoki *et al.*, 2002; Liu *et al.*, 2004; Bommer *et al.*, 2005; Okada *et al.*, 2008; Tremblay *et al.*, 2009). Thus, it was often supposed to play important roles in energy storage and metabolism (Aoki *et al.*, 2002; Okada *et al.*, 2008; Tremblay *et al.*, 2009). In mildly obese bombesin receptor subtype-3 mice, a mouse model of obesity and metabolic syndrome, *Dro1* was shown to be up-regulated in brown adipose tissue and was therefore hypothesized to have a unique function in thermogenesis (Aoki *et al.*, 2002). Furthermore, *Dro1* expression was demonstrated to be down-regulated in epididymal white adipose tissue of several obese mouse models, an effect probably induced by obesity-related low-grade inflammation as treatment of 3T3-L1 adipocytes with insulin, tumor necrosis factor- α (TNF- α), H₂O₂ and hypoxia resulted in reduced *Dro1* mRNA levels (Okada *et al.*, 2008). *In vitro* studies reported *DRO1* to be an adipocyte secreted protein and it was proposed to be a novel adipokine, which might influence whole-body energy homeostasis and contribute to metabolic disorders in obesity (Okada *et al.*, 2007; Tremblay *et al.*, 2009).

Recent findings indicate that *Dro1* plays an important role during adipogenesis, as *Dro1* knockdown in preadipocyte clonal cells (3T3-L1) significantly impaired their ability to differentiate into adipocytes and accumulate lipids. During adipocyte differentiation *Dro1* was found to be expressed in a biphasic manner. While proliferating 3T3-L1 preadipocytes show relatively low *Dro1* mRNA levels, expression increases dramatically when cells reach postconfluency. *Dro1* expression is highly reduced during

early differentiation but increases again in the late stage of adipocyte differentiation (Tremblay *et al.*, 2009). The transition from undifferentiated preadipocytes into lipid-filled fat cells is hallmarked by a series of transcriptional changes. CCAAT/enhancer binding protein alpha (C/EBP α), a basic leucine-region zipper protein and the nuclear receptor peroxisome proliferator activated receptor gamma (PPAR γ), both master regulators of adipogenesis, promote transcription of early adipogenic genes that are required for fatty acid uptake, triglyceride formation and lipid metabolism (Ross *et al.*, 2000; Vázquez-Vela *et al.*, 2008). It was postulated that DRO1 indirectly induces C/EBP α and PPAR γ expression by repression of canonical Wnt/ β -catenin signaling pathway (Tremblay *et al.*, 2009).

The canonical Wnt/ β -catenin pathway plays a crucial role during cell proliferation, cell differentiation and embryonic development and is considered the predominant regulator of adipogenesis (Ross *et al.*, 2000; Bennet *et al.*, 2002; Clevers, 2006). In short, in the absence of a Wnt signal, β -catenin becomes phosphorylated by glycogen synthase kinase-3 (GSK-3) which results in ubiquitination and subsequent destruction of β -catenin by the proteasome. Binding of secreted Wnt to the Frizzled-receptor inhibits the destruction complex, thus leading to the stabilization and accumulation of β -catenin in the cytoplasm and its translocation to the nucleus. Once there, it binds to transcription factors of the T-cell factor/lymphoid enhancing factor (TCF/LEF) family, leading to the transcriptional activation or repression of target genes (Logan and Nusse *et al.*, 2004; Clevers, 2006).

In 3T3-L1 cells depleted for *Dro1* the activity of the Wnt signaling pathway was actually increased compared to controls. Interestingly, over-expression of *Dro1* also impaired adipocyte differentiation by a mechanism that does not influence canonical Wnt signaling and which still remains to be determined (Tremblay *et al.*, 2009). This phenomenon - inhibition of adipogenesis upon over-expression and knockdown of the same gene - is already known for other modulators of adipogenesis (Ross *et al.*, 2000; Wang *et al.*, 2006; Cheung *et al.*, 2007).

2.2 Intestine

2.2.1 Overview

The intestine comprises two anatomically and functionally distinct segments, the small intestine and the large intestine. Both sections share a general structure in the

organization of the gut wall constituted by several tissue layers, including, from within outwards, the tunica mucosa, tela submucosa, tunica muscularis and tunica serosa.

The tunica mucosa, adjoining the gut lumen, is subdivided into the lamina epithelialis mucosae, composed of a columnar epithelium, lamina propria mucosae, comprising connective tissue, vasculature and lymphatic tissue, and lamina muscularis mucosae, constituted by a thin smooth muscle layer. To increase the absorbent capacity of the gut, the columnar epithelial cells are fitted with microvilli.

The tela submucosa is represented by connective tissue, blood vessels, nerves and vegetative ganglion cells (plexus submucosus).

Throughout the whole intestine, lymphoid tissue is scattered in the lamina propria mucosae and tela submucosa, referred to as the gut-associated lymphatic tissue (GALT). The tunica muscularis comprises two smooth muscle layers, a circularly arranged inner layer (stratum circulare) and a longitudinally arranged outer layer (stratum longitudinale). Between those layers lies a varying amount of connective tissue, containing vegetative nerve cells (plexus myentericus).

The tunica serosa includes a single-layered epithelium and a small amount of connective tissue (Hees and Sinowatz, 2000; Hedrich *et al.*, 2004).

2.2.2 Small intestine

The main function of the small intestine is to digest and reabsorb nutrients with the aid of bile from the liver and enzymes from the pancreas. The small intestine is divided into three sections, duodenum, jejunum and ileum. In the small intestine the absorbent surface is enlarged by alternating fingerlike protrusions (villi) which are composed of lamina epithelialis mucosae and lamina propria mucosae. Villi, projecting into the intestinal lumen, alternate with invaginations called crypts of Lieberkühn. The length of the intestinal villi decreases from the duodenum to the ileum. The lamina epithelialis mucosae consists of four differentiated cell types: absorbent epithelial cells, representing the predominant cell type, goblet cells, enteroendocrine cells and Paneth cells (Hees and Sinowatz, 2000). Goblet cells, named after their characteristic cup-like shape, are exocrine cells displaying many secretory granules and are found regularly at the bottom of the crypts. They secrete high-molecular-weight glycoproteins called mucins which form a protective mucus blanket overlaying the intestinal surface (Hees and Sinowatz, 2000; Specian *et al.*, 1991). A small number of the epithelial surface lining cells is represented by enteroendocrine cells which secrete various hormones, e.g.

serotonin and secretin (Hees and Sinowatz, 2000; Schonhoff *et al.*, 2004). In the small intestine, in contrast to the large intestine, a fourth type of epithelial cells is present, the Paneth cell. These cells are located at the base of the crypt and secrete lysozyme, antimicrobial peptides and growth factors (Porter *et al.*, 2002; Yeung *et al.*, 2011). The lamina propria mucosae comprises solitary lymph nodes and large amounts of lymphocytes, plasma cells and granulocytes. Duodenal tubuloalveolar glands (Brunner`s glands), located in the lamina propria mucosae and tela submucosa, secrete alkaline mucus which forms a protective blanket against the acidic content of the gastric juice. Aggregated lymph nodes (Peyer`s patches) of the tela submucosa are characteristic for the ileum (Hees and Sinowatz, 2000). The surface of the Peyer`s patches features M-cells which serve to sample antigens (Hedrich *et al.*, 2004).

Every day, more than 10^{11} enterocytes are shed into the gut lumen, thus the intestinal epithelium has to undergo continuous replacement (Potten and Loeffler, 1990). The cells composing the columnar single layer intestinal epithelium derive from a multipotent stem cell population located basolaterally in the crypts. These stem cells divide and give rise to transient progenitor cells which proliferate in the lower third of the crypt (“transit-amplifying” crypt compartment), migrate upwards towards the tip of the villus, and differentiate along the way into the different mature cell types. Fully differentiated mouse enterocytes reach the surface epithelium after a journey of three to five days where they undergo apoptosis and are shed into the gut lumen (Giles *et al.*, 2003; Sancho *et al.*, 2003, Schonhoff *et al.*, 2004; Simons and Clevers, 2011). Paneth cells also derive from the stem cells residing at the bottom of the crypt, however, differentiation of progenitor cells takes place during a downward migration towards a Paneth cells compartment at the base of the crypt, where they reside for about 20 d, after which they are phagocytosed (Sancho *et al.*, 2003; Buske *et al.*, 2011; Simons and Clevers, 2011; Yeung *et al.*, 2011). Proliferation, migration and differentiation in the intestinal epithelium are regulated by the canonical Wnt signaling pathway. Proliferating and undifferentiated stem and precursor cells at the bottom of the crypt exhibit high nuclear β -catenin levels allowing for the expression of β -catenin/TCF target genes. During migration towards the surface of the epithelium Wnt signaling decreases, resulting in cell cycle arrest and differentiation (Stappenbeck *et al.*, 1998; Radtke and Clevers, 2005; Clevers, 2006; Yeung *et al.*, 2011). On the contrary, in Paneth cells Wnt signaling promotes terminal differentiation (Clevers, 2006).

2.2.3 Large intestine

The large intestine is subdivided into three segments, the caecum, the colon and the rectum. The main function of this compartment lies in its capacity to reabsorb water, electrolytes, and vitamins. In the large intestine the mucous membrane forms crypts of Lieberkühn, but no villi. The lamina epithelialis mucosae comprises absorbent epithelial cells, enteroendocrine and mucin-secreting goblet cells, but no Paneth cells are found. The number of goblet cells is increased in comparison to the small intestine (Stappenbeck *et al.*, 1998; Hees and Sinowatz, 2000; Hedrich *et al.*, 2004; Simons and Clevers, 2011).

In the mouse, the ascending and transverse parts of the colon exhibit transverse folds, whereas the descending colon and rectum have longitudinal folds (Hedrich *et al.*, 2004). The assertions made above for the small intestine relating to the epithelial renewal also largely apply to the large intestine (Hees and Sinowatz, 2000; Hedrich *et al.*, 2004).

2.2.4 Genetics of colorectal cancer

Colorectal cancer is the major cause of non-smoking-related cancer mortality in the Western World (Parkin *et al.*, 2005; World Cancer Research Fund, 2007). In the general population the lifetime risk of colorectal cancer is about 5 to 6% (Hawk and Levin, 2005). Approximately 95% of colorectal cancers are adenocarcinomas (in the following referred to as colorectal cancer) (World Cancer Research Fund, 2007).

Eighty percent of all colorectal malignancies develop spontaneously, only 20% being due to a hereditary cancer syndrome (Kerber *et al.*, 2005). Colorectal carcinomas evolve from preexisting adenomatous lesions of the intestinal glandular epithelium (Fearon and Vogelstein, 1990; Bienz and Clevers, 2000; Fearon, 2011). The adenoma-carcinoma sequence is a progressive multistep process involving the sequential accumulation of genetic alterations that account for novel or increased function of oncogenes and inactivation of tumor suppressor genes (Fearon and Vogelstein, 1990; Arnold *et al.*, 2005; Fearon, 2011). Oncogenes are always activated by somatic alterations, that is, the mutation arises in non-germ cells during lifetime, in consequence of specific point mutations, gene rearrangements, chromosome rearrangements or amplifications (Fearon, 2011). Defects of tumor suppressor genes can be caused by both inherited and somatic alterations and result from localized mutations, complete loss of the gene or epigenetic alterations, e.g. transcriptional silencing due to promoter hypermethylation (Arnold *et al.*, 2005, Fearon, 2011; Curtin *et al.*, 2011). A substantial

fraction of colorectal carcinomas display microsatellite instability, i.e. mutations in microsatellite sequences caused by mutations in the DNA mismatch-repair system, which can initiate and promote tumor formation when oncogenes and/or tumor suppressor genes are involved (Arnold *et al.*, 2005, Fearon, 2011). In most cases of sporadic colon cancers, loss of specific chromosomal regions affecting one allele of certain tumor suppressor genes (“loss of heterozygosity” (LOH)) occurs, with particularly high frequencies on chromosome 17p (protein 53 (*p53*)), 18q (deleted in colorectal cancer (*DCC*), mothers against decapentaplegic homolog 2 (*SMAD2*), mothers against decapentaplegic homolog 4 (*SMAD4*) and 5q (adenomatous polyposis coli (*APC*)) (Fearon and Vogelstein, 1990; Arnold *et al.*, 2005; Fearon, 2011). The acquirement of an inactivating somatic mutation in the remaining wildtype allele promotes tumor development due to perturbation of critical signaling pathways controlling cellular metabolism, proliferation, differentiation and survival (Fearon, 2011; Hanahan and Weinberg, 2011). Inactivation of the *APC* tumor suppressor gene as a consequence of mostly truncating mutations and LOH, respectively, plays a leading role in the initiation of sporadic colorectal neoplasms and is present in about 80% of colorectal adenomas and carcinomas (Nishisho *et al.*, 1991; Powell *et al.*, 1992; Polakis, 1999; Fearon 2011). In familial adenomatous polyposis (FAP), an inherited form of colorectal cancer, a germline mutation within the *APC* gene promotes the development of a multitude (hundreds to thousands) of adenomatous polyps in the large intestine (Lynch, 2003; Logan and Nusse, 2004; Arnold *et al.*, 2005; Fearon, 2011). In the majority of sporadic colorectal tumors as well as tumors from FAP patients, both *APC* alleles are inactivated (Bienz and Clevers, 2000). *APC* is part of a multiprotein destruction complex which plays a crucial role in Wnt signaling by the regulation of intracellular β -catenin levels. *APC* dysfunction leads to the stabilization and accumulation of β -catenin that translocates into the nucleus, complexes with DNA-binding proteins of the TCF/LEF family and activates the transcription of genes regulating cell proliferation, migration and differentiation (Bienz and Clevers, 2000; Giles *et al.*, 2002; Arnold *et al.*, 2005; Aoki *et al.*, 2007). The disruption of the Wnt signaling pathway perturbs normal intestinal homeostasis and finally triggers adenoma development (Bienz and Clevers, 2000; Giles *et al.*, 2002; Arnold *et al.*, 2005). In the intestinal epithelium, stabilized β -catenin is supposed to impair enterocyte differentiation and migration, implicating an expansion of the “transit-amplifying” crypt compartment (Bienz and Clevers, 2000). In the murine intestine, loss of *APC* was found

to induce hyperproliferation in the crypt compartment, to abrogate cell migration and to interfere with differentiation (Sansom *et al.*, 2004; Andreu *et al.*, 2005). Colorectal adenomas may progress stepwise to carcinomas through the accumulation of multiple independent somatic alterations in further tumor suppressor genes (e.g. *p53*, *SMAD4*, *SMAD2*) and oncogenes (e.g. *KRAS*, *BRAF*) (Arnold *et al.*, 2005).

2.3 Adipose tissue

2.3.1 Overview

Adipose tissue is a multi-depot organ comprising several subcutaneous and visceral sites that are distributed over the body (Gesta *et al.*, 2007; Cinti, 2009). In addition to mature adipocytes, which represent the major cell type, adipose tissue includes fibroblasts, macrophages, vascular cells, preadipocytes, and nerves, collectively referred to as the stromal vascular fraction (Hausman *et al.*, 2001, Gesta *et al.*, 2007; Vazquez-Vela *et al.*, 2008). According to their unique morphology and distinct function, two different types of adipocytes, brown and white, are distinguishable and organized in two tissues, the white adipose tissue and the brown adipose tissue. Both cell types are able to store triglycerides and release fatty acids (Cinti, 2005). In rodents, adipose tissue was found to exhibit pronounced plasticity as white adipocytes have the ability to transdifferentiate into brown adipocytes and *vice versa*, according to biological requirements (Cinti, 2005; Cinti, 2009). During embryogenesis, adipose tissue origins from mesenchymal stem cells. These cells give rise to undifferentiated preadipocytes which differentiate into adipocytes (Gregoire *et al.*, 1998; Gesta *et al.*, 2007). Preadipocytes are fibroblast-like cells which reside in adipose tissue and bear the ability to proliferate and differentiate into mature adipocytes (Gregoire *et al.*, 1998; Hausman *et al.*, 2001). It remains unknown whether brown and white adipocytes and adipocytes from different fat depots evolve from the same type of preadipocytes (Gesta *et al.*, 2007). After birth, adipose tissue grows rapidly, due to both an increase in fat cell size (adipocyte hypertrophy) and the addition of new adipocytes (adipocyte hyperplasia), a process collectively termed adipogenesis (Hausman *et al.*, 2001; Vazquez-Vela *et al.*, 2008). As mature adipocytes are postmitotic, additional adipocytes can only origin from preadipocytes (Hausman *et al.*, 2001). Adipogenesis is mediated by hormones, cytokines, and growth factors and implicates down-regulation of the canonical Wnt signaling pathway and expression of transcription factors of the C/EBP and PPAR families, especially C/EBP α and PPAR γ (Gregoire *et al.*, 1998; Ross *et al.*, 2000;

Kennel *et al.*, 2005; Christodoulides *et al.*, 2006; Gesta *et al.*, 2007; Hausman *et al.*, 2001). Adipogenesis takes place within cell clusters and is closely interrelated with angiogenesis (Nishimura *et al.*, 2007). Most likely the proliferation of preadipocytes is induced by circulating factors and neuronal inputs as well as paracrine and autocrine factors secreted from the various cells composing adipose tissue (Lau *et al.*, 1996; Serrero and Lepak, 1996; Hausman *et al.*, 2001).

2.3.2 White adipose tissue

White adipocytes are spherical cells which store triglycerides in a single large lipid droplet that accounts for more than 90% of the cell's volume. A single fat pad contains adipocytes of variable size, ranging from 10 μm to 100 μm , depending on the size of the fat vacuole. White adipose tissue is the primary site for the storage of dietary energy in the form of triglycerides (Cinti, 2005). Dietary lipids are enzymatically hydrolyzed in the proximal intestinal lumen by lipases leading to the production of non-esterified fatty acids which are taken up by the enterocytes (Bamba and Rader, 2007). In the enterocyte, free fatty acids are re-esterified to triglycerides and packaged with apolipoprotein B-48 and other lipids to form so-called chylomicrons. Chylomicrons are secreted into the intestinal lymph and reach the systemic circulation *via* the thoracic duct. In the capillaries of adipose tissue, hydrolysis of chylomicron-triglycerides into non-esterified fatty acids is mediated by lipoprotein lipase which is synthesized by adipocytes, anchored to proteoglycans on the endothelial surface and dependent on its cofactor apoC-II, an integral part of chylomicrons. The non-esterified fatty acids are taken up by adipocytes where they are re-esterified into triglycerides for energy storage (Bamba und Rader, 2007). In times of energy deprivation, free fatty acids and glycerol are generated by lipolysis of triglycerides and released into the circulation, thereby providing an energy source for other tissues, mainly the skeletal muscle (Ahima and Osei, 2008; Bays *et al.*, 2008; Guilherme *et al.*, 2008 Karpe *et al.*, 2011). Uptake of circulating free fatty acids by adipocytes plays only a minor role compared to fatty acid uptake from hydrolysis of chylomicron-triglycerides (Bamba and Rader, 2007).

Furthermore, white adipose tissue functions as an endocrine organ because of its capacity to secrete a variety of hormones and cytokines, so called adipokines (Vazquez-Vela *et al.*, 2008; Singla *et al.*, 2010). Adipokines not only participate in the control of energy metabolism (e.g. leptin, adiponectin, resistin, visfatin), they also play a role in immunological responses (TNF- α , monocyte chemotactic protein-1 (MCP-1)) and the

regulation of blood pressure (e.g. apelin) (Gregoire *et al.*, 1998; Ailhaud, 2006; Vazquez-Vela *et al.*, 2008; Bays *et al.*, 2008). Leptin was the first adipokine described and constitutes an important regulator of energy homeostasis and body weight as it provides a satiety signal to the central nervous system. After food intake leptin is secreted from adipocytes into the blood circulation and binds to receptors expressed by hypothalamic neurons. Thereby a signal transduction cascade is activated that results in a decrease in energy consumption and an activation of energy expenditure pathways. Moreover, leptin, together with adiponectin, enhances insulin sensitivity (Gregoire *et al.*, 1998; Ahima and Osei, 2008; Guilherme *et al.*, 2008; Morris and Rui, 2009; Singla *et al.*, 2010). There is also strong evidence that autocrine and paracrine signaling pathways as well as neuronal influences play an important role in the maintenance of adipose tissue homeostasis (Ahima and Osei, 2008).

2.3.3 Brown adipose tissue

Brown adipocytes store triglycerides in the form of many lipid droplets, thus showing a multilocular appearance. Brown adipose tissue is more densely vascularized and innervated than white adipose tissue, and brown adipocytes possess large characteristic mitochondria containing the protein uncoupling protein 1 (UCP1), a member of the mitochondrial carrier family. Brown adipose tissue is primarily located in the intrascapular region and is most abundant at birth as it is replaced by white adipose tissue during aging (Gesta *et al.*, 2007). The main function of brown adipose tissue is the generation of body heat from triglycerides and fatty acids in a process called (non-shivering) thermogenesis. Combustion of fatty acids in the respiratory chain results in an electrochemical proton gradient between the outer and inner mitochondrial membrane. In brown fat mitochondria UCP1, the equivalent of an H⁺ transporter, is able to release the energy stored in this proton gradient in the form of heat (Cannon and Nedergaard, 2004; Gesta *et al.*, 2007; Ravussin and Galgari, 2011). Thermogenesis is under the control of the sympathetic nervous system and is activated by a temperature below thermoneutrality. Under conditions of increased thermogenetic demand, new brown adipocytes can either derive from preadipocytes by adipogenesis or by direct transformation of white into brown adipocytes (Cinti, 2009).

2.3.4 Obesity

Obesity (also termed adiposity) is characterized by an excessive growth of white adipose tissue caused by an increase in energy uptake and a decrease in energy expenditure. Obesity is defined in humans by a body mass index (body weight (kg) divided by (body height (m))²; BMI) greater than 30. In industrialized countries obesity is a major health problem (World Health Organization (WHO), 2011). In 2008, according to the WHO, 1.5 billion adults were overweight (BMI greater than 25), of these 200 million men and 300 million women were considered obese. Moreover, nearly 43 million children under the age of five were overweight in 2010.

In times of positive caloric balance, adipose tissue expands due to a rising deposit of triglycerides. This is accomplished through increases in adipocyte size (adipocyte hypertrophy) as well as increases in adipocyte number (adipocyte hyperplasia) (Hausman *et al.*, 2001; Vazquez-Vela *et al.*, 2008). During the development of obesity in young animals (early-onset obesity), adipogenesis contributes far more to the increase of fat mass than in older animals (late-onset obesity) as the capacity of preadipocytes to become fully functional mature adipocytes declines in adult life (Lemonnier, 1972; DiGirolamo *et al.*, 1998; Hausman *et al.*, 2001; Vazquez-Vela *et al.*, 2008). In times of positive energy balance, storage of excess energy is initially accomplished by adipocyte hypertrophy (Guilherme *et al.*, 2008; Hausman *et al.*, 2001). Adipocytes, however, possess only a restricted capacity for cell expansion, hence if adipocytes reach a critical cell size further energy can only be stored by an increase in adipocyte number. This critical cell size is assumed to be genetically determined and specific for each fat depot that means some fat depots are more prone to undergo hyperplasia than other (Hausman *et al.*, 2001). In rodents, for example, perirenal and inguinal fat pads have a high tendency to hyperplasia whereas hypertrophy is more characteristic for epididymal and mesenteric fat depots (DiGirolamo *et al.*, 1998). Hypertrophic adipocytes are more prone to undergo necrotic-like cell death than non-hypertrophic adipocytes (up to 30-fold), thus it was suggested that with increasing obesity only the switch from adipocyte hypertrophy to hyperplasia is able to further increase the lipid storage capacity of adipose tissue (Cinti *et al.*, 2005). Moreover, adipocyte hypertrophy was linked to adipocyte dysfunction given that a high degree of hypertrophy in comparison to hyperplasia is related with the risk to develop metabolic disease (Ravussin and Smith, 2002; Bays *et al.*, 2008). Obesity is strongly associated with a number of chronic diseases such as coronary atherosclerotic heart disease, gout,

restrictive lung disease, gall bladder disease, some forms of cancer, degenerative arthritis, infertility, and sleep apnoea (Montague and O'Rahilly, 2000; Hausman *et al.*, 2001; Singla *et al.*, 2010). There are also several metabolic complications of obesity (termed metabolic syndrome), including impaired glucose tolerance, insulin resistance, often giving way to β -cell failure, type 2 diabetes, dyslipidemia, hypertension, and premature heart disease (Bays *et al.*, 2008; Singla *et al.*, 2010). In humans, visceral adipose tissue accumulation is supposed to be associated with increased mortality and a higher risk to develop metabolic disease (Montague and O'Rahilly, 2000; Bays *et al.*, 2008; Singla *et al.*, 2010).

Excess body fat storage is often accompanied by insulin resistance that is characterized by decreased insulin-stimulated glucose uptake and metabolism in adipocytes and skeletal muscle and by impaired suppression of hepatic glucose output. There is strong evidence that these changes in glucose metabolism are due to defective signaling from the insulin receptor and down-regulation of the glucose transporter type 4 (GLUT-4) (Singla *et al.*, 2010). Furthermore, adiposity leads to a rise in basal lipolysis in adipose tissue and impaired trapping of fatty acids in adipocytes implicating elevated circulating free fatty acids. Elevated circulating fatty acid levels result in ectopic lipid accumulation in the pancreas, muscle and liver and strongly influences cellular glucose uptake, thus being one of the main factors causing insulin resistance (Boden, 2008; Guilherme *et al.*, 2008; Vazquez-Vela *et al.*, 2008; Singla *et al.*, 2010).

The endocrine function of adipose tissue is highly impaired in obesity. With increasing body fat mass the release of adipokines from adipose tissue becomes more and more dysregulated, thus disrupting physiological whole-body energy homeostasis (Ahima and Osei, 2008). Most adipokines (e.g. leptin, TNF- α , interleukin-6 (IL-6) and resistin) are upregulated in obesity, however, adiponectin levels are inversely related to adiposity (Ahima and Osei, 2008; Vazquez-Vela *et al.*, 2008). Hyperthrophic adipocytes secrete high amounts of leptin, however, in adiposity non-adipose tissues have developed leptin resistance and high circulating leptin levels promote insulin resistance (Ahima and Osei, 2008; Vazque-Vela *et al.*, 2008; Morris *et al.*, 2009).

Given that adipose tissue contains all the components of the renin-angiotensin system and constitutes a major source of extra-hepatic angiotensinogen, it is supposed that adipose tissue directly contributes to obesity-related hypertension (Ailhaud, 2006).

Moreover, obese adipose tissue develops a chronic low-inflammatory state that is due to an increase in the secretion of pro-inflammatory factors (e.g. TNF- α , IL-6, MCP-1)

from and a decreased production of anti-inflammatory factors (e.g. transforming growth factor- β (TGF- β)) by adipocytes. Thereby, immunoreactive cells, primarily bone-marrow derived macrophages, are attracted and accumulate in adipose tissue in an amount that is positively correlated with adipocyte size and BMI (Bays *et al.*, 2008; Singla *et al.*, 2010; Guilherme *et al.*, 2008; Weisberg *et al.*, 2003; Wellen and Hotamisligil, 2003). Macrophages were found to be predominantly localized around dead adipocytes, hence it was supposed that necrotic-like cell death of hypertrophic adipocytes contributes to the aggregation of macrophages in adipose tissue (Cinti *et al.*, 2005). Activated macrophages secrete a plethora of inflammatory cytokines, especially TNF- α , which strongly enhances lipolysis and impairs triglyceride deposition in adipocytes, thus contributing to excess blood levels of free fatty acids and triglycerides and finally to insulin resistance, type 2 diabetes and ectopic lipid deposition (Guilherme *et al.*, 2008; Weisberg *et al.*, 2003).

3. Animals, Materials and Methods

3.1 Animals

3.1.1 *Dro1* constitutive knockout mice (*Dro1*^{-/-})

Dro1 constitutive knockout mice (in the following designated as knockouts or *Dro1*^{-/-} mice) were generated by gene targeting using a Cre-loxP-mediated recombination system (Fig. 3.1). For generation of the targeting construct, the essential exon 2 of the *Dro1* gene and 5' and 3' homology arms were amplified by PCR from genomic DNA of E14 mouse embryonic stem cells. In doing so, a loxP site was added to the end of the 5' homology arm. A targeting vector was created by insertion of the PCR products into the multiple cloning site of the pPNT4 (Conrad *et al.*, 2003) cloning vector that also carried a neomycin resistance gene, a thymidine kinase gene and another loxP sequence. The construct was linearized by *SaII* restriction digest and electroporated into E14 mouse embryonic stem cells. An embryonic stem cell line that had integrated the construct correctly by homologous recombination was identified by Southern blot analysis and microinjected into blastocysts of C57BL/6N mice. Blastocysts were transferred into the uteri of pseudopregnant synchronized foster mothers and the resulting chimeric progeny were intercrossed with C57BL/6N mice to establish a mouse line with floxed *Dro1* alleles (*Dro1*^{fl/fl}). *Dro1*^{fl/fl} females were mated to transgenic males expressing Cre (causes recombination) recombinase, a type 1 topoisomerase from P1 bacteriophage that catalyzes recombination between loxP sites, under control of the cytomegalovirus (CMV) promoter (Schwenk *et al.*, 1995). The heterozygous *Dro1*^{+/-} offspring was bred to obtain *Dro1*^{-/-} mice. In the present study *Dro1*^{fl/fl} mice were used as control animals, in the following referred to as “controls”. *Dro1*^{fl/fl} mice were generated by PD Dr. Marlon R. Schneider and were made available for the present studies.

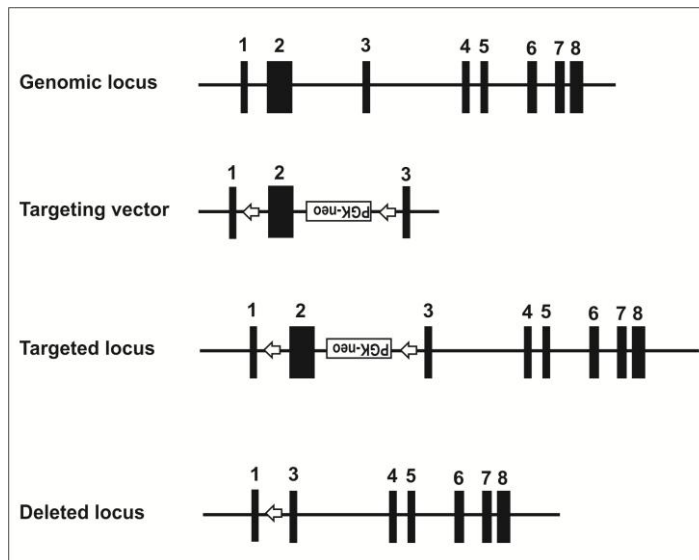


Fig. 3.1 Schematic representation of the strategy employed to generate *Dro1*^{-/-} mice. The essential exon 2 of the *Dro1* gene was flanked by 2 loxP sequences. Cre-recombinase-mediated recombination between loxP sites results in deletion of exon 2 and *Dro1* knockout. Black boxes: exons; White arrows: loxP sites; PGK-neo: phosphoglycerine kinase neomycin resistance cassette.

3.1.2 B6.C-Tg(CMV-cre)1Cgn/J mice

B6.C-Tg(CMV-cre)1Cgn/J mice (Schwenk *et al.*, 1995) were kindly donated by Prof. Dr. Irmgard Förster, Heinrich-Heine-University, Düsseldorf. In this mouse strain the *Cre* gene is under transcriptional control of a human CMV minimal promoter and is expressed during early embryogenesis in all tissues including germ cells. Thus Cre-mediated deletion of the loxP-flanked DNA sequence is ubiquitously present and the acquired mutation is transmitted through the germ-line. The transgene was observed to be linked to the X chromosome (Schwenk *et al.*, 1995).

3.1.3 C57BL/6J-*Apc*^{Min}/J mice

C57BL/6J-*Apc*^{Min}/J mice (in the following referred to as *Apc*^{+Min} mice) were purchased from the Jackson Laboratory (Bar Harbor, USA). *Apc*^{+Min} mice were established from an ethylnitrosourea-treated C57BL/6J male mouse and carry a single autosomal dominant germ-line nonsense mutation at nucleotide 2549 (codon 850) in the *Apc* tumor suppressor gene (Moser *et al.*, 1990; Su *et al.*, 1992). Somatic allelic loss of the remaining *Apc* wild-type locus leads to dysregulation of the Wnt signaling pathway (Levy *et al.*, 1994; Luongo *et al.*, 1994). The resulting phenotype is characterized by a

high predisposition to develop a multitude of tumors of the intestinal tract. Therefore the mutant gene was named multiple intestinal neoplasia (*Min*) (Moser *et al.*, 1989). $Apc^{+/Min}$ mice develop, on average, 30 tumors throughout the entire length of the intestinal tract, though the majority of neoplastic lesions are distributed to the small bowel and few occur in the colon (Moser *et al.*, 1990; Shoemaker *et al.*, 1997; Boivin *et al.*, 2003). $Apc^{+/Min}$ mice die, on average, at 120 d of age in consequence of secondary effects of tumor growth, mainly intestinal bleeding and obturation (Moser *et al.*, 1990; Shoemaker *et al.*, 1997). On the C57BL/6 background all intestinal tumors are adenomas which may, especially in older animals, occasionally progress to adenocarcinomas (Moser *et al.*, 1990; Shoemaker *et al.*, 1997; Boivin *et al.*, 2003). Invasion of tumors into the tela submucosa is uncommon (McCart *et al.*, 2008) and adenocarcinomas possess no metastatic properties (Boivin *et al.*, 2003). Spontaneous colonic ACF formation is rare or absent (Reitmair *et al.*, 1996; Song *et al.*, 2000; Boivin *et al.*, 2003). Tumor burden was observed to be strongly affected by the genetic background due to the presence or absence of genetic modifiers, so called modifiers of *Min* (*Mom*) (Shoemaker *et al.*, 1997; Halberg *et al.*, 2000; McCart *et al.*, 2008). Since mutant homozygotes die early in embryogenesis (Moser *et al.*, 1990; Moser *et al.*, 1995), all studies were conducted in heterozygote mice of both genders. Considering the fact that $Apc^{+/Min}$ females are seldom healthy enough to maintain a pregnancy and feed an eventual litter (Moser *et al.*, 1990), only heterozygote males were used for breeding. $Apc^{+/Min}$ males were mated to $Dro1^{-/-}$ females and the resulting male $Dro1^{+/-};Apc^{+/Min}$ offspring was intercrossed with $Dro1^{-/-}$ females to obtain $Dro1^{-/-};Apc^{+/Min}$ progeny. $Dro1^{fl/fl};Apc^{+/Min}$ mice were used as control animals to $Dro1^{-/-};Apc^{+/Min}$ mice and were bred as described for $Dro1^{-/-};Apc^{+/Min}$ mice. In the following, $Dro1^{fl/fl};Apc^{+/Min}$ mice are entitled as “ $Apc^{+/Min}$ controls”. Mice on the $Apc^{+/Min}$ background were inspected on a daily basis and sacrificed when moribund.

To investigate *Mom1* allele status of $Dro1^{-/-};Apc^{+/Min}$ and $Apc^{+/Min}$ control mice, a 500 bp region of the *Mom1* allele was amplified by PCR using primers Mom1#1 and Mom1#2 (see below for general PCR conditions). PCR products were digested with *Bam*HI (MBI Fermentas, St. Leon-Rot) for 1 h at 37°C and separated along with a molecular weight marker (pUC mix molecular weight marker, MBI Fermentas, St. Leon-Rot) on a 1.5% Tris-acetate-EDTA buffer (TAE) agarose (Invitrogen, Karlsruhe) gel containing ethidium bromide (Roth, Karlsruhe). Electrophoresis was carried out in an agarose gel electrophoresis chamber (MWG-Biotech, Ebersberg) at 120 V for 45 min

in a TAE running buffer. DNA band patterns were visualized with ultraviolet light at 254/366 nm.

Restriction digest:

PCR product	20 µl
<i>Bam</i> HI buffer (MBI Fermentas, St. Leon-Rot)	5 µl
<i>Bam</i> HI restriction enzyme	1 µl
Bidistilled water	24 µl

50x TAE running buffer

Tris (Roth, Karlsruhe)	242.0 g
Glacial acetic acid (Roth, Karlsruhe)	57.1 ml
Ethylenediaminetetraacetic acid (EDTA), 0.5 M, pH 8.0 (VWR International, Darmstadt)	100 ml
Bidistilled water up to	1 l

3.1.4 Animal maintenance

Animals were maintained under specific pathogen free conditions in a closed barrier system in the facilities of the Gene Center. They were housed separated by sex in type 2 and type 3 Makrolon cages, with a 12 h light cycle at 22°C and 40% humidity. Food and water were provided *ad libitum* and mice were either fed a chow diet (V1536, Ssniff, Soest, Germany; 13.0 MJ/kg, with 9% energy derived from fat, 33% from protein, and 58% from carbohydrate) or, to induce obesity, a high fat diet (D12492 mod., Ssniff, Soest, Germany; 25.2 MJ/kg, with 60% energy derived from fat, 19% from protein, and 21% from carbohydrate). Mice were weaned at an age of 3 weeks and earmarked. In case studies were conducted in mice younger than 3 weeks, foot tattooing was used to identify animals. Cervical dislocation was applied for killing.

Experiments were carried out in accordance with the German Animal Protection Law and were officially sanctioned by the local authorities (AZ 55.2-1-54-2531-126-09).

3.2 Materials and Methods

3.2.1 Mouse Genotyping

3.2.1.1 Sample collection

Samples were collected when mice were 3 to 4 weeks of age by clipping 0.5 mm of the tail tip with a pair of scissors (Aesculap, Tuttlingen). The wound was blotted dry from blood on absorbent paper and closed with Histoacryl[®] liquid skin glue (B. Braun, Melsungen). Samples were immediately frozen on dry ice, transferred to a 1.5 ml centrifuge tube (Eppendorf, Hamburg), and stored at -80°C to prevent DNA degradation.

3.2.1.2 Extraction of DNA from mouse tail tips

Digestion buffer (620 µl) was added to the centrifuge tubes containing the frozen tail tips and the samples were incubated at 56°C overnight with gentle shaking.

Digestion buffer:

Nuclei Lysis Solution (Promega, Mannheim)	500 µl
EDTA, 0.5 M, pH 8.0	120 µl
Proteinase K, 20 mg/ml (Roche, Mannheim)	17.5 µl

The next day 3 µl of RNase (Roche, Mannheim) were added and samples incubated at 37°C for 20 min to degrade RNA. Thereafter 200 µl Protein Precipitation Solution (Promega, Mannheim) were added and the samples were vortexed vigorously at high speed for 20 s. After chilling on ice for 5 min, samples were centrifuged at 14.000 x g for 4 min to pelletize precipitated proteins at the bottom of the tube. The supernatant containing the DNA was carefully transferred to a clean 1.5 ml centrifuge tube containing 600 µl of room temperature isopropanol (Merck, Darmstadt) and the solution was gently mixed by inverting the tubes until white strands of precipitated DNA were visible. To pelletize DNA, samples were centrifuged at 14.000 x g for 1 min. After carefully removing the isopropanol, 600 µl of room temperature 70% ethanol (Merck, Darmstadt) were added to the pellet and the tubes were inverted several times to wash the DNA. Samples were again centrifuged for 1 min at 14.000 x g, the ethanol carefully removed using a pipette and the pellet air-dried for 10 min. To rehydrate DNA, 50 µl of

DNA Rehydration Solution (Promega, Mannheim) were added and samples incubated for 1 h at 65°C.

3.2.1.3 PCR analysis

PCR reactions were prepared on ice using the Taq DNA polymerase Kit (Qiagen, Hilden) and were carried out in a reaction volume of 20 µl in DNase-, RNase and pyrogen-free 100 µl PCR-reaction-tubes (G. Kisker GbR, Steinfurt).

Mastermix preparation (per sample):

PCR buffer, 10x (Qiagen, Hilden)	2.00 µl
dNTPs, 1 mM (MBI Fermentas, St. Leon-Rot)	2.00 µl
Q-Solution (Qiagen, Hilden)	4.00 µl
MgCl ₂ , 25mM (Qiagen, Hilden)	1.25 µl
Sense primer, 2 µM	1.00 µl
Antisense primer, 2 µM	1.00 µl
Bidistilled H ₂ O	7.65 µl
Taq Polymerase, 5U/µl (Qiagen, Hilden)	0.10 µl
Template DNA, about 50 ng/µl	1.00 µl

Mastermix preparation using primers Apc33, Apc34 and Apc758 to genotype Apc^{+/-Min} mice (per sample):

PCR buffer, 10x	2.00 µl
dNTPs, 1 mM	4.00 µl
Q-Solution	4.00 µl
MgCl ₂ , 25 mM	1.25 µl
Primer Apc33	2.00 µl
Primer Apc34	2.00 µl
Primer Apc758	2.00 µl
Bidistilled H ₂ O	1.65 µl
Taq Polymerase, 5U/µl	0.10 µl
Template DNA, about 50 ng/µl	1.00 µl

The reaction took place in a thermal cycler (Biometra, Göttingen) according to the following protocol:

Step 1: 94°C – 4 min	(DNA denaturation)
Step 2: 94°C – 1 min	(DNA denaturation)
Step 3: Annealing temperature	(primer annealing)
Step 4: 72°C – 2 min	(elongation)
Step 5: 72°C – 10 min	(elongation)
Step 6: 4°C	(cooling)

Step 2 to 4 were repeated 35 times (36 amplification cycles in total), thereafter the program continued with step 5. Amplified products and a molecular weight marker were loaded into the slots of 1.5% agarose TAE gels containing ethidium bromide and electrophoresis was carried out in an electrophoresis chamber at 120 V for 45 min in a TAE running buffer. DNA band patterns were visualized with ultraviolet light at 254/366 nm.

3.2.2 Identification of knockout mice by non-radioactive Southern blot

3.2.2.1 Digest, electrophoresis and transfer of DNA

DNA was extracted from liver samples as described above (Chapter 3.2.1.2) and DNA concentration was measured with a spectrophotometer (Beckman, Palo Alto, USA) at 260 and 280 nm. 10 µg of genomic DNA were restriction digested with *Pst*I (MBI Fermentas, St. Leon-Rot) over night at 37°C in a centrifuge tube.

Restriction digest:

Liver genomic DNA, 10 µg	15.0 µl
<i>Pst</i> I restriction enzyme	3.0 µl
Buffer <i>Pst</i> I (MBI Fermentas, St. Leon-Rot)	4.0 µl
Spermidine, 0.1 M (Sigma-Aldrich, Deisenhofen)	1.0 µl
Bidistilled water	17.0 µl

The next day 10 µl of 6x loading dye (MBI Fermentas, St. Leon-Rot) were added to each sample and DNA fragments were separated by electrophoresis on a 0.9% agarose TAE gel containing ethidium bromide for 6 h at 60 V using a TAE running buffer. DNA fragments were visualized by ultraviolet light at 254/366 nm and photographed together

with a ruler. For DNA denaturation, the gel was placed in buffer I (1.5 M NaCl (Roth, Karlsruhe), 0.5 M NaOH (Roth, Karlsruhe)) for 45 min by gently shaking. The gel was rinsed with bidistilled water and transferred to buffer II (1.5 M NaCl, 1.0 M Tris-HCl (Roth, Karlsruhe)) for 30 min to depurinate DNA. In the meantime a nylon membrane (Pall Corporation, Pensacola, USA) was cut to the size of the gel, wetted in bidistilled water for 10 min and incubated in 10x saline-sodium citrate buffer (SSC) until needed. For transfer of DNA, the gel was placed upside down on a piece of filter paper (GE Healthcare, Munich) whose ends were dipped into a 10x SSC reservoir. The gel was carefully covered with the membrane, wetted filter paper, and a stack of tissue towels (both cut to the size of the membrane), and a burden of approximately 1 kg was placed on top. Air bubbles were removed with a glass pipette after each step. Blotting took place over night, so that the buffer was drawn from the buffer reservoir through the gel, the nylon membrane and the filter paper to the stack of dry paper tissues by capillary force. Thereby the DNA fragments were carried to the nylon membrane on which they were immobilized. The next day the membrane was removed and washed in 6x SSC for 5 min. Thereafter it was illuminated with ultraviolet light (120 J/cm^2) for 60 s to cross-link DNA covalently to the membrane.

20x SSC:

NaCl	175.3 g
Sodium citrate (Merck, Darmstadt)	88.2 g
Bidistilled water up to	1 l
Adjusted to pH 7.0	

3.2.2.2 Non-radioactive probe labeling

The digoxigenin (DIG) labeled hybridization probe was generated by PCR from C57BL/6N mice genomic DNA using the DIG Probe Synthesis kit (Roche, Mannheim). The dNTP mixture contains DIG labeled uridine nucleotides, in consequence DIG is incorporated into the nucleic acid probe by the DNA polymerase. Preparation of the PCR reaction was accomplished in 100 μl PCR tubes on ice using primers Dro3'end#1 and Dro3'end#2.

Master mix (per sample):

PCR buffer with MgCl ₂ , 10x (Roche, Mannheim)	5.00 µl
PCR DIG Probe Synthesis mix (Roche, Mannheim)	5.00 µl
Forward primer, 2 µM	5.00 µl
Reverse primer, 2 µM	5.00 µl
Enzyme mix (Roche, Mannheim)	0.75 µl
Bidistilled water	28.25 µl
Template DNA, about 50 ng/µl	1.00 µl

Thermic cycling was carried out in a thermal cycler according to the following protocol:

Step 1: 94°C – 4 min	(DNA denaturation)
Step 2: 94°C – 1 min	(DNA denaturation)
Step 3: 58°C – 1 min	(primer annealing)
Step 4: 72°C – 2 min	(elongation)
Step 5: 72°C – 10 min	(elongation)
Step 6: 4°C	(cooling)

Steps 2 to 4 were repeated 44 times before the program continued with step 5 (45 amplification cycles in total). 5 µl of the amplified product were transferred to a clean 100 µl tube containing 15 µl bidistilled water and 4 µl 6x loading dye. The aliquot was run on a 0.9% agarose TAE gel containing ethidium bromide along with a DNA molecular weight marker. DNA band patterns were visualized by ultraviolet light. The remaining probe was stored at -20°C until needed.

3.2.2.3 Hybridization, washing and detection

For hybridization, washing and detection, the DIG Block and Wash Buffer Set (Roche, Mannheim) was used and all necessary solutions were prepared following the manufacturer`s manual. All washing and incubation steps were performed with gentle agitation at room temperature if not stated differently.

The nylon membrane was placed in a glass hybridization tube (Bachofer, Reutlingen) and incubated in pre-heated DIG Easy Hyb buffer (Roche, Mannheim) for 30 min. 30 µl of the DIG labeled probe were transferred to a 1.5 ml centrifugation tube, heated at 95°C for 5 min, cooled on ice for 2 min and added to the DIG Easy Hyb buffer in the hybridization tube. Hybridization took place over night at 39°C. The next day non-

bound probes were removed by washing the membrane 2 times for 5 min in 2x SSC containing 0.1% sodium dodecyl sulfate (SDS; Merck, Darmstadt) and 2 times for 15 min in 0.5x SSC containing 0.1% SDS at 65°C. Thereafter the membrane was incubated in Washing buffer (Roche, Mannheim) for 5 min, in Blocking solution (Roche, Mannheim) for 1 h and finally treated for 30 min with alkaline phosphatase conjugated Anti-DIG-AP Fab fragments (Roche, Mannheim) diluted 1: 10.000 in Blocking solution. Unbound Anti-DIG-AP Fab fragments were eliminated by rinsing the membrane 2 times for 15 min with Washing buffer. Next, the membrane was removed from the hybridization tube, placed with the DNA side facing up in a hybridization bag and 2 ml of CSPD ready-to-use detection solution (Roche, Mannheim) were applied and spread evenly and without air bubbles over the membrane. After 5 min, excess liquid was removed from the hybridization bag, the edges were heat-sealed and the membrane was exposed to a chemiluminescence film (GE Healthcare, Munich) until the required signal strength was achieved.

3.2.3 Evaluation of gene expression at the RNA level

3.2.3.1 Extraction of RNA from tissues

Mice were killed by cervical dislocation and tissue samples (liver, muscle, heart, white adipose tissue and brown adipose tissue) excised immediately. The intestine was excised and the faecal content rinsed out with 1x phosphate buffered saline (PBS) using cannula (B.Braun, Melsungen) and syringe (Codan Medical ApS, Roedby, Denmark). The intestine was opened longitudinally, laid open and small intestinal epithelium and colon epithelium were scraped off with cover glass slides (VWR International, Darmstadt) and transferred to 1.5 ml centrifuge tubes. Samples were frozen on dry ice and stored at -80°C. For RNA isolation, frozen tissue samples (~50-100 mg) were transferred to 5 ml plastic tubes (Greiner Bio-One, Frickenhausen) containing 1 ml of Trizol reagent (Invitrogen, Karlsruhe) and homogenised for 60 s using a homogenizer (ART Labortechnik, Müllheim) at 23500 rpm. To avoid cross-contamination the tip of the homogenizer was cleaned with diethylpyrocarbonate-treated (DEPC; Sigma-Aldrich, Deisenhofen) water and 0.2 M NaOH between samples. The lysate was centrifuged at 12.000 x g for 10 min at 4°C and the supernatant was transferred to a clean 2 ml centrifuge tube (Eppendorf, Hamburg). Samples were incubated for 5 min at room temperature, 0.2 ml chloroform (Merck, Darmstadt) were added and the solution shaken vigorously by hand for 15 s. Phase separation was achieved by incubating

samples for 3 min at room temperature and centrifugation at 12.000 x g for 15 min at 4°C. The upper clear, aqueous phase which contains the RNA fraction was transferred to a clean 1.5 ml centrifuge tube. To precipitate RNA, 0.5 ml isopropanol was added and the tubes were inverted several times. Incubation was carried out for 10 min at room temperature and RNA was pelletized by centrifugation at 12.000 x g for 10 min at 4°C. After decantation of the supernatant, the RNA was washed with 0.5 ml of ice-cold 75% ethanol and samples centrifuged at 7.500 x g for 5 min at 4°C. The ethanol was carefully removed with a pipette, the pellet air-dried for 3 min and resuspended in 100 µl DEPC-treated water. For RNA cleanup the RNeasy Mini kit (Quiagen, Hilden) was used according to the manufacturer`s manual. RNA was finally dissolved in 50 µl DEPC-treated water and stored at -80°C.

10x PBS:

NaCl	80.0 g
Na ₂ HPO ₄ (Merck, Darmstadt)	14.7 g
KCl (Merck, Darmstadt)	2.0 g
KH ₂ PO ₄ (Merck, Darmstadt)	2.4 g
Bidistilled water up to	1 l
Adjusted to pH 7.4	

3.2.3.2 cDNA synthesis

RNA concentration was measured with a spectrophotometer and samples diluted in DEPC-treated water to a final RNA concentration of 0.5 µg/µl. Genomic DNA was removed from the RNA preparation using DNase I, Amplification Grade (Invitrogen, Karlsruhe).

DNaseI digest (per sample):

DNase I reaction buffer, 10x (Invitrogen, Karlsruhe).	2 µl
DNase I Amp Grade, 1U/ µl (Invitrogen, Karlsruhe).	2 µl
DEPC-treated water	8 µl
RNA preparation, 0.5 µg/µl	8 µl

After an incubation for 15 min at room temperature, the DNase I was inactivated by the addition of 2 µl of 25 mM EDTA solution (Invitrogen, Karlsruhe) to the reaction

mixture and heating for 10 min at 65°C. cDNA was synthesized using the SuperScript First Strand cDNA Synthesis System (Invitrogen, Karlsruhe) in a final reaction volume of 55 µl. PCR reactions were prepared in DNase-, RNase and pyrogen-free 0.5 ml centrifuge tubes (Eppendorf, Hamburg) on ice as follows:

RNA/ primer mixture (per sample):

dNTPs, 10 mM	2.75 µl
Random hexamer primer (Invitrogen, Karlsruhe)	2.75 µl
Template RNA, 4 µg	22.0 µl

cDNA synthesis mix (per sample):

RT buffer, 10x (Invitrogen, Karlsruhe)	5.5 µl
MgCl ₂ , 25 mM (Invitrogen, Karlsruhe)	11.0 µl
DTT, 0.1 M (Invitrogen, Karlsruhe)	5.5 µl
RNaseOUT, 40 U/ µl (Invitrogen, Karlsruhe)	2.75 µl
Superscript III RT, 200 U/ µl (Invitrogen, Karlsruhe)	2.75 µl

The RNA/ primer mixture was incubated at 65°C for 5 min and chilled on ice for 1 min. The cDNA synthesis mix was intermixed and reverse transcription was carried out as follows:

- Step 1: 25°C – 10 min
- Step 2: 42°C – 50 min
- Step 3: 70°C – 15 min
- Step 4: 4°C – 1 min

Finally RNA was degraded by addition of 2.75 µl of RNase H (Invitrogen, Karlsruhe) and incubation at 37°C for 20 min.

3.2.3.3 Quantitative real-time PCR (RT-PCR)

PCR reactions were prepared in 96 well real-time PCR plates (Eppendorf, Hamburg) in a total reaction volume of 20 µl using the Taq DNA polymerase Kit and HotStar Taq polymerase (Quiagen, Hilden). The intercalating dye SYBR[®] Green (Lonza, Basel, Switzerland) was used as fluorescent reporter in the reaction.

Mastermix (per reaction):

PCR buffer, 10x	2.0 µl
MgCl ₂ , 25 mM	1.0 µl
Q-Solution	4.0 µl
dNTPs, 10mM	0.5 µl
Forward primer, 10 µM	1.0 µl
Reverse primer, 10 µM	1.0 µl
SYBR [®] Green, 1: 2000	0.8 µl
HotStar Taq, 5 U/ µl	0.2 µl
Bidistilled water	7.5 µl
cDNA	2.0 µl

Real-time PCR plates were sealed using a heat sealing foil (Eppendorf, Hamburg) and DNA was amplified and quantified in a Mastercycler[®] ep realplex PCR machine (Eppendorf, Hamburg) according to the following protocol:

Step 1: 95°C	– 15 min (DNA denaturation)
Step 2: 95°C	– 30 s (DNA denaturation)
Step 3: 55°C	– 30 s (primer annealing)
Step 4: 72°C	– 30 s (elongation)
Step 5: 82°C	– 20 s (DNA quantification)
Step 6: 95°C	– 15 s (DNA denaturation)
Step 7: 60°C	– 15 s
Step 8: Heating to 95°C	– 20 min (melting curve determination)
Step 9: 95°C	– 15 s

Steps 2 to 5 were repeated 55 times (56 amplification cycles in total) whereupon the program continued with step 6. The amount of *Dro1* cDNA was compared to the amount of the housekeeping gene *Gapdh* and each sample was normalized on the basis of its *Gapdh* content.

3.2.4 Evaluation of gene expression at the protein level

3.2.4.1 Extraction of proteins from tissues

Tissue samples (heart, lung, liver, spleen, kidney, intestine, white adipose tissue, skeletal muscle) were frozen on dry ice and stored at -80°C until needed. Approximately 50 mg of frozen tissue samples were transferred to a 5 ml plastic tube containing 400 μl of protein extraction buffer and homogenized at 23500 rpm for 30 s. To avoid protein carryover between samples the homogenizer was rinsed with bidistilled water after each sample. The homogenate was transferred to a 1.5 ml centrifuge tube, incubated for 5 min at 95°C , cooled down on ice for 5 min, and centrifuged for 5 min at 4°C and $13.000 \times g$. The supernatant containing the proteins was transferred to a fresh 1.5 ml centrifuge tube and samples were stored at -20°C until needed.

Protein extraction buffer:

Tris, 1M, pH 7.5	2 ml
Triton X-100 (Roth, Karlsruhe)	2 ml
Laemmli buffer, 5x	20 ml
Bidistilled water	76 ml

5x Laemmli buffer:

Tris, 1M, pH 6.8	65.5 ml
Glycerol (Roth, Karlsruhe)	100.0 ml
EDTA, 0.5M, pH 8.0	2.0 ml
SDS	20.0 g
Bromphenol blue (Serva, Heidelberg)	0.1%
Bidistilled water up to	200 ml

3.2.4.2 Determination of protein concentration

To determine the protein content of the samples, a bicinchoninic acid (BCA) protein assay was performed. For generation of a standard curve, serial dilutions of a bovine serum albumin (BSA; Roth, Karlsruhe) stock solution (4 mg/ml) were prepared. 10 μl of the samples of unknown protein concentration and of the standards were added into the wells of a 96-well plate (Becton Dickinson, Heidelberg) individually and intermixed

with 200 μ l CuSO₄-BCA solution and 40 μ l 1x PBS. The reaction was incubated for 30 min at 37°C and the absorbance was measured at 562 nm in a micro-plate reader (Tecan, Männedorf, Switzerland). For generation of a standard curve, protein concentrations of standards were plotted versus their absorbance. To obtain protein concentration in the unknown samples their absorbance was applied to the standard curve.

CuSO₄-BCA solution:

CuSO ₄ solution (Sigma-Aldrich, Deisenhofen)	70 μ l
BCA (Sigma-Aldrich, Deisenhofen)	3430 μ l

3.2.4.3 SDS-Polyacrylamide gel electrophoresis (SDS-PAGE)

Protein separation was performed using the Mini Protean[®] 3 cell system (Bio-Rad, Munich). Preparation of the separating gel was accomplished in a 50 ml glass beaker under continuous agitation and poured into the space between the glass plates of the system, leaving space for the stacking gel. To ensure a plain surface the gel was covered with bidistilled water. After polymerization for 1 h the stacking gel was prepared accordingly, poured on top of the separating gel and a comb was inserted. After polymerization, the plates were implanted into the electrophoresis chamber filled with SDS-PAGE electrophoresis buffer and the comb was removed. Prior to loading, 20 μ g of each protein sample was transferred to a fresh 1.5 centrifuge tube, filled up with 1x Laemmli buffer to 30 μ l, incubated at 95°C for 5 min and chilled on ice. In some experiments 5% 2-mercaptoethanol (Merck, Darmstadt) was added to the protein samples. Samples were loaded into the wells of the gel along with a molecular weight marker (PageRuler[™] Prestained Protein Ladder, MBI Fermentas, St. Leon-Rot) and separated by electrophoresis on the stacking gel at 100 V for 15 min and on the separating gel at 140 V until the dye front run off the bottom of the gel.

Separating gel (12%):

Tris, 0.5 M, pH 8.8	2.5 ml
Acrylamide, 30% (Bio-Rad, Munich)	4.0 ml
SDS, 10%	100 µl
Ammonium persulfate, 10% (Bio-Rad, Munich)	50 µl
Temed (Bio-Rad, Munich)	5 µl
Bidistilled water	3.35 ml

Stacking gel (5%):

Tris, 0.5 M, pH 6.8	1.25 ml
Acrylamide, 30%	1.5 ml
SDS, 10%	100 µl
Ammonium persulfate, 10%	100 µl
Temed	5 µl
Bidistilled water	3.35 ml

SDS-PAGE electrophoresis buffer:

Tris	30.3 g
Glycine (Merck, Darmstadt)	144 g
SDS	10 g
Bidistilled water up to	1 l

3.2.4.4 Blotting

Transfer of the separated proteins was performed using a semidry electroblotting apparatus (Bio-Rad, Munich). A polyvinylidene difluoride (PVDF) membrane (Millipore, Billerica, USA) was cut the size of the gel and kept in methanol (Merck, Darmstadt) until needed. Two sheets of blotting paper (Bio-Rad, Munich) were soaked in 200 ml of 1x transfer buffer containing 40 ml methanol. One sheet of blotting paper was placed onto the semidry blotter and covered with the membrane. The gel was taken out of the electrophoresis apparatus, placed on top of the membrane and covered with another sheet of blotting paper. Between each step air bubbles were removed by use of a pipette. The upper electrode was put onto the blotting apparatus and blotting was carried out at 15 mA for 1 h.

10x transfer buffer:

Tris	58.2 g
Glycine	29.2 g
SDS	3.7 g
Bidistilled water up to	1 l

3.2.4.5 Detection

After blotting, the PVDF membrane was placed in a glass hybridization tube and incubated in 1x Tris buffered saline Tween20 (TBST) containing 5% instant skimmed milk powder (Roth, Karlsruhe) for 60 min, washed 2 times with 1x TBST for 5 min and treated with the primary antibody diluted in 1x TBST containing 1% milk powder for 60 min. The membrane was washed 3 times for 5 min with 1x TBST, incubated with the secondary antibody diluted 1: 10.000 in 1x TBST containing 1% milk powder for 60 min and washed 2 times with 1x TBST for 20 min. For detection, the membrane was treated with 2 ml ECL Western blotting Detection Reagent (GE Healthcare, Munich), enveloped in plastic foil and exposed to a chemiluminiscence film until the required signal strength was achieved. All incubation steps were carried out at room temperature with gentle agitation.

To remove primary and secondary antibodies the membrane was treated with Restore Western Blot Stripping Buffer (Thermo Scientific, Rockford, USA) for 10 min, washed 3 times for 1 min with bidistilled water and washed 2 times for 5 min with 1x TBST.

25x TBS:

Tris	60 g
NaCl	200 g
HCl, 12 N (Merck, Darmstadt)	7.9 ml
Bidistilled water up to	1 l
Adjusted to pH 7.6	

1x TBST:

25x TBS	40 ml
Tween [®] 20 (Sigma-Aldrich, Deisenhofen)	2 ml
Bidistilled water up to	1 l

Primary antibodies:

Mouse anti-actin antibody (MP Biomedicals, Solon, USA), diluted 1: 1000

Rabbit anti-CCDC80 antibody (Acris, Herford), diluted 1: 5000

Rabbit anti-CCDC80 antibody (Sigma-Aldrich, Deisenhofen), diluted 1: 1000

Secondary antibodies:

Donkey anti-rabbit antibody (GE Healthcare, Munich), diluted 1: 10.000

Goat anti-mouse antibody antibody (MP Biomedicals, Solon, USA), diluted 1: 10.000

3.2.5 Histological analysis**3.2.5.1 Hematoxylin and eosin (H&E) staining**

Heart, lung, liver, spleen, kidney, intestine and the cranial tip of the epididymal white adipose tissue depot were dissected, the intestine processed as described in Chapter 3.2.6.1, samples placed in a histology cassette (Medite, Burgdorf) and fixed in 4% buffered formaldehyde solution at 4°C for a minimum of 24 h. Samples were dehydrated, embedded in paraffin, and 4 µm tissue sections were cut and mounted on glass microscope slides (Menzel-Gläser, Braunschweig). After the sections dried for 3 d at room temperature they were deparaffinized in Roti[®]-Histol (Roth, Karlsruhe) for 40 min and rehydrated in a descending graded alcohol series (100% ethanol, 90% ethanol, 80% ethanol, 70% ethanol, 50% ethanol) down to bidistilled water. They were stained in hematoxylin solution according to Mayer (Sigma-Aldrich, Deisenhofen) for 2 min, rinsed under running tap water for approximately 10 min and counterstained in eosin solution (Medite, Burgdorf) for 2.5 min. Next, slices were rinsed in bidistilled water, dehydrated in an ascending graded alcohol series (50% ethanol, 70% ethanol, 80% ethanol, 90% ethanol, 100% ethanol) to Roti[®]-Histol and mounted with mounting medium (VWR International, Darmstadt) and cover glass slides. Histopathologic analysis of H&E-stained tissue sections was performed in a blinded manner by Dr. Jens Neumann, Institute of Pathology, University of Munich.

4% buffered formaldehyde solution:

Paraformaldehyde (Sigma-Aldrich, Deisenhofen)	40 g
10x PBS	100 ml
NaOH, 5 M	250 µl
Bidistilled water up to	1 l
Adjusted to pH 7.4	

3.2.5.2 Periodic acid Schiff (PAS) staining

Intestines were processed, formaldehyde fixed and paraffin embedded as described in Chapter 3.2.6.1. PAS staining was performed according to a standard protocol at the Institute of Pathology, University of Munich. The number of PAS-positive cells per total cells in the crypt-villus axis of the small intestine was counted in 20 crypts per mouse.

3.2.5.3 Elastic van Gieson (EvG) staining

Livers were formaldehyde fixed and paraffin embedded as described in Chapter 3.2.5.1. EvG staining was performed according to a standard protocol at the Institute of Pathology, University of Munich. Histopathologic examination of EvG-stained tissue sections was performed in a blinded manner by Dr. Jens Neumann, Institute of Pathology, University of Munich.

3.2.6 Immunohistochemistry (IHC)**3.2.6.1 Bromodeoxyuridine (BrdU) staining**

BrdU is a proliferation marker that is incorporated, instead of thymidine, into the newly synthesized DNA of cycling cells. To analyse cell proliferation in the intestine, mice were injected intraperitoneally with BrdU (30 mg/kg body weight; Roche, Mannheim) 1 h prior to sacrifice. Mice were killed and the intestine excised immediately. The caecum was discarded and the colon and small intestine rinsed with 1x PBS to remove fecal material. The small intestine was cut equally into 3 pieces. Each intestine section was curled up in a histology cassette and fixed in 4% buffered formaldehyde solution at 4°C for 48 h. After the samples were dehydrated and embedded in paraffin, 4 µm tissue sections were sliced and mounted on superfrost glass microscope slides (Menzel Gläser, Braunschweig). Slices were dried for 1 week at room temperature, and baked at 45°C

for 1 h to improve the adherence of the tissue to the glass microscope slides and to melt the paraffin. They were deparaffinised and rehydrated as described above (Chapter 3.2.5.1) and heat-induced epitope retrieval was performed by cooking in Target Retrieval Solution (Dako, Hamburg) at 99°C for 40 min. Cooled slices were washed 2 times in 1x TBS for 2 min, incubated in rabbit serum (PromoCell, Heidelberg) diluted 1: 10 in 1x TBS for 30 min and treated with rat anti-BrdU primary antibody (Serotec, Düsseldorf) diluted 1: 50 in 1x TBS for 1 hour. The slices were washed 2 times for 2 min in 1x TBS and incubated in 3% H₂O₂ (Roth, Karlsruhe) for 10 min. The samples were then washed 3 times in 1x TBS for 2 min and incubated in rabbit anti-rat secondary antibody (Serotec, Düsseldorf) diluted 1: 50 in 1x TBS for 30 min. They were washed again 3 times for 2 min in 1x TBS and subsequently treated with diaminobenzidine solution (Sigma-Aldrich, Deisenhofen) until the required staining strength was achieved. The staining reaction was stopped by washing in 1x TBS. Next, slices were stained in hematoxylin solution according to Mayer for 30 s, rinsed under running tap water for approximately 10 min, dehydrated to Roti[®]-Histol as described above (Chapter 3.2.5.1) and mounted with mounting medium and cover glass slides. All incubation, washing and staining steps were carried out at room temperature. To evaluate intestinal proliferation the number of BrdU-stained cells was counted in 20 crypts of the small intestine and 20 crypts of the colon per mouse.

10x TBS:

NaCl	80.0 g
Tris	30.0 g
Bidistilled water up to	1 l
Adjusted to pH 7.4	

3.2.6.2 Matrix metalloproteinase-7 (MMP-7) staining

MMP-7 staining was performed to identify Paneth cells. Intestines were processed, formaldehyde fixed and paraffin embedded as described above (Chapter 3.2.6.1) and 4 µm tissue sections were cut, mounted on superfrost microscope glass slides and dried at 37°C for 3 d. For antigen unmasking, deparaffinised sections were sub-boiled at 95°C for 40 min in 10 mM sodium citrate buffer (pH 6.0). Cooled sections were incubated in methanol containing 3% H₂O₂ for 30 min, washed 3 times for 5 min in 1x PBS, treated with 0.5% BSA dissolved in 1x PBS for 30 min and incubated overnight at 4°C in goat

anti-MMP-7 (Santa Cruz Biotechnology, Heidelberg) primary antibody diluted 1: 100 in 1x PBS. Next day sections were washed 3 times for 5 min in 1x PBS and incubated in donkey anti-goat biotinylated secondary antibody (Santa Cruz Biotechnology, Heidelberg) diluted 1: 200 in 1x PBS for 30 min. After being treated with avidin-biotin-peroxidase complexes (Vector Laboratories, Burlingame, USA) for 30 min, the sections were washed 3 times for 5 min in 1x PBS and incubated in diaminobenzidine solution for 10 min. The staining reaction was stopped by washing for 5 min in 1x PBS. Finally, the sections were washed for 5 min in bidistilled water, stained in hematoxylin solution according to Mayer for 30 s, rinsed under running tap water for approximately 10 min, dehydrated to Roti[®]-Histol as described above (Chapter 3.2.5.1) and mounted with mounting medium and cover glass slides. Incubation, washing and staining steps were performed at room temperature if not differently stated.

3.2.6.3 Cleaved caspase-3 staining

To identify apoptotic cells, cleaved caspase-3 staining was performed on intestinal tissue sections. Intestines were processed, formaldehyde fixed and paraffin embedded as described above (Chapter 3.2.6.1), and 4 µm tissue sections were cut, mounted on superfrost microscope glass slides and dried at 37°C overnight. Sections were deparaffinised in Roti[®]-Histol for 10 min, incubated in ethanol for 10 min and treated with 96% ethanol for 2 min before being transferred to methanol containing 3% H₂O₂. For antigen retrieval, slices were cooked in 1x TBS containing 0.001% Tween[®]20 in a pressure cooker. After incubation in 1x TBS containing 5% goat serum (Sigma-Aldrich, Deisenhofen), the sections were treated with avidin blocking reagent (Vector Laboratories, Burlingame, USA) for 15 min, washed in 1x TBS for 1 min, and treated with biotin blocking reagent (Vector Laboratories, Burlingame, USA) for 15 min. After being incubated with primary rabbit anti-cleaved caspase-3 antibody (Cell Signaling, Danvers, USA) diluted 1: 200 in 1x TBS, sections were washed 3 times for 5 min in 1x TBS and incubated with goat anti-rabbit secondary antibody (DAKO, Hamburg) diluted 1: 200 in 1x TBS. Sections were then treated with avidin-biotin-peroxidase complexes for 30 min, washed 2 times in 1x TBS for 5 min and incubated with diaminobenzidine solution for 5 min. Thereafter slices were processed as described above (Chapter 3.2.6.2). The number of cleaved caspase-3-positive cells was counted in 50 crypt-villus units in the small intestine and in 100 crypts in the colon per mouse.

3.2.6.4 β -catenin staining

Intestines were processed, formaldehyde fixed and paraffin embedded as described above (Chapter 3.2.6.1). Immunohistochemistry of β -catenin in the intestine was performed by the Institute of Pathology, University of Munich. β -catenin-stained intestinal sections were evaluated for the accumulation of nuclear β -catenin by 2 investigators who were blinded to the experimental groups. Within neoplastic tissue the percentage of nuclear β -catenin-positive cells was estimated.

3.2.6.5 Ki-67 staining

Intestines were processed, formaldehyde fixed and paraffin embedded as described above (Chapter 3.2.6.1). Immunohistochemistry of Ki-67 in the intestine was performed by the Institute of Pathology, University of Munich. The percentage of Ki-67-positive cells within neoplastic tissue was estimated by 2 investigators who were blinded to the experimental groups.

3.2.7 Analysis of body and organ growth

Body weight of mice was recorded using a laboratory scale (BP4100S, Sartorius, Göttingen). Nose-rump-length (NRL), defined as the distance from the tip of the nose to the base of the tail, was measured under anesthesia with the aid of a ruler. Anesthesia was induced by intraperitoneal injection of ketamine (100 mg/kg body weight, Bremer Pharma, Warburg) and xylazine (5 mg/kg body weight, Selectavet, Munich). To determine organ weight, the animals were killed, the organs (heart, lungs, liver, spleen, kidneys) immediately excised, blotted dry from blood on absorbent paper and weighted to the nearest mg with a laboratory scale (BP221S, Sartorius, Göttingen). For bilateral organs the paired weight was recorded. Carcass weight was determined after the removal of organs, fat pads, skin and head. For long bone size analysis, femora were dissected, coarsely freed from surrounding tissue, incubated in 1x PBS at 80°C for 2 h, and maintained in 1% papain (Merck, Darmstadt) at 37°C overnight. After the bones were cleaned with water and dried at 37°C overnight, their length was determined with a slide rule.

3.2.8 Analysis of adipose tissue parameters

3.2.8.1 Total body fat content

Total body fat content and lean mass were analyzed in live mice by magnetic resonance imaging (MRI) using the Minispec LF50 (Bruker, Karlsruhe). After recording their body weight, the mice were placed in a perforated plastic cylinder (Bruker, Karlsruhe), carefully restrained with the aid of a plastic plunger (Bruker, Karlsruhe) and inserted into the Minispec LF50 for a 2 min lasting measurement. Total body fat and lean mass values in percent were converted to fat in g. To guarantee accurate measurement and to reduce stress in animals, analyses did not start before the mice were 4 weeks of age.

3.2.8.2 Fat pad weight

Mice were sacrificed, and the epididymal, abdominal and subcutaneous white fat pads were excised and weighted to the nearest mg using a laboratory scale.

3.2.9 Analysis of liver triglyceride content

At necropsy the liver was resected, frozen on dry ice and stored at -80°C until needed. 50 mg of frozen tissue were transferred to a 5 ml tube containing 500 μl of 0.9% NaCl solution and homogenized at 23500 rpm for 60 s. To avoid sample carryover the tip of the homogenizer was rinsed with 0.9% NaCl for 30 s after each sample. The homogenate was centrifuged at $14.000 \times g$ for 1 min to pelletize tissue debris and the supernatant containing the triglycerides was transferred to a clean centrifuge tube. The triglyceride content of the supernatant was determined by use of the Triglyceride FS Kit (DiaSys, Holzheim). The principle of this test involves enzymatic hydrolysis of triglycerides by lipase into glycerol and free fatty acids. The glycerol produced is then measured in a series of enzymatic reactions by the formation of a quinoneimine dye. To create a standard curve for triglyceride concentration, a dilution series of the Triglyceride FS standard (200 mg triglycerides/dl; DiaSys, Holzheim) was prepared. 10 μl of the supernatant or standard were pipetted in duplicate into the wells of a 96-well plate, treated with 10 μl of 1% dioxycholic acid (Merck, Darmstadt) and incubated for 5 min at 37°C with gentle agitation. 200 μl of Triglyceride FS reagent (DiaSys, Holzheim) were added to each well, incubated for 20 min at 37°C with gentle shaking and absorbance was measured in a micro-plate reader at 495 nm against blank. A standard curve was generated by plotting absorbance of standards versus their

triglyceride concentration. Triglyceride content of samples was calculated with the aid of the standard curve.

3.2.10 Evaluation of serum parameters

3.2.10.1 Blood collection

Blood was drawn from the retro-orbital sinus with heparinized capillary tubes (Brand, Gießen) under ketamine and xylazine injection narcosis (Chapter 3.2.7) and collected in a 1.5 ml centrifugation tube. Blood samples were centrifuged at 7.000 x *g* for 10 min at 4°C to isolate serum. Serum was stored in aliquots of 50 µl at -80°C until use.

3.2.10.2 Serum free fatty acids

Free fatty acids were determined in 10 µl of serum using the Free Fatty Acid Quantification Kit (Abcam, Cambridge, United Kingdom) according to the manufacturer`s manual. The principle of the assay is the conversion of fatty acids to their CoA derivatives, which are subsequently oxidized with the concomitant generation of color.

3.2.10.3 Serum triglycerides

Serum triglycerides were measured with the Triglyceride FS Kit. For information on the principle of the test and preparation of the standard curve see above (Chapter 3.2.9). 10 µl of serum and 200 µl of Triglyceride FS reagent were intermixed in the wells of a 96-well plate in duplicate, incubated for 20 min at 37°C with gentle shaking and absorbance was measured in a micro-plate reader at 495 nm against blank. Triglyceride concentration of serum samples was calculated using a standard curve.

3.2.11 Analysis of glucose tolerance and insulin tolerance

After mice were fasted for 16 h (5 pm to 9 am), blood glucose level was measured in a drop of blood from the tail vein using a glucometer (Abbot, Ludwigshafen). Subsequently mice were injected intraperitoneally either with glucose solution (1.5 g/kg body weight; B. Braun, Melsungen) for glucose tolerance test or with insulin (0.75 U/kg body weight; B. Braun, Melsungen) for insulin tolerance test. In both assays blood glucose levels were determined 20, 40, 60 and 120 min after administration of glucose or insulin.

3.2.12 Evaluation of preadipocyte differentiation in primary cell culture

Stromal vascular (SV) cells were isolated, cultured and differentiated according to Hausman *et al.*, 2008.

3.2.12.1 Isolation of SV cells

For isolation of SV cells, inguinal fat pads of 5 mice were pooled. Mice were killed by cervical dislocation, the lower abdominal area disinfected with isopropanol and the abdominal skin incised in the mid-line. Inguinal fat pads were dissected using sterile instruments and transferred to a 10 cm Petri dish (Becton Dickinson, Heidelberg) filled with 20 ml prewarmed DMEM/F12 medium (PAA Laboratories GmbH, Pasching, Austria) containing 100 units penicillin (Sigma-Aldrich, Deisenhofen) and 0.1 mg streptomycin (Sigma-Aldrich, Deisenhofen) per ml (in the following referred to as DMEM/F12 medium). Inguinal fat pads were transferred to a sterile 100 ml glass beaker, and minced with sterile pointed scissors. After adding 10 ml of digestion buffer, the beaker content was transferred to a 100 ml Erlenmeyer flask.

Digestion buffer:

HEPES (Sigma-Aldrich, Deisenhofen)	0.1 M
NaCl	0.12 M
KCl	50 mM
D-glucose (Sigma-Aldrich, Deisenhofen)	5 mM
BSA	1.5%
Calcium chloride (Merck, Darmstadt)	1 mM
Collagenase type I (Sigma-Aldrich, Deisenhofen)	10.000 U
Dissolved in bidistilled water	

Following incubation in a rotating shaker (Infors AG, Bottmingen) for 60 min at 37°C and 115 rpm, the undigested tissue was removed by pouring the solution through a 100 µm nylon cell strainer (Becton Dickinson, Heidelberg) into a 50 ml centrifugation tube (Becton Dickinson, Heidelberg). Additional 20 ml of DMEM/F12 medium were added and the cell suspension centrifuged at 200 x g for 10 min at room temperature to pelletize SV cells. The supernatant was removed and cells resuspended in 30 ml of fresh DMEM/F12 medium containing 10% fetal bovine serum (FBS; Biochrom AG, Berlin). To remove cell clumps, the cell suspension was filtered through a 40 µm nylon cell

strainer (Becton Dickinson, Heidelberg) into a 50 ml centrifugation tube. After centrifugation at 200 x g for 10 min at room temperature, the supernatant was discarded, cells resuspended in 7.5 ml of DMEM/F12 medium containing 10% FBS and plated in 12 well cell culture plates (Becton Dickinson, Heidelberg) at a density of 4.8×10^3 cells/cm².

3.2.12.2 Maintenance and differentiation of SV cells

One day after plating, the medium was replaced with DMEM/F12 medium containing 5% FBS and exchanged every 2 d until the cells became confluent. Differentiation of preadipocytes was induced by incubating confluent cells with induction medium for 72 h.

Induction medium:

Dexamethasone (Sigma-Aldrich, Deisenhofen)	0.1 µM
IBMX (Sigma-Aldrich, Deisenhofen)	250 µM
Insulin	17 nM
Dissolved in DMEM/F12 medium containing 5% FBS	

The induction medium was exchanged for DMEM/F12 medium containing 10% FBS and 17 nM insulin. The insulin containing medium was removed after 72 h and replaced with DMEM/F12 medium containing 10% FBS. Every other day 70% of the medium was substituted with fresh DMEM/F12 medium containing 10% FBS until cells were filled with lipid droplets.

3.2.12.3 Oil red O staining

Adipocyte lipid droplets were identified by oil red O staining. The medium was removed, each well rinsed with 500 µl 1x PBS and cells fixed by addition of 1 ml 4% buffered formaldehyde solution. After 10 min the fixative was removed, cells rinsed with 60% isopropanol for 30 s and oil red O stain (0.34 mM oil red O (Sigma-Aldrich, Deisenhofen), dissolved in 60% isopropanol) applied 1 ml per well for 10 min. Cells were rinsed again with 60% isopropanol for 30 s and 500 µl 1x PBS were added to each well. Oil red O staining was accomplished according to Ramírez-Zacarías *et al.*, 1992.

3.2.12.4 Differentiation scoring

To evaluate differentiation properties of SV cells the number and size of oil red O-stained lipid droplets were counted by computer image analysis. Oil red O-stained wells were viewed under a light microscope (Olympus, Hamburg) at 100x magnification and areas showing a high density of lipid droplets were photographed with a digital camera (Olympus, Hamburg). Images were processed with GIMP Portable (Freeware, Copyright by John T. Haller) so that all colors, except red, were removed. The following commands were used for the conversion: Color saturation (All: -100, Red: +100), Transparency, New layer (Layer fill type: White), Lower layer. An accurate conversion was ensured by comparing the converted images to the original images. Photos were converted into black and white and the quantity and mean area of black particles were analyzed with Image J (Freeware) using the following commands: Image (8-bit), Threshold (Default, Red), Analyze Particles (Size: 10-Infinity; Circularity: 0.00-1.00). To minimize incorrectness caused by staining artifacts values less than 10^2 pixel were excluded from analysis. An example of digital image processing is shown in Fig. 3.2.

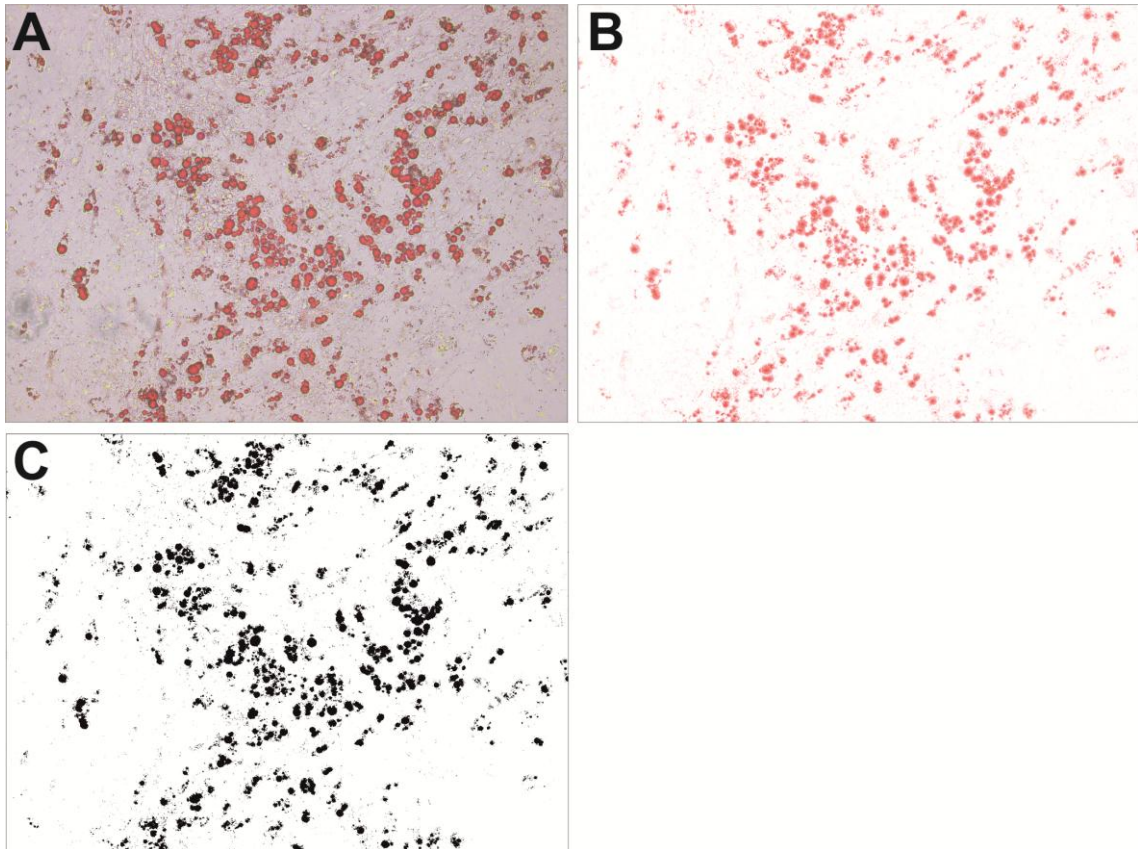


Fig. 3.2 Oil red O-stained differentiated SV cells were photographed at 100x magnification (A). All colors except red were erased by digital image processing (B) and photos converted into black and white (C). The number and mean area of black particles were counted by computer image analysis.

3.2.13 Analysis of aberrant crypt foci (ACF)

3.2.13.1 Tissue collection

Mice were sacrificed at the age of 5 and 10 weeks, respectively. The colon was excised and rinsed with 1x PBS to remove fecal content. After the colon was cut into 2 equal sections, each segment was put on a Super Frost microscope glass slide, opened longitudinally and laid open. A piece of filter paper cut the size of the glass slide was placed on the top and attached by the aid of paper clips. Samples were fixed in 4% buffered formaldehyde solution at 4°C for a minimum of 24 h.

3.2.13.2 Methylene blue staining

The formaldehyde-fixed intestinal sections on the microscope glass slides were washed 2 times for 10 min in 1x PBS. Filter paper and paper clips were removed and samples stained in 0.1% methylene blue staining solution (Sigma-Aldrich, Deisenhofen) for

3 min. The colon was mounted with liquid gelatin (Merck, Darmstadt) and a cover glass slide, and the samples were stored at 4°C until the gelatin solidified. Methylene blue staining was accomplished according to Bird, 1987.

3.2.13.3 ACF scoring

Whole-mount colonic samples were placed under a dissecting microscope (Zeiss, Jena) and examined at 25x magnification. The criteria used to identify ACF were increased crypt size (in comparison to most crypts in the field), round or elongated luminal openings and a thickened layer of epithelial cells that stain more intensely with methylene blue (Bird, 1987; Fenoglio-Preiser and Noffsinger, 1999; Boivin *et al.*, 2003; Gupta *et al.*, 2008).

3.2.14 Analysis of weight and length of the intestine

Mice were sacrificed and the intestine excised immediately. The caecum was discarded and the small intestine and colon rinsed with 1x PBS to remove fecal material. Small intestine and colon were weighted to the nearest mg with a laboratory scale and their length was measured with a ruler.

3.2.15 Analysis of intestinal neoplastic lesions

3.2.15.1 Tissue collection

Mice were killed, the intestine dissected and transferred to a plastic dish containing 1x PBS. The caecum was discarded and the colon and small intestine rinsed with 1x PBS to remove fecal material. The small intestine was cut into 3 equal segments and each intestinal section was placed on a piece of filter paper, opened longitudinally, laid open and fixed in 4% buffered formaldehyde solution at 4°C for a minimum of 24 h.

3.2.15.2 Tumor scoring

Formaldehyde-fixed intestinal sections were placed under running water for 10 min to remove excess formaldehyde. The intestine was detached from the filter paper and tumor number and their maximum diameter were determined under a dissecting microscope at 10x magnification. Depending on their size, tumors of the small intestine were classified into the categories “ ≤ 2 mm” and “ > 2.5 mm”. Because of uncertainty about the precise anatomic demarcation, the colon and rectum were scored as “colon”.

A quantity of small intestinal lesions and all colonic tumors sized > 2 mm in diameter were resected including adjacent normal tissue, dehydrated and embedded in paraffin. 4 µm tissue sections were cut in parallel with the mucosal surface, mounted on glass microscope slides and stained with H&E. Histopathologic analysis of neoplastic lesions was performed in a blinded manner by Dr. Jens Neumann, Institute of Pathology, University of Munich, using standard criteria for the classification of human adenomas of the colon and the assessment of the degree of dysplasia. The diagnosis intramucosal adenocarcinoma was made for lesions with high grade dysplasia/IEN in combination with focal invasion of the lamina propria mucosae. Adenocarcinomas invading through the lamina muscularis mucosae into the tela submucosa were termed invasive adenocarcinoma.

3.2.16 Statistical analysis

All data are displayed as means ± standard deviation. All data were analyzed for normal distribution using Kolmogorov-Smirnov test with Dallal-Wilkinson-Lilliefors P value (GraphPad Prism version 4.00 for Windows, GraphPad software, San Diego, USA). To analyze significance of differences, two-tailed Student's t-test (normally distributed data) or two-tailed Mann Whitney U test (not normally distributed data) were performed (GraphPad Prism version 4.00 for Windows). Body weight gain, total body fat gain and lean mass gain were evaluated by 2-factorial ANOVA (GraphPad Prism version 4.00 for Windows). P values < 0.05 were considered to be statistically significant.

3.2.17 Primer sequences

Sequences of the primers used in the experiments are the following:

<u>Name</u>	<u>Sequence</u>
β-actinFW	5'-GGCATCGTGATGGACTCC-3'
β-actinRV	5'-GTCGGAAGGTGGACAGGG-3'
Apc33	5'-GCCATCCCTTCACGTTAG-3'
Apc34	5'-TTCCACTTTGGCATAAAGGC-3'
Apc758	5'-TTCTGAGAAAGACAGAAGTTA-3'
Cre1	5'-AATCGCCATCTTCCAGCAGG-3'

<u>Name</u>	<u>Sequence</u>
Cre2	5'-GATCGCTGCCAGGATATACG-3'
Dro3'end#1	5'-GCA AAG CTC TAG ATA AGC CAG-3'
Dro3'end#2	5'-ACT CCT GTT CAT AAT GGC CAG-3'
Dro1homo1	5'-TTCTTTAACTATCTCCTGCCC-3'
Dro1homo2	5'-CATCATTGTATTATCCACTTGG-3'
Dro1rec	5'-ACGTGTCTCTGAGTTTCACAAC-3'
mDro1FW	5'-CTTCCTCCTGCTCCAGTCAC-3'
mDro2RV	5'-CTGGATAGGCAGTGGTGGTT-3'
mGapdhFW	5'-TCATCAACGGGAAGCCCATCAC-3'
mGapdhRV	5'-AGACTCCACGACATACTCAGCACCG-3'
Mom1#1	5'-GTC-CAA-GGG-AAC-ATT-GCG-3'
Mom1#2	5'-AGA-ACA-GGT-GAT-TTG-GCC-C-3'

3.2.18 Materials

3.2.18.1 Machines

Agarose gel electrophoresis chamber	MWG-Biotech, Ebersberg
Analytical balance	Sartorius, Göttingen
Benchtop 96 tube working rack	Stratagene, La Jolla, USA
Blunt forceps	Aesculap, Tuttlingen
Digital camera	Olympus, Hamburg
Dissecting microscope	Zeiss, Jena
Fine scissors	Aesculap, Tuttlingen
Gel documentation system	Intas, Göttingen
GIMP Portable	Freeware, Copyright by John T. Haller
Glucometer Precision	Abbott, Ludwigshafen
GraphPad Prism version 4.00 for Windows	GraphPad software, San Diego, USA
Heating plate with magnetic stirrer	IKA process Equipment, Staufen
Homogenizer	ART Labortechnik, Müllheim
Hybridization oven	Saur, Reutlingen
Hybridization tube	Bachofer, Reutlingen
Image J	Freeware
Incubator	Heraeus, Munich

Laboratory scale, BP221S	Sartorius, Göttingen
Laboratory scale, BP4100S	Sartorius, Göttingen
Light microscope	Olympus, Hamburg
Mastercycler [®] ep realplex PCR machine	Eppendorf, Hamburg
MicroPlate reader	Tecan, Männedorf, Switzerland
Microwave	Siemens, Munich
Mini Protean [®] 3 cell system	Bio-Rad, Munich
Minispec LF50	Bruker, Karlsruhe
Mouse restrainer	Bruker, Karlsruhe
Pointed scissors	Aesculap, Tuttlingen
Rotating shaker	Infors AG, Bottmingen
Semidry electroblotting apparatus	Bio-Rad, Munich
Spectrophotometer	Beckman, Palo Alto, USA
Table centrifuge (5417R)	Eppendorf, Hamburg
Thermal cycler	Biometra, Göttingen
Thermomixer 5436	Eppendorf, Hamburg
UV-Crosslinker	Biometra, Göttingen

3.2.18.2 Consumables

Blotting paper	Bio-Rad, Munich
Cannulas	B.Braun, Melsungen
Centrifugation tube (15 ml, 50 ml)	Becton Dickinson, Heidelberg
Centrifuge tube (0.5 ml, 1.5 ml, 2.0 ml)	Eppendorf, Hamburg
Chemoilluminescence film	GE Healthcare, Munich
Cover glass slides	VWR International, Darmstadt
Disposable syringes (2, 5, 10, 20 ml)	Codan Medical ApS, Roedby, Denmark
Filter paper	GE Healthcare, Munich
Glass microscope slides	Menzel-Gläser, Braunschweig
Heat sealing foil	Eppendorf, Hamburg
Heparinized capillary tubes	Brand, Gießen
High fat diet	ssniff, Soest
Histology cassettes	Medite, Burgdorf
Multi-well cell culture plates	Becton Dickinson, Heidelberg

Nylon cell strainer (40 μ m, 100 μ m)	Becton Dickinson, Heidelberg
Nylon membrane	Pall Corporation, Pensacola, USA
PCR-reaction-tubes	G. Kisker GbR, Steinfurt
Petri dishes (diameter 10 cm)	Becton Dickinson, Heidelberg
Plastic tubes (5 ml)	Greiner Bio-One, Frickenhausen
PVDF membrane	Millipore, Billerica, USA
Real-time PCR plates (96 well)	Eppendorf, Hamburg
Standard chow	ssniff, Soest
Super Frost microscope glass slides	Menzel Gläser, Braunschweig

3.2.18.3 Chemicals

2-mercaptoethanol	Merck, Darmstadt
Acrylamide, 30%	Bio-Rad, Munich
Agarose	Invitrogen, Karlsruhe
Ammonium persulfate, 10%	Bio-Rad, Munich
Anti-DIG-AP Fab fragments	Roche, Mannheim
Avidin blocking reagent	Vector Laboratories, Burlingame, USA
Avidin-biotin-peroxidase complexes	Vector Laboratories, Burlingame, USA
<i>Bam</i> HI buffer	MBI Fermentas, St. Leon-Rot
<i>Bam</i> HI restriction enzyme	MBI Fermentas, St. Leon-Rot
Bichinonic acid	Sigma-Aldrich, Deisenhofen
Biotin blocking reagent	Vector Laboratories, Burlingame, USA
Blocking solution	Roche, Mannheim
BrdU	Roche, Mannheim
Bromphenol blue	Serva, Heidelberg
BSA	Roth, Karlsruhe
Buffer <i>Pst</i> I	MBI Fermentas, St. Leon-Rot
Calcium chloride	Merck, Darmstadt
Chloroform	Merck, Darmstadt
Collagenase type I	Sigma-Aldrich, Deisenhofen
CSPD ready-to-use detection solution	Roche, Mannheim

CuSO ₄	Sigma-Aldrich, Deisenhofen
DEPC	Sigma-Aldrich, Deisenhofen
D-Glucose	Sigma-Aldrich, Deisenhofen
Diaminobenzidine	Sigma-Aldrich, Deisenhofen
Diethylpyrocarbonate	Sigma-Aldrich, Deisenhofen
DIG Block and Wash Buffer Set	Roche, Mannheim
DIG Easy Hyb buffer	Roche, Mannheim
DIG Probe Synthesis kit	Roche, Mannheim
DMEM/F12 cell culture medium	PAA Laboratories GmbH, Pasching, Austria
DNA Rehydration Solution	Promega, Mannheim
DNase I Amp Grade, 1U/ µl	Invitrogen, Karlsruhe.
DNase I reaction buffer, 10x	Invitrogen, Karlsruhe
DNase I, Amplification Grade	Invitrogen, Karlsruhe
dNTPs (dATP, dTTP, dCTP, dGTP)	MBI Fermentas, St. Leon-Rot
Donkey anti-goat biotinylated antibody	Santa Cruz Biotechnology, Heidelberg
DTT, 0.1 M	Invitrogen, Karlsruhe
ECL Western blotting detection reagent	GE Healthcare, Munich
EDTA solution, 25 mM	Invitrogen, Karlsruhe
EDTA	VWR International, Darmstadt
Enzyme mix	Roche, Mannheim
Eosin solution	Medite, Burgdorf
Ethanol	Merck, Darmstadt
Ethidium bromide	Roth, Karlsruhe
FBS	Biochrom AG
Free Fatty Acid Quantification Kit	Abcam, Cambridge, United Kingdom
Gelatin	Merck, Darmstadt
Glacial acetic acid	Roth, Karlsruhe
Glucose solution	B. Braun, Melsungen
Glycerol	Roth, Karlsruhe
Glycine	Merck, Darmstadt
Goat anti-MMP-7 antibody	Santa Cruz Biotechnology, Heidelberg

Goat anti-mouse antibody antibody	MP Biomedicals, Solon, USA
Goat serum	Sigma-Aldrich, Deisenhofen
Goat-anti-rabbit antibody	DAKO, Hamburg
H ₂ O ₂	Roth, Karlsruhe
HCl	Merck, Darmstadt)
Hematoxylin solution according to Mayer	Sigma-Aldrich, Deisenhofen
HEPES	Sigma-Aldrich, Deisenhofen
Hot-start Taq, 5 U/ μ l	Quiagen, Hilden
IBMX	Sigma-Aldrich, Deisenhofen
Isopropanol	Merck, Darmstadt
KCl	Roth, Karlsruhe
Ketamine	Bremer Pharma, Warburg
KH ₂ PO ₄	Merck, Darmstadt
Loading dye (6x)	MBI Fermentas, St. Leon-Rot
Methanol	Merck, Darmstadt
Methylene Blue	Sigma-Aldrich, Deisenhofen
MgCl ₂ , 25 mM	Invitrogen, Karlsruhe
MgCl ₂ , 25mM	Qiagen, Hilden
Milk powder	Roth, Karlsruhe
Molecular weight marker	MBI Fermentas, St. Leon-Rot
Mounting medium	VWR International, Darmstadt
Mouse anti-actin antibody	MP Biomedicals, Solon, USA
Na ₂ HPO ₄	Merck, Darmstadt
NaCl	Roth, Karlsruhe
NaOH	Roth, Karlsruhe
Nuclei Lysis Solution	Promega, Mannheim
Oil red O	Sigma-Aldrich, Deisenhofen
PageRuler TM Prestained Protein Ladder SM0671	MBI Fermentas, St. Leon-Rot
Papain	Merck, Darmstadt
Paraformaldehyde	Sigma-Aldrich, Deisenhofen
PCR buffer with MgCl ₂ , 10x	Roche, Mannheim
PCR buffer, 10x	Qiagen, Hilden
PCR DIG Probe Synthesis mix	Roche, Mannheim
Penicillin	Sigma-Aldrich, Deisenhofen

Protein Precipitation Solution	Promega, Mannheim
Proteinase K	Roche, Mannheim
<i>Pst</i> I restriction enzyme	MBI Fermentas, St. Leon-Rot
pUC mix molecular weight marker	MBI Fermentas, St. Leon-Rot
Q-Solution	Qiagen, Hilden
Rabbit anti-CCDC80 antibody	Acris, Herford
Rabbit anti-CCDC80 antibody	Sigma-Aldrich, Deisenhofen
Rabbit anti-cleaved caspase-3 antibody	Cell Signaling, Danvers, USA
Rabbit anti-rat antibody	Serotec, Düsseldorf
Rabbit serum	PromoCell, Heidelberg
Random hexamer primer	Invitrogen, Karlsruhe
Rat anti BrdU primary antibody	Serotec, Düsseldorf
Restore Western Blot Stripping Buffer	Thermo Scientific, Rockford, USA
RNase	Roche, Mannheim
RNase H	Invitrogen, Karlsruhe
RNaseOUT, 40 U/ μ l	Invitrogen, Karlsruhe
RNeasy Mini kit	Quiagen, Hilden
Roti [®] -Histol	Roth, Karlsruhe
RT buffer, 10x	Invitrogen, Karlsruhe
SDS	Merck, Darmstadt
Sodium citrate	Merck, Darmstadt
Spermidine (0.1 M)	Sigma-Aldrich, Deisenhofen
Streptomycin	Sigma-Aldrich, Deisenhofen
SuperScript First Strand cDNA Synthesis	Invitrogen, Karlsruhe
Superscript III RT, 200 U/ μ l	Invitrogen, Karlsruhe
SYBR [®] Green	Lonza, Basel, Switzerland
Taq DNA polymeras Kit	Quiagen, Hilden
Taq Polymerase, 5U/ μ l	Quiagen, Hilden
Target Retrieval Solution	Dako, Hamburg
Temed	Bio-Rad, Munich
Triglyceride FS Kit	DiaSys, Holzheim
Triglyceride FS reagent	DiaSys, Holzheim
Triglyceride FS standard,200 mg/dl	DiaSys, Holzheim
Tris	Roth, Karlsruhe

Tris-HCl	Roth, Karlsruhe
Triton X-100	Roth, Karlsruhe
Trizol	Invitrogen, Karlsruhe
Tween [®] 20	Sigma-Aldrich, Deisenhofen
Washing buffer	Roche, Mannheim

3.2.18.4 Drugs

Dexamethasone	Sigma-Aldrich, Deisenhofen
Insulin rapid	B. Braun, Melsungen
Histoacryl [®] liquid skin glue	B. Braun, Melsungen
Xylazine	Selectavet, Munich

4. Results

4.1 Generation of $Dro1^{-/-}$ mice

4.1.1 Establishment of $Dro1^{-/-}$ mice

One of the embryonic E14 stem cell clones identified for correct construct integration into the *Dro1* allele was injected into blastocysts from C57BL/6N mice. Transplantation of blastocysts into the uteri of pseudopregnant foster mothers resulted in the birth of 14 mice of which 8 were identified as being chimeric. Crossing of chimeras into the C57BL/6N background and screening of the progeny by PCR identified 3 animals to transmit a loxP-flanked *Dro1* allele through the germ-line. A $Dro1^{-/-}$ line was established by intercrossing mice carrying loxP-flanked *Dro1* alleles homozygously to mice expressing Cre-recombinase under control of the CMV promoter. $Dro1^{-/-}$ mice were viable and fertile, showed no increased morbidity or mortality, and litters from $Dro1^{-/-}$ parents were similar in number of progeny (Fig. 4.1A) and gender distribution (Fig. 4.1B) as compared to litters from control mice. Genotyping was performed by PCR analysis from genomic tail tip DNA using primers Dro1homo1 and Dro1homo2 to detect the wildtype and floxed *Dro1* locus and primers Dro1homo1 and Dro1rec to detect the deleted *Dro1* locus (Fig. 4.2). Primers Cre1 and Cre2 were employed to identify Cre transgenic mice (Fig. 4.2).

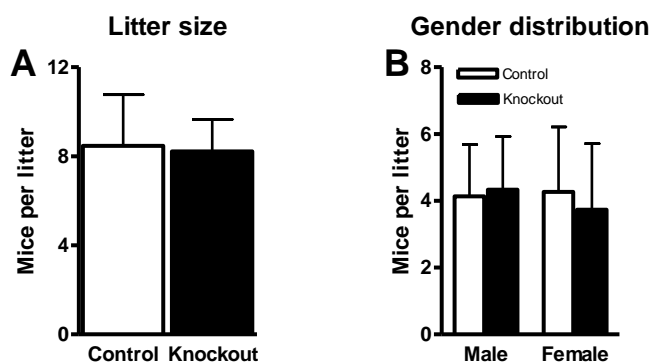


Fig. 4.1 Litter size (A) and gender distribution (B) in litters from $Dro1^{-/-}$ (knockout) parents (n=18 litters) and control animals (n=15 litters).

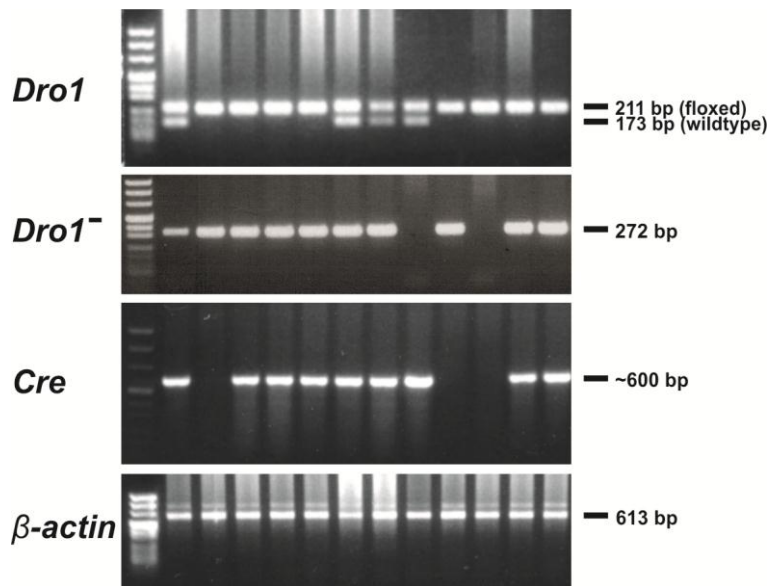


Fig. 4.2 PCR analysis of the *Dro1*, *Cre* and β -actin locus. Primers Dro1homo1 and Dro1homo2 were derived from sequences upstream of exon 2 and on exon 2 resulting in a 173 bp fragment for the wildtype and a 211 bp fragment for the floxed *Dro1* locus. To detect the deleted *Dro1* locus primers Dro1homo1 and Dro1rec were derived from sequences upstream and downstream of exon 2, resulting in a 272 bp product for the deleted locus. Primers Cre1 and Cre2 were employed to identify Cre transgenic mice. PCR for the housekeeping gene β -actin was used as loading control.

4.1.2 Analysis of genomic recombination

To verify Cre-recombinase-mediated deletion of *Dro1*, Southern blot analysis with liver genomic DNA from 8-week-old $Dro1^{fl/fl}$, $Dro1^{-/-}$ and wildtype mice was performed. As expected, digest with *PstI* resulted in restriction fragments of 7.6 kb (genomic locus), 7.0 kb (floxed locus), and 6.4 kb (deleted locus) (Fig. 4.3B). *PstI* restriction sites and calculated restriction fragment sizes are displayed in Fig. 4.3A. Deletion of exon 2 on the *Dro1* gene was also confirmed by PCR analysis from genomic tail tip DNA using primers Dro1homo1 and Dro1rec. Primers were derived from sequences upstream and downstream of exon 2, resulting in a 272 bp product for the deleted locus (Fig. 4.2).

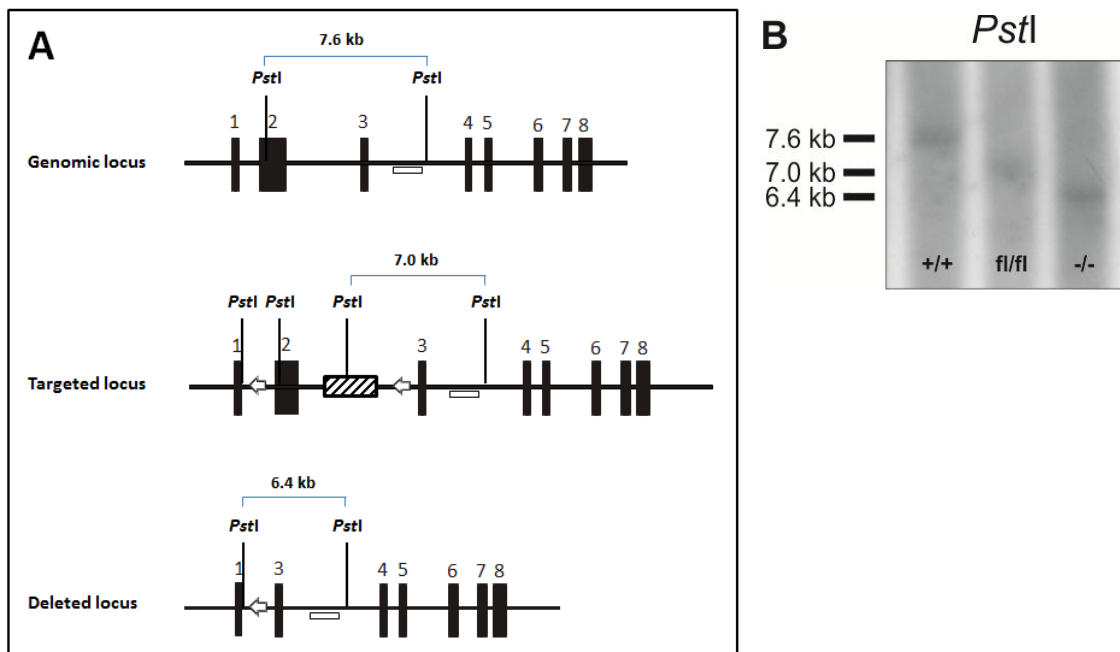


Fig. 4.3 (A) Schematic representation of the strategy employed for Southern blot analysis of the *Dro1* locus. *PstI* restriction sites, the probe binding site and expected restriction fragment sizes are indicated. Black boxes: Exons; White box: Probe binding site; Shaded box: PGK-neo; White arrows: loxP sequences. (B) Southern blot analysis of genomic liver DNA digested with *PstI* from wildtype (+/+), *Dro1*^{fl/fl} (fl/fl) and *Dro1*^{-/-} (-/-) mice.

4.1.3 Expression analysis

To investigate *Dro1* expression in *Dro1*^{-/-} mice RNA was extracted from liver, heart, muscle, white adipose tissue, brown adipose tissue, small intestinal epithelium and colon epithelium of *Dro1*^{-/-} and control animals at 4 month of age (n=3/ group). Quantitative RT-PCR analysis from cDNA using primers mDro1#1 and mDro1#2 failed to detect any significant *Dro1* expression in tissues of *Dro1*^{-/-} mice, confirming the genetic deletion of *Dro1* (Fig. 4.4A). Moreover, PCR analysis from cDNA using primers Dro1homo1 and Dro1homo2 detected a 211 bp fragment in several tissues of control (*Dro1*^{fl/fl}) animals that is absent in *Dro1*^{-/-} mice (Fig. 4.4B).

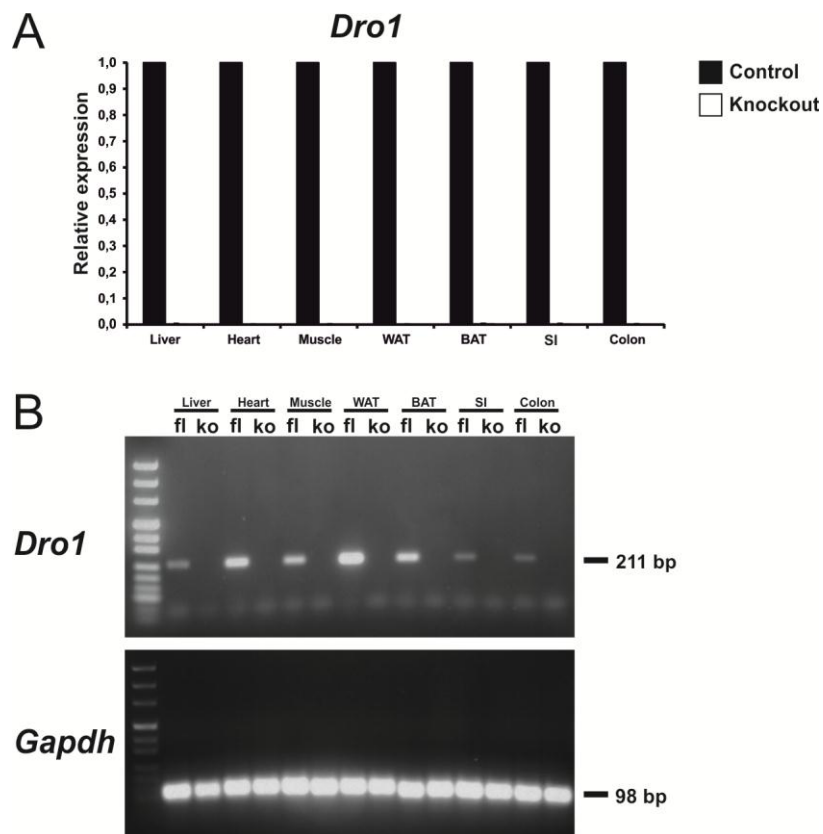


Fig. 4.4 (A) *Dro1* expression was evaluated by quantitative RT-PCR analysis from cDNA in various tissues of *Dro1*^{-/-} and control animals (n=3/ group). Shown is one representative data set (n=1/ group, analyses done in duplicates) and *Dro1* expression is presented relative to controls. Primers mDro1#1 and mDro1#2 were derived from sequences on exon 2. WAT: White adipose tissue; BAT: Brown adipose tissue; SI: Small intestine. (B) Gel electrophoresis of *Dro1* PCR products using primers Dro1homo1 and Dro1homo2 from cDNA detected a 211 bp fragment in several tissues of control (*Dro1*^{fl/fl}) animals that is absent in *Dro1*^{-/-} mice. PCR of *Gapdh* demonstrates that equal amounts of cDNA were employed.

4.1.4 Protein analysis

For further investigation of *Dro1* expression, Western blot analysis of heart, liver, muscle, white adipose tissue and intestinal epithelium from 4-month-old *Dro1*^{-/-} and control mice was performed. It was not possible to detect the mouse DRO1 protein using antibodies raised against human DRO1, indicating antigenic differences between mouse and human DRO1 (data not shown).

4.2 Effects of *Dro1* loss on intestinal tumor formation

DRO1 has been identified in *in vitro* studies as a putative tumor suppressor gene with particular relevance for colorectal carcinogenesis (Bommer *et al.*, 2005). In the following the effect of *Dro1* deficiency on intestinal epithelium homeostasis and intestinal tumor formation was investigated *in vivo*.

4.2.1 Anatomy and histology of the intestine

4.2.1.1 Weight and length of the intestine

To detect changes in intestinal growth, *Dro1*^{-/-} and control mice (n=3/ group) were sacrificed at 2.5 months of age and both the small intestine and colon were weighted and measured. Intestinal length was similar in *Dro1*^{-/-} and control mice and no significant differences in wet weight were observed (Table 4.1).

Table 4.1 Mean intestinal length and wet weight of the small intestine and colon in *Dro1*^{-/-} (knockout) and control mice at the age of 2.5 months (n=3/ group). Values are presented as means and corresponding standard deviations are presented in brackets.

Genotype	Control	Knockout
<u>Length (cm)</u>		
Small intestine	45.6 (2.3)	46.1 (3.6)
Colon	9.9 (0.4)	9.9 (0.1)
<u>Wet weight (g)</u>		
Small intestine	1.17 (0.11)	1.27 (0.25)
Colon	0.29 (0.03)	0.28 (0.01)

4.2.1.2 Intestinal epithelium

Studies in colorectal cancer cell lines suggested *DRO1* to be involved in detachment-induced apoptosis (Bommer *et al.*, 2005), a phenomenon essential for the maintenance of the intestinal epithelium (Grossmann *et al.*, 2002). To determine the consequences of *Dro1* loss on the architecture of the intestinal epithelium, well oriented histological sections of intestinal rolls of 16-week-old *Dro1*^{-/-} and control mice were investigated for pathologic changes. Microscopic analysis of H&E-stained histological sections showed no changes in the intestinal epithelium architecture in *Dro1*^{-/-} mice (n=3; Fig. 4.5A). Evaluation of PAS-stained histological sections of the intestine (n=2/ group) revealed a normal distribution of mucus-producing goblet cells (Fig. 4.5A). The ratio of PAS-positive cells per total cells in the crypt-villus axis of the small intestine, counted in 20 crypts per mouse, was unchanged in *Dro1*^{-/-} mice as compared to controls (n=2/ group; Fig. 4.5C). Loss of *Dro1* had no influence on the positioning of Paneth cells at the bottom of the small intestinal crypts as demonstrated by MMP-7 staining (n=2/ group; Fig. 4.5B). To evaluate intestinal cell proliferation, 16-week-old *Dro1*^{-/-} and control mice (n=3 /group) were subjected to a single intraperitoneal injection of BrdU 1 h before sacrificed. Immunohistochemical detection of BrdU-labeled cells failed to demonstrate an abnormal proliferation rate in the small intestine and colon of *Dro1*^{-/-} mice, as the mean number of BrdU-positive cells, counted in 20 crypts per mouse and intestinal segment, was not significantly different from control mice (Fig. 4.6). Moreover, the positioning of BrdU-positive cells in the crypt was similar in *Dro1*^{-/-} and control mice (Fig. 4.6). As demonstrated by cleaved caspase-3 staining, no significant differences in the mean number of apoptotic cells in the intestinal epithelium of the small intestine (counted in 50 crypt-villus units per mouse) and colon (counted in 100 crypts per mouse) were recorded between control and *Dro1*^{-/-} mice (n=3/ group; Fig. 4.6).

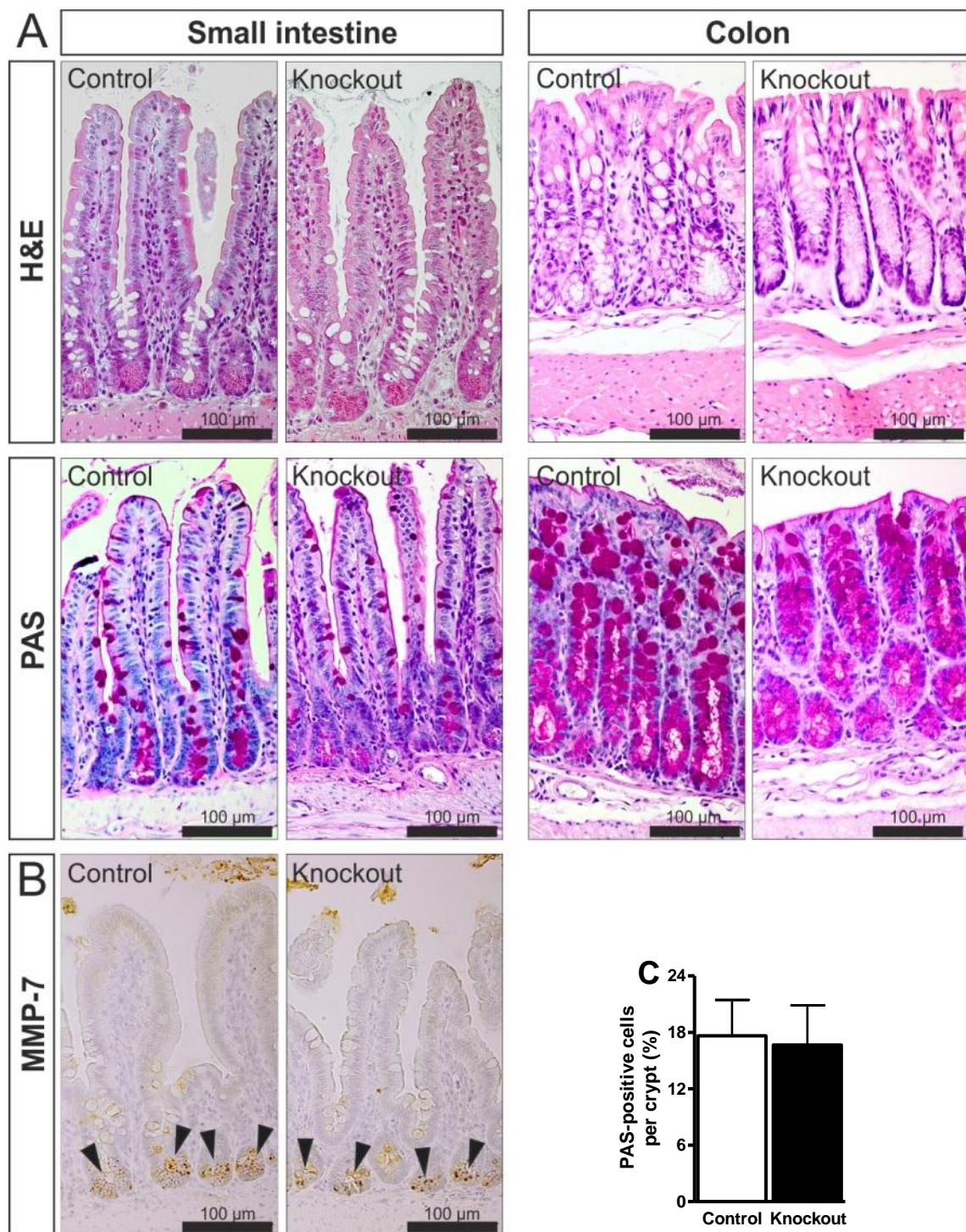


Fig. 4.5 (A) Representative H&E- and PAS-stained intestinal sections from small intestine and colon of 16-week-old $Dro1^{-/-}$ (knockout) and control mice. (B) Immunohistochemical detection of MMP-7 in the small intestine of 16-week-old $Dro1^{-/-}$ (knockout) and control mice. Black arrowheads indicate localization of MMP-7 positive cells. (C) Ratio of PAS-positive cells per total cells in the crypt-villus axis of the small intestine in 16-week-old $Dro1^{-/-}$ (knockout) and control mice, counted in 20 crypts per mouse (n=2/ group).

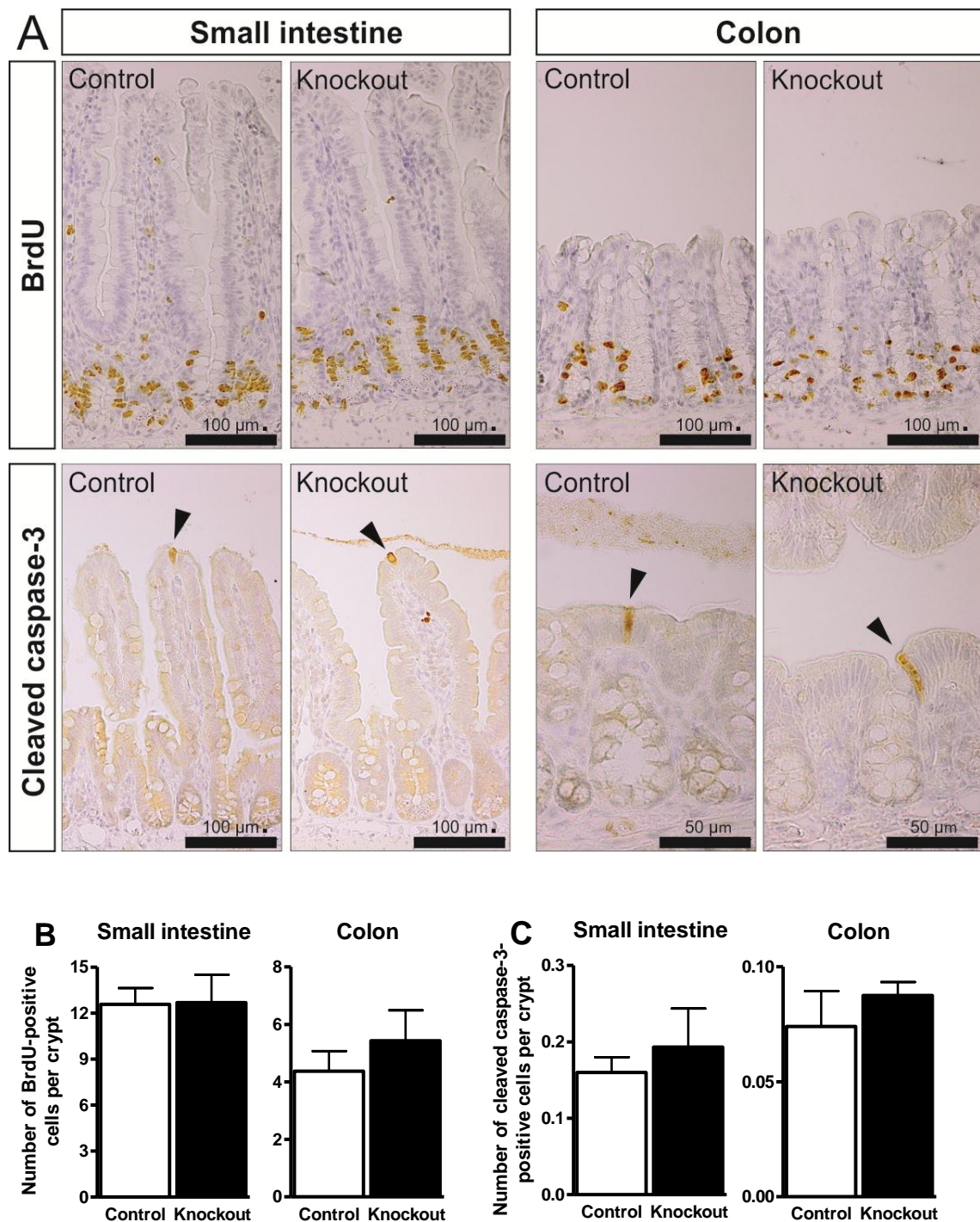


Fig. 4.6 Immunohistochemical detection of BrdU and cleaved caspase-3 in the small intestine and colon of 16-week-old $Dro1^{-/-}$ (knockout) and control mice. (B) Mean number of BrdU-positive cells, counted in 20 crypts per mouse and intestinal segment, in the small intestine and colon of $Dro1^{-/-}$ and control mice ($n=3/$ group). (C) Mean number of cleaved caspase-3-positive cells in the small intestine and colon of $Dro1^{-/-}$ and control mice, counted in 50 crypt-villus units in the small intestinal and 100 crypts in the colon per mouse ($n=3/$ group).

4.2.2 Spontaneous intestinal tumor formation

DRO1 was postulated to be a putative tumor suppressor gene (Bommer *et al.*, 2005). Since loss-of-function mutations in tumor suppressor genes are a key aspect of colorectal carcinogenesis (Fearon and Vogelstein, 1990; Arnold *et al.*, 2005; Fearon, 2011), we investigated whether loss of *Dro1* initiates intestinal neoplasia. *Dro1*^{-/-} (n=13) and control mice (n=16) of both genders were killed at the age of 18 months and the intestines were examined for visible polyps under a dissecting microscope. Independently of the *Dro1* status no intestinal tumors were observed.

4.2.3 Intestinal tumor formation in *Apc*^{+/*Min*} mice

Since *Dro1*^{-/-} mice showed no spontaneous tumor formation in the intestinal tract, we assumed that loss of *Dro1* alone is not sufficient to initiate intestinal tumorigenesis. Therefore, *Dro1*^{-/-} mice were introduced into the *Apc*^{+/*Min*} background, a widely used intestinal tumor mouse model (Moser *et al.*, 1990), to investigate the impact of *Dro1* deficiency in mice already predisposed to tumor formation. *Apc*^{+/*Min*} mice were genotyped by PCR analysis from genomic tail tip DNA using primers *Apc*33, *Apc*34 and *Apc*758 (Fig. 4.7).

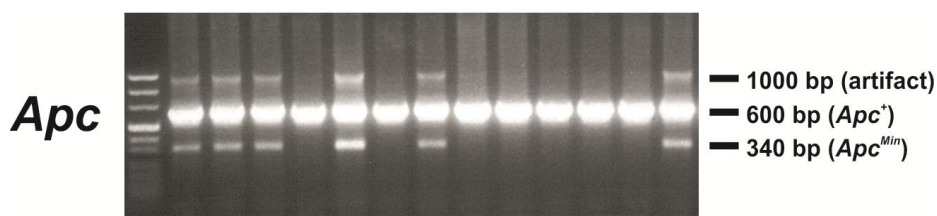


Fig. 4.7 Detection of the *Apc*⁺ and *Apc*^{Min} allele by PCR analysis.

4.2.3.1 Morbidity and mortality

Mice on the $Apc^{+/Min}$ background were surveyed daily for symptoms of illness and sacrificed when moribund. $Dro1^{-/-};Apc^{+/Min}$ mice exhibited significantly reduced survival when compared to $Apc^{+/Min}$ controls ($P=0.0004$; Fig. 4.8). Whereas compound mutant mice were moribund at an average age of 92 d, $Apc^{+/Min}$ control animals survived up to an average age of 142 d. Independently of the *Dro1* status, morbidity was hallmarked by body weight loss, hypothermia, bloody faeces, severe anemia, intestinal prolapse, and lethargy. Necropsy showed that severe symptoms of distress were most probably due to intestinal obstruction by tumor and intestinal hemorrhage.

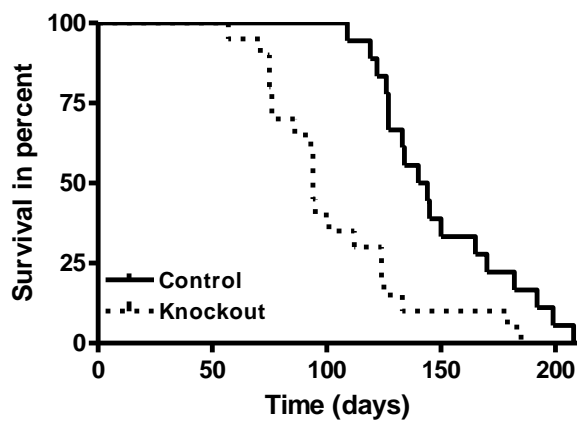


Fig. 4.8 Kaplan-Meier survival curve for $Dro1^{-/-};Apc^{+/Min}$ (knockout; $n=20$) and $Apc^{+/Min}$ control mice (control; $n=18$).

4.2.3.2 Intestinal tumor number and size

To investigate a possible effect of *Dro1* deficiency on tumor formation in $Apc^{+/Min}$ mice, the intestines of $Dro1^{-/-};Apc^{+/Min}$ and $Apc^{+/Min}$ control mice were examined under a dissecting microscope for tumor number, size and localization at different ages. Because of uncertainty about the precise anatomic demarcation, the colon and rectum were scored as “colon”. Tumors of the caecum were not investigated in the present study.

Moribund $Dro1^{-/-};Apc^{+/Min}$ (n=14) as well as $Apc^{+/Min}$ control mice (n=19) developed a multitude of tumors throughout the entire small intestine. Average small intestinal tumor multiplicity was similar in both groups (Fig. 4.9A). Evaluation of mean tumor frequency between different sites of the small intestine showed that the vast majority of small intestinal polyps localized to the middle and distal segment regardless of the *Dro1* status (Fig 4.9B). Likewise, no differences in small intestinal tumor size distribution were recorded (Table 4.2).

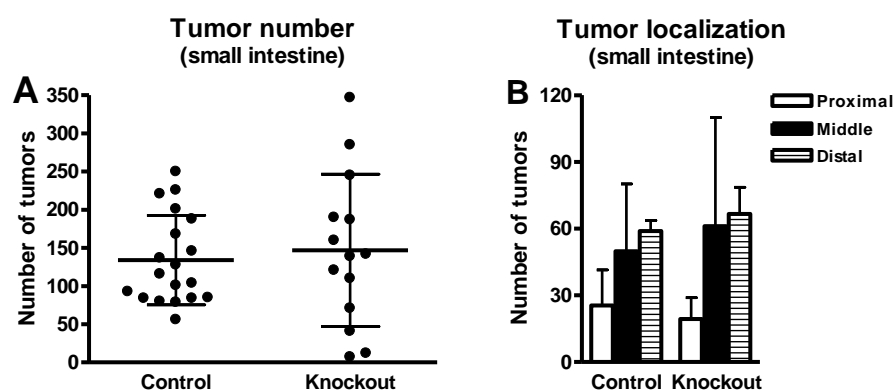


Fig. 4.9 Small intestinal tumor number (A) and distribution of tumors between the proximal, middle and distal section of the small intestine (B) in moribund $Apc^{+/Min}$ control (control; n=19) and $Dro1^{-/-};Apc^{+/Min}$ (knockout; n=14) mice.

Table 4.2 Size distribution of all tumors recorded in the small intestines of moribund $Apc^{+/Min}$ control (control) and $Dro1^{-/-};Apc^{+/Min}$ (knockout) mice.

Genotype	Control (n=19)	Knockout (n=14)
No. of tumors recorded	2547	2057
Thereof ≤ 2.5 mm (%)	2230 (87.6%)	1848 (89.9%)
>2.5 mm (%)	317 (12.4%)	208 (10.1%)

By contrast, differences in colonic tumor frequency between moribund $Dro1^{-/-};Apc^{+/Min}$ (n=17) and $Apc^{+/Min}$ control mice (n=16) were visible to the unaided eye at necropsy (Fig. 4.10). Microscopic analysis revealed a more than 3-fold increase in average colonic tumor number in $Dro1^{-/-};Apc^{+/Min}$ mice as compared to $Apc^{+/Min}$ controls (Fig. 4.11A). Whereas all $Dro1^{-/-};Apc^{+/Min}$ mice were affected by tumors of the colon, only 75% of the $Apc^{+/Min}$ control mice developed colonic polyps. The maximum colonic tumor number presented by a $Dro1^{-/-};Apc^{+/Min}$ mouse was 31, in $Apc^{+/Min}$ controls it was 12 (Fig. 4.11A). To analyze mean distribution of tumors between different sites, the colon was divided into a proximal and distal section. Independently of the *Dro1* status, the majority of colonic tumors localized to the distal section (Fig. 4.11B) and the percentage distribution of polyps between the proximal and distal colon was unchanged by *Dro1* loss ($Dro1^{-/-};Apc^{+/Min}$: 10% proximal, 90% distal; $Apc^{+/Min}$ control: 6% proximal, 94% distal). Notably, a significant rise in mean tumor number in both the proximal and distal colon was observed in $Dro1^{-/-};Apc^{+/Min}$ mice as compared to $Apc^{+/Min}$ controls (Fig. 4.11B). Average tumor size (Fig. 4.11C) and tumor size distribution (Table 4.3) were similar in $Dro1^{-/-};Apc^{+/Min}$ and $Apc^{+/Min}$ control mice. Frequently, tumors of different sizes were observed in the same animal. No visible lymph node or distant metastases were recorded at necropsy, independently of the *Dro1* status.

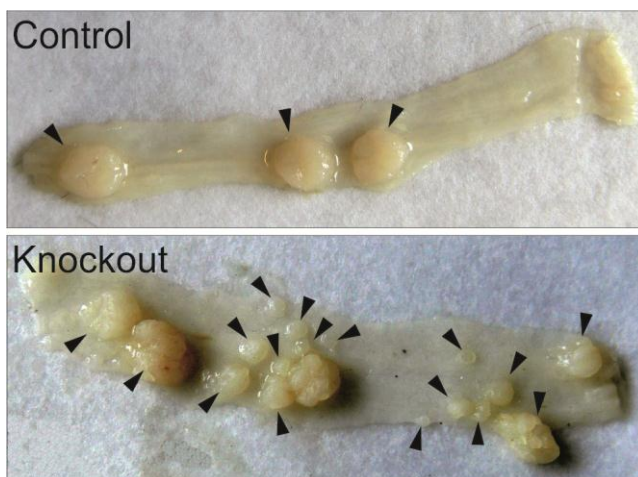


Fig. 4.10 Representative examples of longitudinally opened distal colon sections of a moribund $Apc^{+/Min}$ control (control) and a moribund $Dro1^{-/-};Apc^{+/Min}$ (knockout) mouse. Black arrowheads indicate neoplastic lesions.

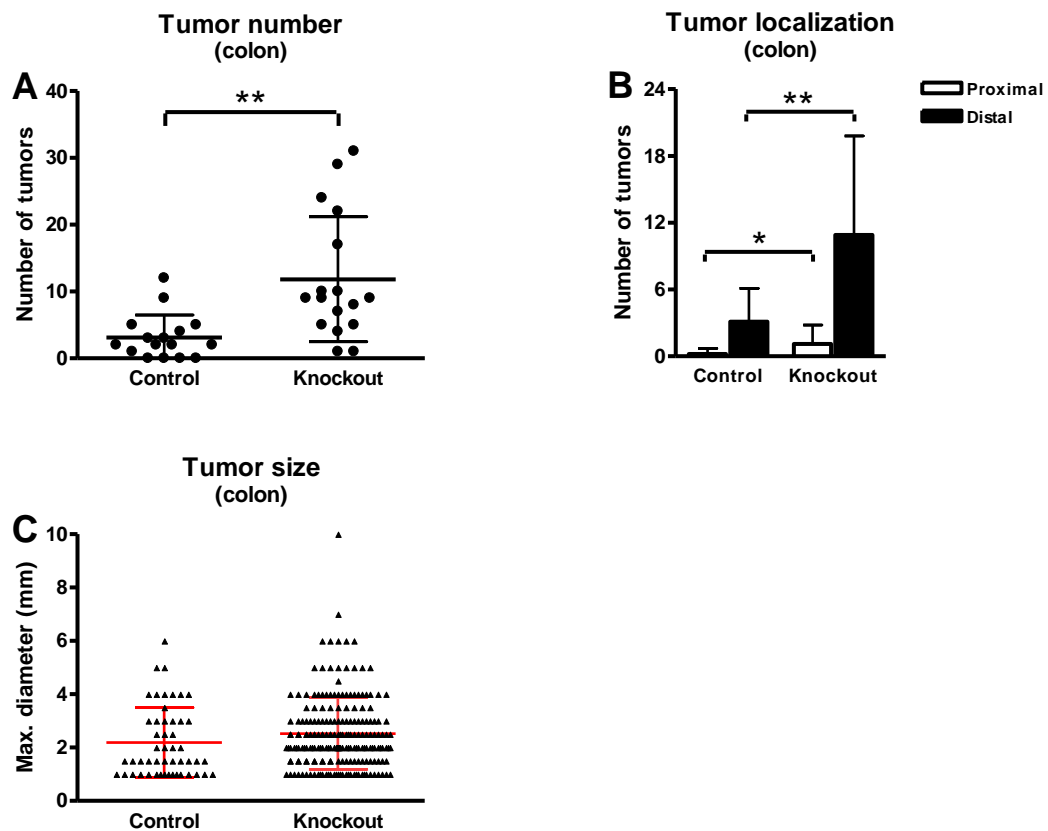


Fig. 4.11 Number of colonic polyps (A), number of tumors recorded for the proximal and distal colon (B), and tumor size (C) in moribund $Dro1^{-/-};Apc^{+/Min}$ (knockout; n=17) and $Apc^{+/Min}$ control (control; n=16) mice. *: $P \leq 0.05$; **: $P \leq 0.01$.

Table 4.3 Size distribution of all colonic polyps recorded in moribund $Apc^{+/Min}$ control (control) and $Dro1^{-/-};Apc^{+/Min}$ (knockout) mice.

Genotype	Control (n=16)	Knockout (n=17)
No. of tumors recorded	50	201
Thereof ≤ 2.5 mm (%)	34 (68.0%)	138 (68.7%)
> 2.5 mm (%)	16 (32.0%)	63 (31.3%)

To obtain insight into developmental aspects of tumor formation, $Dro1^{-/-};Apc^{+/Min}$ and $Apc^{+/Min}$ control mice were sacrificed at 5 and 10 weeks of age and the intestines were carefully examined.

Small intestinal lesions were already present in 5-week-old animals of both groups. In the cohort of 8 $Dro1^{-/-};Apc^{+/Min}$ mice, 3 animals exhibited a total of 4 small intestinal lesions which were all localized to the proximal section. In age-matched $Apc^{+/Min}$ controls (n=7), a total of 8 tumors developed in 4 mice, thereof 5 localized to the proximal, 1 to the middle and 2 to the distal segment. By 10 weeks of age the mean frequency of tumors of the small intestine was reduced in $Dro1^{-/-};Apc^{+/Min}$ mice when compared to $Apc^{+/Min}$ controls but statistical significance was not reached (P=0.40; Fig. 4.12A). Consistent with findings in moribund animals, no differences in mean tumor frequency between different sites of the small intestine were observed (Fig. 4.12B).

At the age of 5 weeks, mice were free of colonic polyps independently of the *Dro1* status. However, by 10 weeks of age, colonic tumors were frequently observed in $Dro1^{-/-};Apc^{+/Min}$ mice (in 9 out of 10 mice) but were rather rarely present in $Apc^{+/Min}$ controls (in 3 out of 8 mice). A significant increase in mean colonic tumor multiplicity was recorded in 10-week-old $Dro1^{-/-};Apc^{+/Min}$ mice (n=10) compared to similarly aged $Apc^{+/Min}$ controls (n=8; Fig. 4.12C). Analysis of tumor distribution between the proximal and distal colon showed that lesions were solely committed to the distal section. The proximal colon was tumor free in both groups.

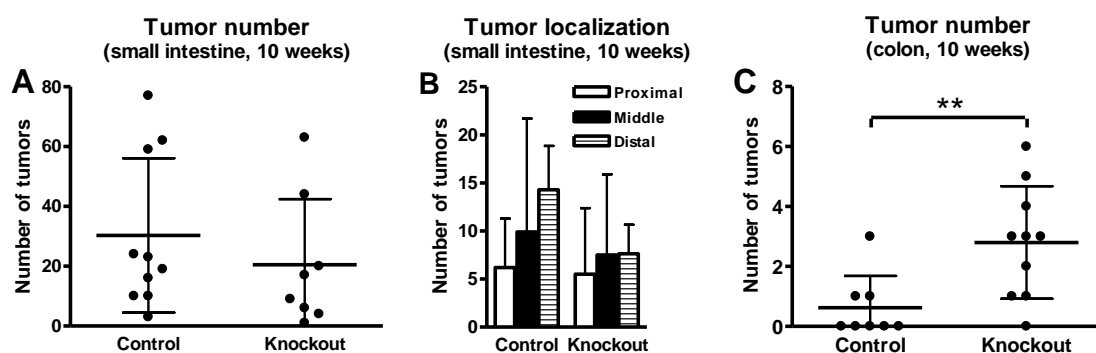


Fig. 4.12 Small intestinal tumor number (A) and distribution of tumors between the proximal, middle and distal section of the small intestine (B) in $Apc^{+/Min}$ control (control; n=10) and $Dro1^{-/-};Apc^{+/Min}$ mice (knockout; n=8) at the age of 10 weeks. (C) Intestinal colonic tumor number in $Apc^{+/Min}$ control (control; n=8) and $Dro1^{-/-};Apc^{+/Min}$ mice (knockout; n=10) at the age of 10 weeks. **: P ≤ 0.01.

4.2.3.3 Tumor histology

A large number of representative small intestinal polyps and all colonic tumors > 2 mm in diameter were isolated from the intestines of moribund $Dro1^{-/-};Apc^{+/Min}$ (n=21) and $Apc^{+/Min}$ control (n=19) mice and investigated by microscopic analysis of several H&E-stained serial sections.

Histologically, tumors (n=60) isolated from the small intestines of moribund $Dro1^{-/-};Apc^{+/Min}$ mice corresponded to tubular adenomas with focal high grade dysplasia/intraepithelial neoplasia (IEN) of the epithelium (Table 4.4A). The same was true for the vast majority (49 of the 50) of lesions resected from the small intestines of moribund $Apc^{+/Min}$ control mice (Table 4.4A). Noteworthy, a single lesion isolated from a control mouse euthanized at 144 d of age presented an invasive adenocarcinoma with infiltration of tumor cells into the tela submucosa.

Microscopic evaluation of 83 colonic tumors resected from the colons of moribund $Dro1^{-/-};Apc^{+/Min}$ mice revealed that 54 polyps (~65%) resembled tubular adenomas with focal high grade dysplasia/IEN and 29 lesions (~35%) had progressed to malignancy (adenoma/adenocarcinoma ratio of ~2: 1; Table 4.4A). Seventeen (~59%) of the 29 adenocarcinomas featured intramucosal adenocarcinomas, the remaining (~41%) were characterized as invasive adenocarcinoma penetrating through the lamina muscularis mucosae. In the cohort of 21 $Dro1^{-/-};Apc^{+/Min}$ mice, 10 animals (48%) harbored at least one colonic tumor with malignant growth features. Notably, 28 of the 29 adenocarcinomas located to the distal colon. In contrast, colonic adenocarcinomas did not develop in the colons of $Apc^{+/Min}$ control mice. Polyps isolated from the colons of $Apc^{+/Min}$ control mice were classified, without exception, as tubular adenomas with focal high grade dysplasia/IEN of the epithelium (Table 4.4A). Small intestinal and colonic adenomas in $Dro1^{-/-};Apc^{+/Min}$ mice were histologically similar to $Apc^{+/Min}$ control tumors. Representative pictures of H&E-stained sections from tumors from moribund $Apc^{+/Min}$ control and $Dro1^{-/-};Apc^{+/Min}$ mice are shown in Fig. 4.13.

Tumor progression was investigated more closely by histopathologic analysis of tumors from 10-week-old $Apc^{+/Min}$ control and $Dro1^{-/-};Apc^{+/Min}$ mice. Assessment of a large number of small intestinal polyps showed that all lesions featured adenomas with high grade dysplasia/IEN of the epithelium regardless of the *Dro1* status (Table 4.4B). Histopathologic analysis of 14 colonic tumors from $Dro1^{-/-};Apc^{+/Min}$ mice revealed that 10 lesions resembled adenomas with high grade dysplasia/IEN and 4 had progressed to intramucosal adenocarcinoma (adenoma/adenocarcinoma ratio 2.5: 1; Table 4.4B). By

contrast, 5 of the 6 colonic polyps from $Apc^{+/Min}$ control mice were adenomas with high grade dysplasia/IEN and a single adenocarcinoma was observed (Table 4.4B).

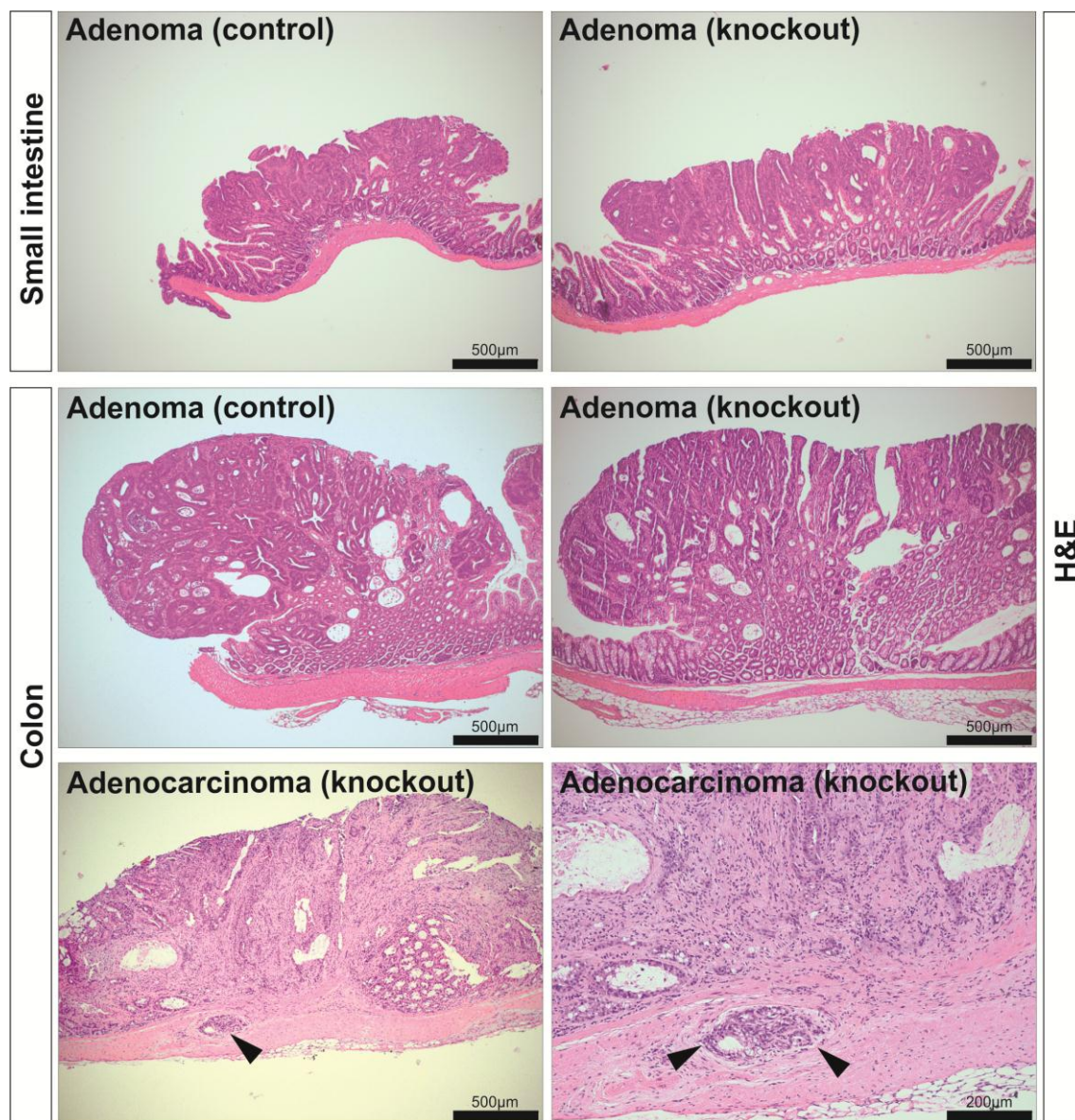


Fig. 4.13 Representative H&E-stained tissue sections from small intestinal and colonic tumors from moribund $Dro1^{-/-};Apc^{+/Min}$ (knockout) and $Apc^{+/Min}$ control (control) mice. Black arrowheads indicate invasion of tumor cells through the lamina muscularis mucosae into the tela submucosa.

Table 4.4 Histopathologic classification of tumors dissected from the small intestine and colon of moribund (A) and 10-week-old (B) $Apc^{+/Min}$ control (control) and $Dro1^{-/-}; Apc^{+/Min}$ (knockout) mice. For histopathologic classification, small intestinal tumors were selected at random. Colonic polyps > 2.0 mm in diameter were analyzed

A		
Moribund mice		
Genotype	Control (n=19)	Knockout (n=21)
<u>Small intestine</u>		
No. of tumors analyzed	60	50
Thereof adenoma	59 (98.3%)	50 (100%)
adenocarcinoma	1 (1.7%)	-
<u>Colon</u>		
No. of tumors analyzed	15	83
Thereof adenoma	15 (100%)	54 (65.1%)
adenocarcinoma	-	29 (34.9%)
B		
10 weeks of age		
Genotype	Control (n=15)	Knockout (n=16)
<u>Small intestine</u>		
No. of tumors analyzed	50	50
Thereof adenoma	50 (100%)	50 (100%)
adenocarcinoma	-	-
<u>Colon</u>		
No. of tumors analyzed	6	14
Thereof adenoma	5 (83.4%)	10 (71.4%)
adenocarcinoma	1 (16.6%)	4 (28.6%)

4.2.3.4 Tumor proliferation rate

The ability to sustain chronic proliferation constitutes the most fundamental hallmark of cancer cells (Hanahan and Weinberg, 2011). To investigate a probable effect of *Dro1* deficiency on the cellular proliferation rate in colorectal tumors of moribund $Apc^{+/Min}$ mice, immunohistochemical staining of Ki-67, a cell cycle related protein, was performed on tissue sections of $Apc^{+/Min}$ adenomas (n=11), $Dro1^{-/-};Apc^{+/Min}$ adenomas (n=15) and $Dro1^{-/-};Apc^{+/Min}$ adenocarcinomas (n=14). Compared to normal intestinal epithelium, cellular proliferation was disorganized and profoundly increased in all categories of lesions analyzed (Fig. 4.14A). Quantification of the number of Ki-67-positive cells revealed that, on average, the percentage of proliferating cells was unchanged between $Dro1^{-/-};Apc^{+/Min}$ adenomas, $Dro1^{-/-};Apc^{+/Min}$ adenocarcinomas and $Apc^{+/Min}$ control adenomas (Fig. 4.14B). Furthermore, no differences in the distribution of Ki-67 cells throughout neoplastic lesions were observed (Fig. 4.14A).

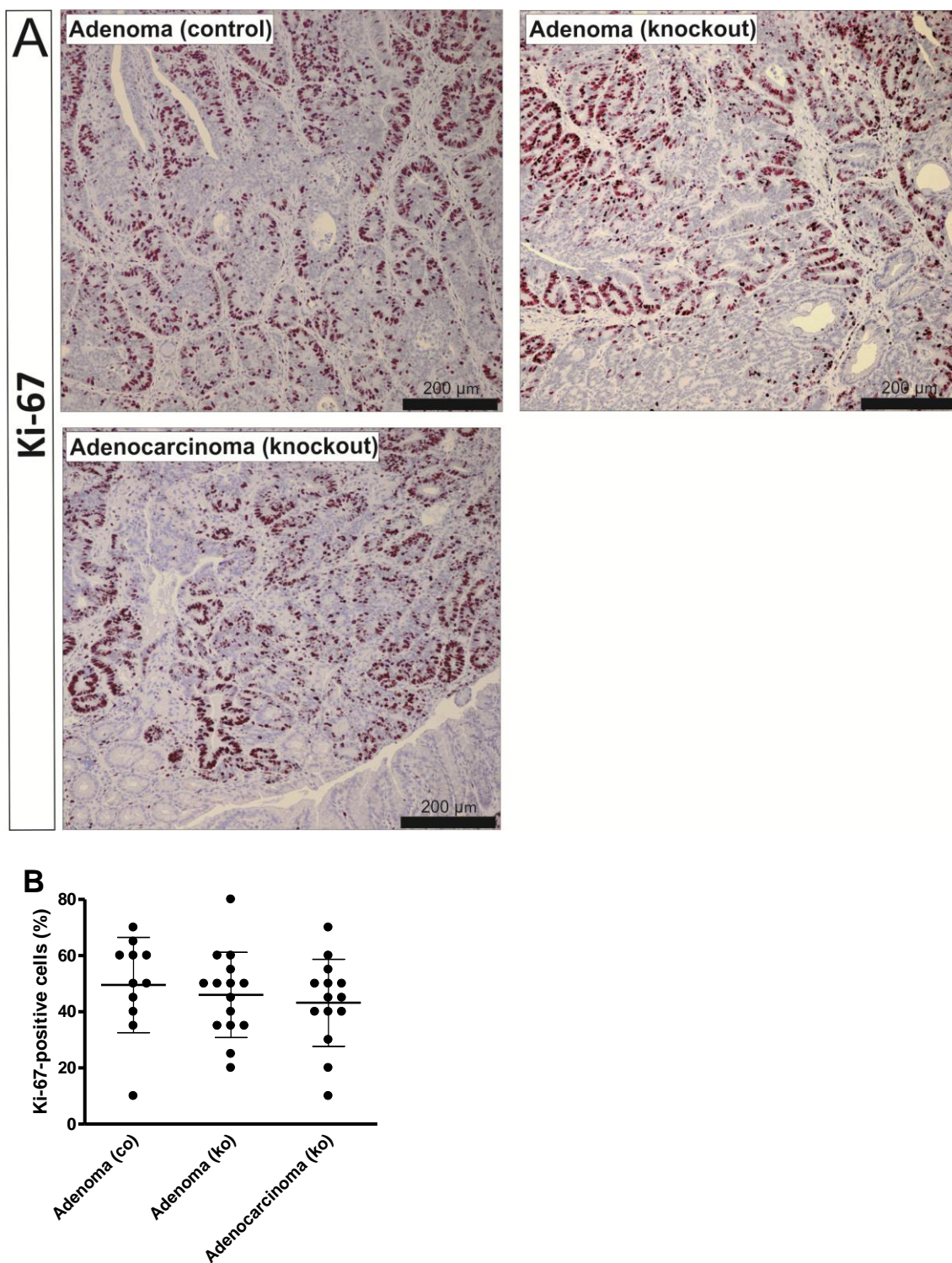


Fig. 4.14 (A) Immunohistochemical staining of Ki-67 in colorectal tumors isolated from moribund $Apc^{+/Min}$ control (control) and $Dro1^{-/-};Apc^{+/Min}$ (knockout) mice. (B) Quantification of Ki-67-positive cells in colonic tumors of moribund $Apc^{+/Min}$ control and $Dro1^{-/-};Apc^{+/Min}$ mice (n=11 for $Apc^{+/Min}$ control adenomas, n=15 for $Dro1^{-/-};Apc^{+/Min}$ adenomas, n=14 for $Dro1^{-/-};Apc^{+/Min}$ adenocarcinomas).

4.2.3.5 Nuclear β -catenin accumulation

To investigate whether loss of *Dro1* impacts accumulation of nuclear β -catenin within colonic tumors of moribund $Apc^{+/Min}$ mice, immunohistochemical staining of β -catenin was performed on $Apc^{+/min}$ control adenomas (n=12), $Dro1^{-/-};Apc^{+/Min}$ adenomas (n=11) and $Dro1^{-/-};Apc^{+/Min}$ adenocarcinomas (n=14).

Elimination of *Dro1* had no influence on β -catenin staining patterns in morphologically normal intestinal epithelium, in which β -catenin was distributed to the cell membrane and was rarely observed in cells located at the crypt base (Fig. 4.15A).

Within neoplastic tissue nuclear β -catenin staining was strongly increased compared to normal intestinal epithelium independent of the *Dro1* status and malignant progression (Fig. 4.15A). The mean percentage of tumor cells exhibiting positive nuclear β -catenin staining was similar in $Dro1^{-/-};Apc^{+/Min}$ adenomas when compared to adenomas derived from $Apc^{+/Min}$ control mice (Fig. 4.15B). Furthermore, no significant differences in the mean percentage of β -catenin positive nuclei were observed between adenomas and adenocarcinomas from $Dro1^{-/-};Apc^{+/Min}$ mice (Fig. 4.15B).

The staining intensity within the nucleus was evaluated by scoring changes in the intensity of staining relative to normal epithelium within the same section. Nearly all lesions were characterized by strong nuclear β -catenin staining. Noteworthy, low levels of nuclear staining were only observed within an $Apc^{+/Min}$ control adenoma.

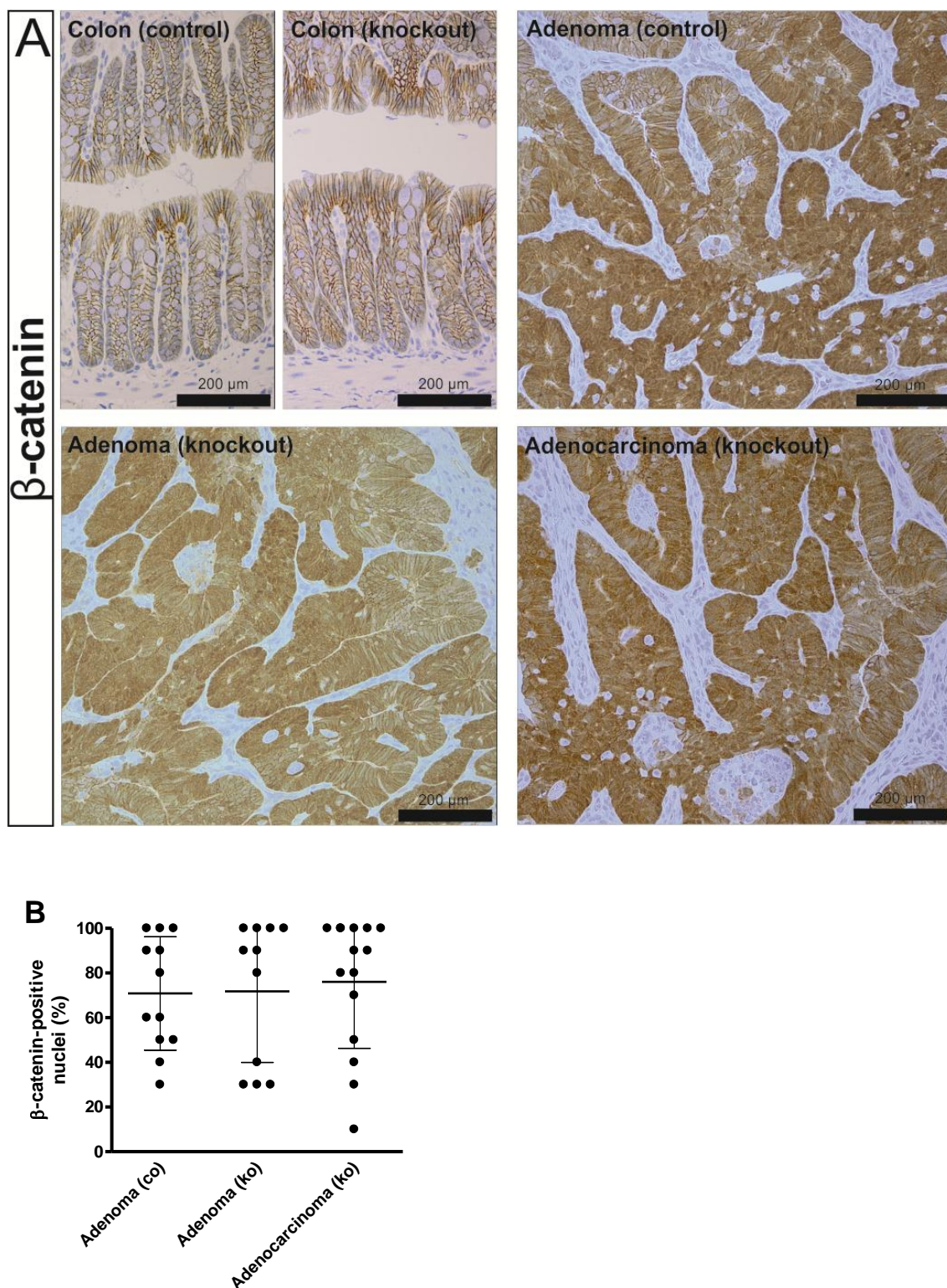


Fig. 4.15 (A) Immunohistochemical staining of β -catenin in the normal intestinal epithelium, in colorectal adenoma and in adenocarcinoma from moribund $Apc^{+/Min}$ control (control) and $Dro1^{-/-};Apc^{+/Min}$ (knockout) mice. (B) Percentage of β -catenin-positive nuclei in colonic tumors from moribund $Apc^{+/Min}$ (co) and $Dro1^{-/-};Apc^{+/Min}$ (ko) mice (n=12 for $Apc^{+/Min}$ control adenomas, n=11 for $Dro1^{-/-};Apc^{+/Min}$ adenomas, n=14 for $Dro1^{-/-};Apc^{+/Min}$ adenocarcinomas).

4.2.3.6 ACF formation

ACF are putative precursor lesions of colorectal adenomas in humans and some mouse strains of intestinal cancer (McLellan and Bird, 1988a; Fenoglio-Preiser and Noffsinger, 1999; Boivin *et al.*, 2003; Gupta and Schoen, 2009). To investigate whether *Dro1* loss regulates the development of ACF in $Apc^{+/Min}$ mice, $Dro1^{-/-};Apc^{+/Min}$ and $Apc^{+/Min}$ control mice were sacrificed at the age of 5 (n=5/ group) and 10 (n=5/ group) weeks and whole-mount colon preparations were investigated for early morphologic changes of colonic crypts by methylene blue staining and trans-illumination. No ACF were observed in $Apc^{+/Min}$ mice independently of the *Dro1* status. Representative pictures of methylene blue stained whole-mount colon samples are displayed in Fig. 4.16.

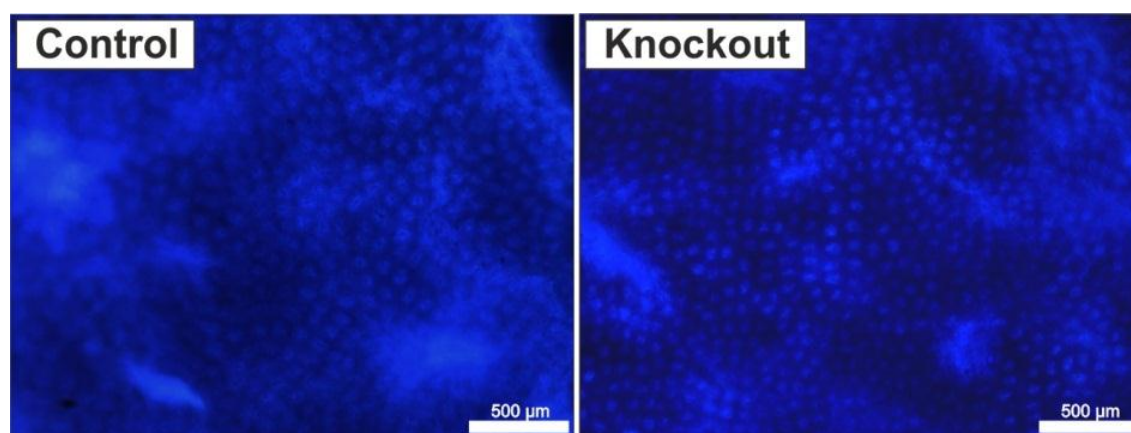


Fig. 4.16 Representative pictures of whole-mount distal colon samples from 10-week-old $Apc^{+/Min}$ control (control) and $Dro1^{-/-};Apc^{+/Min}$ (knockout) mice stained with methylene blue.

4.2.3.7 *Mom1* status

As the genetic background strongly influences tumor burden in $Apc^{+/Min}$ mice (Gould *et al.*, 1996; McCart *et al.*, 2008), the *Mom1* allele status of $Dro1^{-/-};Apc^{+/Min}$ and $Apc^{+/Min}$ control mice was examined (n=15/ group). In order to detect a *Bam*HI restriction site present in the resistant *Mom1* allele ($Mom1^R$) but absent in the sensitive *Mom1* allele ($Mom1^S$), a *Mom1* PCR product was generated from tail tip genomic DNA, digested with *Bam*HI and separated by gel electrophoresis. $Dro1^{-/-};Apc^{+/Min}$ as well as $Apc^{+/Min}$ control mice were found to carry the $Mom1^S$ allele homozygously (Fig. 4.17).

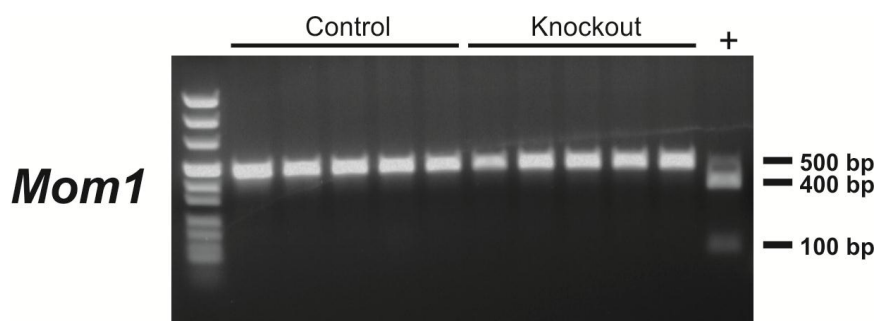


Fig. 4.17 Evaluation of the *Mom1* allelic status of *Dro1*^{-/-};*Apc*^{+/*Min*} (knockout) and *Apc*^{+/*Min*} control (control) mice. Representative gel electrophoresis of *Mom1* PCR products digested with *Bam*HI. The 500 bp fragment indicates absence of a *Bam*HI restriction site and is characteristic for the *Mom1*^S allele. The 400 bp and 100 bp fragments are characteristic for the *Mom1*^R allele.

4.3. Effects of *Dro1* loss on body growth

Since *Dro1* has been implicated in energy homeostasis, body weight regulation, and obesity (Aoki *et al.*, 2002; Okada *et al.*, 2008; Tremblay *et al.*, 2009) a possible effect of *Dro1* deficiency on body growth was investigated under standard feeding conditions and when mice were exposed to a high-fat diet.

4.3.1 Standard feeding conditions

4.3.1.1 Body weight

To ascertain whether inactivation of *Dro1* affects body weight gain, selected litters of *Dro1*^{-/-} parents or control parents were weighted weekly from the 11th day of life until 15 weeks of age. *Dro1*^{-/-} mice of both genders showed normal development until 10 (males) and 12 (females) weeks of age after which a significant increase in body weight was observed when compared to gender-matched controls (Fig. 4.18A). Examination of 6- and 18-month-old mice also revealed profound differences in body weight between *Dro1*^{-/-} and control mice (4.18B and 4.18C).

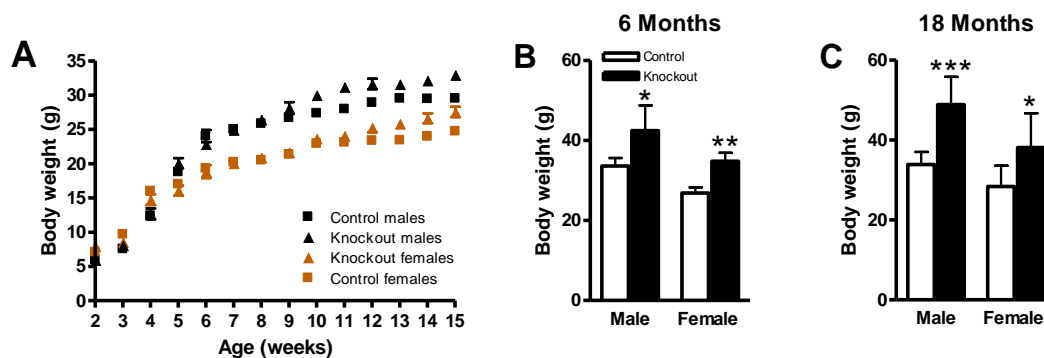


Fig. 4.18 (A) Body weight gain in *Dro1*^{-/-} (knockout) and control males (n=9 for *Dro1*^{-/-} males and n=13 for control males) and females (n=10 for *Dro1*^{-/-} females and n=8 for control females) fed a standard diet. *Dro1*^{-/-} males exhibited significantly enhanced body weight from week 10 as compared to control males. Increase in body weight in *Dro1*^{-/-} females as compared to control females was significant from week 12. $P \leq 0.001$ for males and $P \leq 0.01$ for females at 15 weeks of age. (B, C) Body weight in *Dro1*^{-/-} (knockout) and control mice of both genders at 6 (B) and 18 (C) months of age (n=5/ group for males and n=6/ group for females at 6 months, n=7/ group for males at 18 months and n=6/ group for females at 18 months). Legend displayed in (B) applies to (C). *: $P \leq 0.05$; **: $P \leq 0.01$; ***: $P \leq 0.001$.

4.3.1.2 Longitudinal growth

Since changes in longitudinal body growth may account for differences in body weight, the length of the femora and the nose-rump-length (NRL) were investigated in 6-month-old *Dro1*^{-/-} and control mice. Both parameters were found to be similar in *Dro1*^{-/-} and control mice (Fig. 4.19A and 4.19B). Notably, by 6 months of age relative nose-rump-length calculated as body weight divided by NRL (g/cm) was significantly increased in *Dro1*^{-/-} mice of both genders as compared to gender-matched controls (Fig. 4.19C).

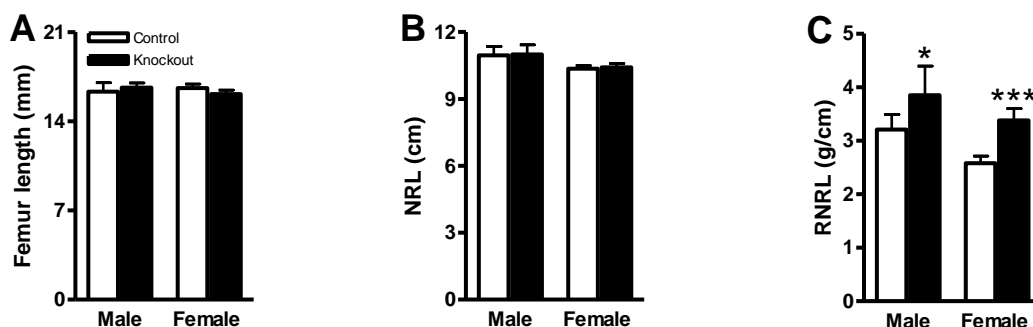


Fig. 4.19 Femur length (A), nose-rump-length (NRL) (B), and relative nose-rump-length (RNRL) (C) in 6-month-old *Dro1*^{-/-} (knockout) and control animals of both genders (n=5/ group for males and n=6/ group for females). Legend displayed in (A) applies to all figures. *: $P \leq 0.05$; ***: $P \leq 0.001$.

4.3.1.3 Organ growth

To determine a possible effect of *Dro1* ablation on organ and carcass weight, *Dro1*^{-/-} and control mice were sacrificed at various stages of life. The weight of the following organs was examined: heart, lungs, liver, spleen and kidneys.

Necropsy of 2-month-old animals revealed similar heart, lung, liver, kidney and carcass weight in *Dro1*^{-/-} and control mice of both sexes. Absolute and relative spleen weight was significantly increased in 2-month-old *Dro1*^{-/-} males as compared to age and gender-matched controls; females showed an increase in spleen weight but statistical significance was not reached.

At the age of 6 months a significant rise in liver, spleen and carcass weight was detected in both genders of *Dro1*^{-/-} mice as compared to age- and gender-matched controls. Moreover, the weight of lungs and kidneys was profoundly increased in 6-month-old *Dro1*^{-/-} males. The absolute heart weight was increased but statistical significance was

not reached. When related to body weight, changes in the weight of lungs, liver, spleen, kidneys and carcass did not persist. Notably, the relative weight of heart and kidneys was significantly decreased in $Dro1^{-/-}$ females but was unchanged in $Dro1^{-/-}$ males as compared to age- and gender-matched control mice. Absolute and relative organ weights are presented in Table 4.5 and Table 4.6. Microscopic evaluation of H&E-stained histological sections of heart, lung, spleen, liver and kidney from 2 (n=3) and 6 (n=6) months old $Dro1^{-/-}$ mice revealed no obvious pathologic alterations in organ architecture.

Table 4.5 Absolute organ weight in male (A) and female (B) $Dro1^{-/-}$ (knockout) and control mice at the age of 2 (n=3/ group) and 6 months (n=5/ group for males and n=6/ group for females at 6 months). Values are presented as means and corresponding standard deviations are displayed in brackets. *: $P \leq 0.05$; **: $P \leq 0.01$; ***: $P \leq 0.001$. (-) indicates the absence of significant differences.

A	Organ weights (mg), males					
	2 months		Δ	6 months		Δ
	Control	Knockout		Control	Knockout	
Heart	144 (9)	159 (31)	-	176 (19)	235 (64)	-
Lungs	156 (11)	162 (6)	-	189 (33)	240 (39)	*
Liver	1233 (100)	1387 (39)	-	1634 (144)	2492 (274)	**
Spleen	59 (13)	91 (9)	*	73 (11)	118 (23)	*
Kidneys	295 (11)	338 (43)	-	397 (53)	548 (14)	**
Carcass	11324 (836)	11297 (607)	-	14172 (532)	16791 (415)	***

B	Organ weights (mg), females					
	2 months		Δ	6 months		Δ
	Control	Knockout		Control	Knockout	
Heart	127 (12)	110 (12)	-	140 (6)	152 (20)	-
Lungs	159 (13)	143 (6)	-	181 (20)	214 (48)	-
Liver	1065 (137)	1110 (77)	-	1376 (186)	1811 (327)	**
Spleen	86 (14)	110 (20)	-	82 (12)	125 (17)	***
Kidneys	262 (9)	257 (24)	-	308 (22)	326 (21)	-
Carcass	9977 (319)	9292 (392)	-	11003 (703)	13881 (568)	***

Table 4.6 Relative organ weight in male (A) and female (B) $Dro1^{-/-}$ (knockout) and control mice at the age of 2 (n=3/ group) and 6 months (n=5/ group for males and n=6/ group for females at 6 months). Values are presented as means and corresponding standard deviations are displayed in brackets. *: $P \leq 0.05$; **: $P \leq 0.01$; ***: $P \leq 0.001$. (-) indicates the absence of significant differences.

A						
Relative organ weights (% of body weight), males						
	2 months		Δ	6 months		Δ
	Control	Knockout		Control	Knockout	
Heart	0.55 (0.05)	0.60 (0.10)	-	0.52 (0.05)	0.57 (0.18)	-
Lungs	0.59 (0.07)	0.61 (0.03)	-	0.56 (0.08)	0.57 (0.07)	-
Liver	4.65 (0.17)	5.23 (0.35)	-	4.86 (0.82)	5.99 (1.08)	-
Spleen	0.22 (0.04)	0.34 (0.04)	*	0.22 (0.02)	0.29 (0.07)	-
Kidneys	1.12 (0.10)	1.28 (0.18)	-	1.18 (0.10)	1.33 (0.24)	-
Carcass	42.68 (0.26)	42.57 (1.35)	-	42.21 (1.57)	40.5 (1.48)	-

B						
Relative organ weights (% of body weight), females						
	2 months		Δ	6 months		Δ
	Control	Knockout		Control	Knockout	
Heart	0.56 (0.06)	0.51 (0.09)	-	0.52 (0.04)	0.44 (0.07)	*
Lungs	0.70 (0.05)	0.66 (0.07)	-	0.67 (0.07)	0.62 (0.16)	-
Liver	4.68 (0.47)	5.13 (0.09)	-	5.12 (0.61)	5.23 (1.05)	-
Spleen	0.35 (0.08)	0.51 (0.06)	-	0.30 (0.06)	0.36 (0.06)	-
Kidneys	1.15 (0.05)	1.09 (0.05)	-	1.15 (0.08)	0.94 (0.08)	***
Carcass	43.95 (0.19)	42.99 (1.08)	-	40.98 (2.26)	40.01 (2.89)	-

4.3.1.4 Total body fat and lean mass

To evaluate changes in body composition, total body fat content and lean mass were determined weekly in $Dro1^{-/-}$ and control males from 4 to 15 weeks of age by MRI. $Dro1^{-/-}$ males exhibited a significant increase in lean mass compared to controls by week 9 onwards (Fig. 4.20A). Total body fat tended to be higher in $Dro1^{-/-}$ males but statistical significance was not reached (Fig. 4.20B).

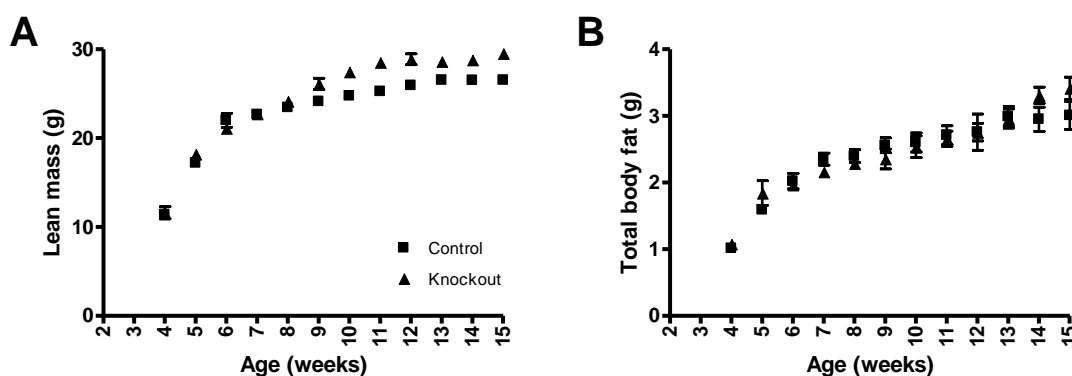


Fig. 4.20 Lean mass (A) and total body fat (B) gain in $Dro1^{-/-}$ (knockout; n=9) and control males (n=13). Increase in lean mass in $Dro1^{-/-}$ males was significant from week 9 onwards as compared to control males ($P \leq 0.001$ at 15 weeks of age). No significant differences in total body fat were observed ($P=0.32$ at 15 weeks of age). Legend displayed in (A) applies to both figures.

4.3.1.5 Fat pad growth

To investigate changes in fat pad growth the main white adipose tissue depots of 2- and 6-month-old $Dro1^{-/-}$ and control mice of both genders were weighted and their relative contribution to body weight was calculated. Analyses involved the epididymal, abdominal and subcutaneous fat pads in males and the abdominal (including ovarian and periovarian fat) and subcutaneous fat pads in females. At 2 months of age, when body weight of $Dro1^{-/-}$ mice was not significantly different from that of control mice, no significant differences in white adipose tissue mass were recorded between $Dro1^{-/-}$ and control mice (Fig. 4.21A and 4.21B).

By 6 months of age when profound differences in body weight were present, substantial changes in fat pad weight were observed (Fig. 4.21C and 4.21D). $Dro1^{-/-}$ males exhibited significantly enlarged epididymal, abdominal and subcutaneous fat pads when

compared to age- and gender-matched controls (Fig. 4.21C). In $Dro1^{-/-}$ females a significant rise in abdominal fat was recorded and the weight of the subcutaneous fat pad tended to be increased but statistical significance was not reached (Fig. 4.21D). Substantial changes in fat pad weight between $Dro1^{-/-}$ and control mice persisted when fat pad weight was related to body weight (Fig. 4.21). Evaluation of H&E-stained histological sections of the cranial tip of epididymal white adipose tissue from 2- and 6-month-old $Dro1^{-/-}$ males revealed no obvious pathologic changes.

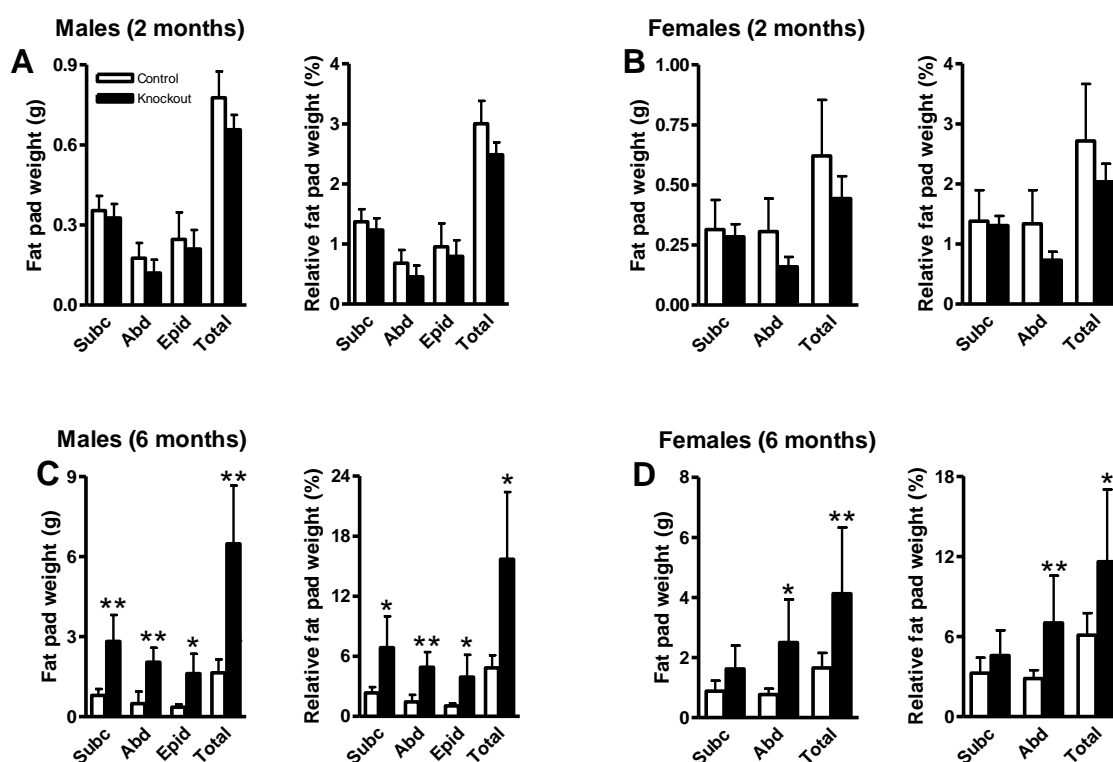


Fig. 4.21 Absolute and relative weights of the subcutaneous (subc), abdominal (abd) and epididymal (epid) white fat pads in $Dro1^{-/-}$ (knockout) and control males (A, C) and females (B, D) at 2 (A, B) and 6 (C, D) months of age. Relative fat pad weight was calculated as percent of body weight. (n=3/ group for both genders at 2 months, n=5/ group for males and n=6/ group for females at 6 months). Legend displayed in (A) applies to all figures. *: $P \leq 0.05$; **: $P \leq 0.01$.

4.3.1.6 Glucose metabolism

To detect possible changes in glucose metabolism, intraperitoneal glucose tolerance test was performed in 14-week-old *Dro1*^{-/-} (n=9) and control (n=12) males. At this age body mass was significantly enhanced in *Dro1*^{-/-} males when compared to control males (32.12 g ± 1.99 g in *Dro1*^{-/-} males compared to 29.46 g ± 1.45 g in control males. $P \leq 0.01$). Fasted blood glucose levels were similar in *Dro1*^{-/-} and control mice and *Dro1*^{-/-} mice cleared the administrated glucose as efficiently from the blood as controls (Fig. 4.22).

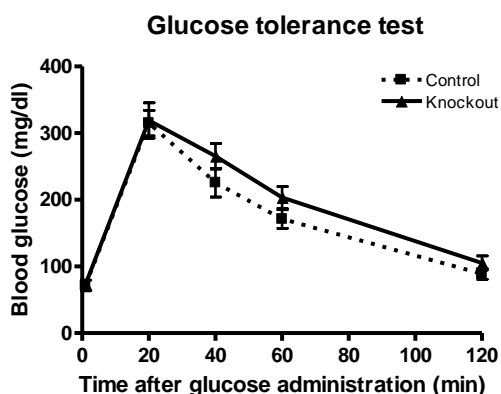


Fig. 4.22 Intraperitoneal glucose tolerance test in 14-week-old *Dro1*^{-/-} (knockout; n=9) and control males (n=12).

4.3.1.7 Serum triglycerides and free fatty acids

To elucidate a possible effect of *Dro1* deficiency on serum lipids, triglycerides and free fatty acids were measured in the serum of 2- and 6-month-old *Dro1*^{-/-} and control mice. At 2 months of age serum triglycerides tended to be lower in *Dro1*^{-/-} mice as compared to controls and by 6 months of age the decrease reached significance (Fig. 4.23A). Serum free fatty acid levels were unchanged in *Dro1*^{-/-} mice when compared to controls at 2 as well as 6 months of age (4.23B).

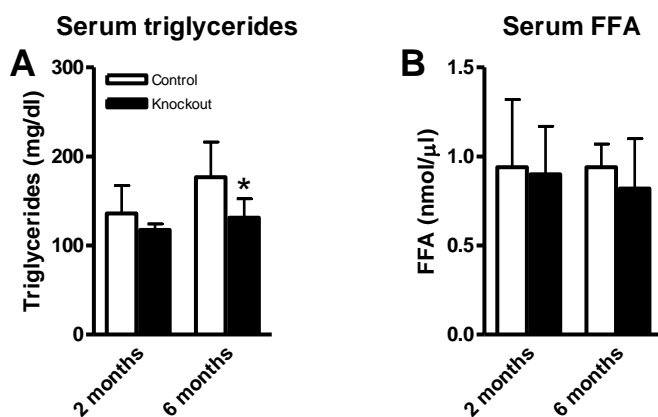


Fig. 4.23 Serum triglycerides (A) and free fatty acids (FFA) (B) in $Dro1^{-/-}$ (knockout) and control mice at the age of 2 (n=3/ group) and 6 months (n=6/ group). Legend displayed in (A) applies to (B). *: $P \leq 0.05$.

4.3.2 High-fat diet feeding conditions

Since $Dro1^{-/-}$ mice of both sexes exhibited an overweight phenotype under standard feeding conditions, the impact of *Dro1* elimination on the development of diet-induced obesity was investigated. Thus, $Dro1^{-/-}$ and control mice (n=9/ group) were fed a high-fat diet in which the majority of caloric intake (60%) is from fat for 16 weeks beginning at 11 days of age (first day of solid food intake). The following experiments were conducted in male mice as changes in adipose tissue mass were more pronounced in $Dro1^{-/-}$ males than in females when fed a standard diet.

4.3.2.1 Body weight, body fat and lean mass

To investigate the effect of *Dro1* deficiency on body weight gain in mice maintained on a high-fat diet, body weight was measured weekly starting from the 11th day of life until 17 weeks of age. No significant differences in weight curves were found between $Dro1^{-/-}$ and control mice in the first 7 weeks of life. However, from week 8 onwards $Dro1^{-/-}$ mice were significantly heavier than controls (Fig. 4.25A). After being exposed to a high-fat diet for 16 weeks $Dro1^{-/-}$ mice exhibited 43.9% more body weight than controls. Fig. 4.24 demonstrates the dramatic phenotype.

To analyze how changes in body weight correlate with changes in total body fat and lean mass in high-fat diet-fed mice, MRI measurement was performed weekly starting from the 4th week of life. By week 8 onwards $Dro1^{-/-}$ mice exhibited a significant increase in lean mass (Fig. 4.25B) and body fat (Fig. 4.25C) as compared to controls.

Throughout the whole time-course a severe rise in body fat was detected in $Dro1^{-/-}$ mice whereas body fat only slightly increased in controls after week 9 (Fig. 4.25C).

At the age of 15 weeks body weight, body fat and lean mass were significantly increased in high-fat diet-fed $Dro1^{-/-}$ mice compared to their normal-fed counterparts. Control mice also exhibited higher body weight and body fat under high-fat diet than under normal diet but the difference was statistically significant only for body fat. Lean mass in controls was unchanged by high-fat diet. Changes in body weight, body fat and lean mass in knockout and control mice under normal diet and high-fat diet are displayed in Table 4.6.

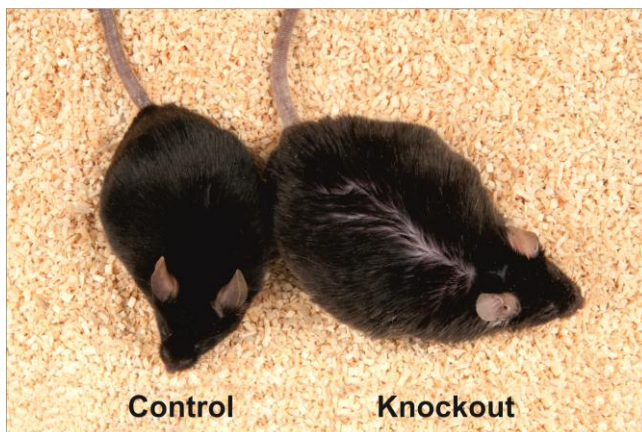


Fig. 4.24 Representative picture of a control and $Dro1^{-/-}$ (knockout) mouse after exposed to a high-fat diet for 16 weeks.

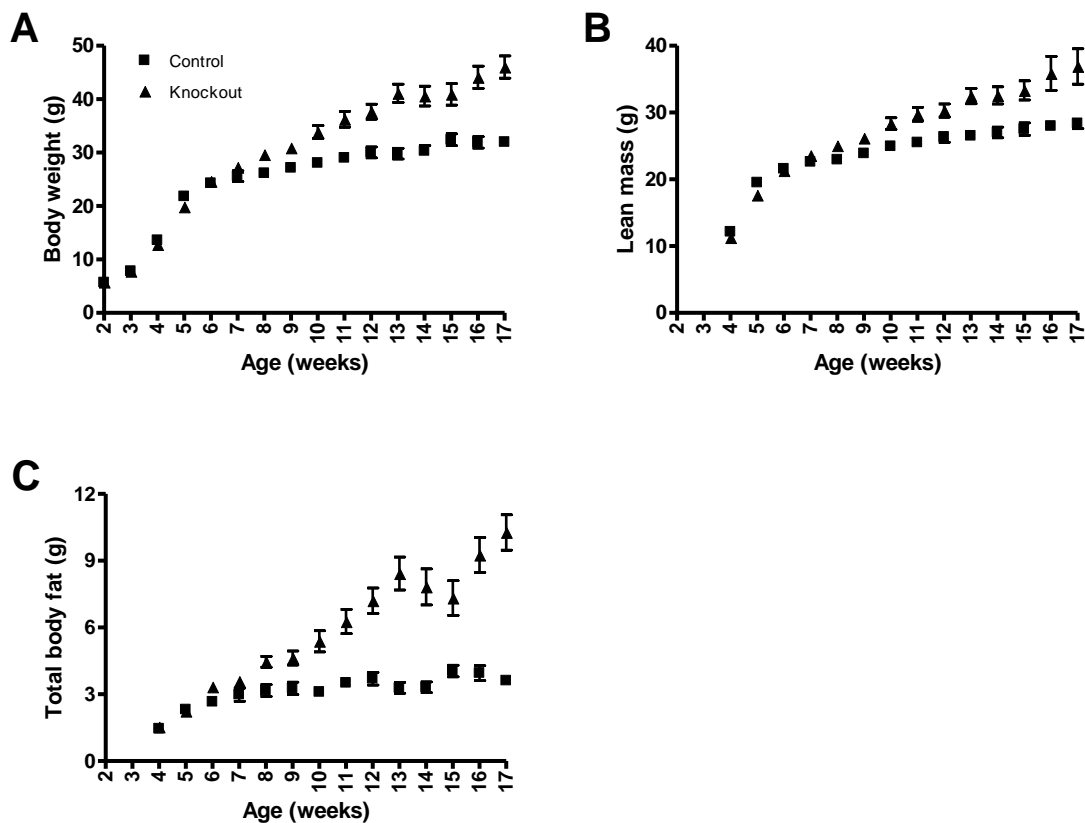


Fig. 4.25 Body weight (A), lean mass (B) and total body fat (C) gain in $Dro1^{-/-}$ (knockout) and control males ($n=9$ / group) maintained on a high-fat diet for 16 weeks beginning at the 11th day of age. Increases in body weight, body fat and lean mass were continually significant after week 8. $P \leq 0.001$ for body weight and body fat and $P \leq 0.05$ for lean mass at 17 weeks of age. Legend displayed in (A) applies to all figures.

Table 4.6 Comparison of body weight, body fat and lean mass between normal-fed (n=9 for $Dro1^{-/-}$ males and n=13 for control males) and high-fat diet-fed (n=9/ group) control mice and $Dro1^{-/-}$ (knockout) mice at 15 weeks of age. Values are presented as means and standard deviations (brackets). *: $P \leq 0.05$; **: $P \leq 0.01$; ***: $P \leq 0.001$. (-) indicates the absence of significant differences.

	Normal diet	High-fat diet	Δ	Increase (%)
Body weight				
Control	30.82 (1.94)	31.56 (3.47)	-	+ 2.39
Knockout	33.06 (1.85)	40.92 (5.70)	**	+ 23.41
Body fat				
Control	3.40 (0.53)	4.04 (0.79)	*	+ 18.78
Knockout	3.41 (0.50)	7.55 (2.11)	***	+ 121.24
Lean mass				
Control	27.42 (1.43)	27.51 (2.8)	-	+ 1.04%
Knockout	29.65 (1.36)	33.37 (4.05)	*	+ 12.53%

4.3.2.2 Glucose metabolism

To assess the response to glucose administration under high-fat diet feeding, an intraperitoneal glucose tolerance test was performed in 14-week-old $Dro1^{-/-}$ and control mice (after they had been exposed to a high-fat diet for 13 weeks). $Dro1^{-/-}$ mice showed significantly higher levels of blood glucose after fasting for 16 h when compared to controls. Moreover their ability to clear glucose from the blood was substantially decreased (Fig. 4.26A).

An intraperitoneal insulin tolerance test was accomplished one week later to investigate the role of insulin resistance in the glucose response. Fasted blood glucose levels tended to be higher in $Dro1^{-/-}$ mice but statistical significance was not reached. In addition, knockout mice showed a markedly attenuated glucose lowering rate after insulin injection when compared to controls (Fig. 4.26B).

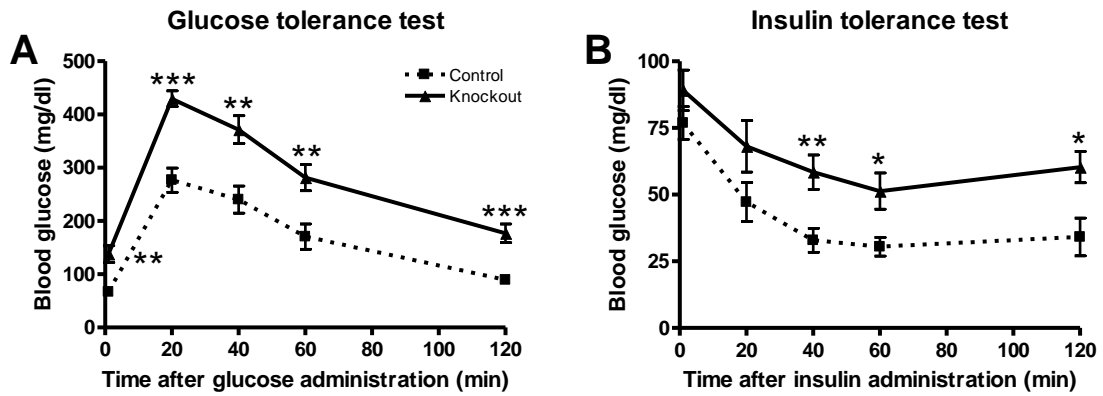


Fig. 4.26 Intraperitoneal glucose tolerance (A) and insulin tolerance (B) tests in $Dro1^{-/-}$ and control mice ($n=9/$ group) after being fed a high-fat diet for 13 and 14 weeks, respectively. Legend displayed in (A) applies to (B). *: $P \leq 0.05$; **: $P \leq 0.01$; ***: $P \leq 0.001$.

4.3.2.3 Organ growth

After knockout and control mice had been exposed to a high-fat diet for 16 weeks they were sacrificed and the organs and carcass were weighted. In accordance with our findings in normal-fed mice, $Dro1^{-/-}$ mice exhibited significantly increased absolute weight of lungs, liver, spleen, kidneys and carcass when compared to controls (Table 4.7). When related to body weight, the weight of heart, lungs, kidneys and carcass was over-proportionally decreased in $Dro1^{-/-}$ mice as compared to controls (Table 4.7). Noteworthy, the liver was remarkably pale and saffron-colored in all $Dro1^{-/-}$ mice but in none of the controls (Fig. 4.27).

Table 4.7 Absolute and relative organ weight in $Dro1^{-/-}$ (knockout) and control (n=9/group) males maintained on a high-fat diet for 16 weeks starting from the 11th day of life. Values are presented as means. Corresponding standard deviations are displayed in brackets. *: $P \leq 0.05$; **: $P \leq 0.01$; ***: $P \leq 0.001$. (-) indicates the absence of significant differences.

	Organ weights (mg)			Relative organ weights (% of body weight)		
	Control	Knockout	Δ	Control	Knockout	Δ
Heart	173 (21)	204 (63)	-	0.54 (0.05)	0.44 (0.11)	*
Lungs	193 (23)	218 (15)	*	0.66 (0.03)	0.48 (0.06)	***
Liver	1491 (192)	2105 (479)	**	4.65 (0.33)	4.55 (0.69)	-
Spleen	92 (63)	199 (81)	**	0.28 (0.16)	0.45 (0.19)	-
Kidneys	398 (43)	468 (71)	*	1.24 (0.07)	1.02 (0.12)	***
Carcass	14012 (1113)	16849 (2116)	**	43.23 (0.90)	37.14 (3.13)	***

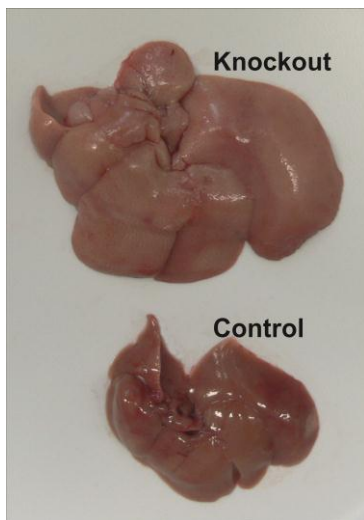


Fig. 4.27 Representative picture of a liver from a $Dro1^{-/-}$ (knockout) and control mouse after fed a high-fat diet for 16 weeks starting from the 11th day of life.

4.3.2.4 Fat pad growth

To investigate the effect of *Dro1* loss on fat pad weight under high-fat diet feeding conditions, the epididymal, abdominal and subcutaneous fat pads of *Dro1*^{-/-} and control mice were weighted after mice had been exposed to a high-fat diet for 16 weeks. Consistent with profound changes in body weight and total body fat content, these fat compartments were dramatically enlarged in *Dro1*^{-/-} males as compared to controls (Fig. 4.28A and Fig.4.29). These changes persisted when fat pad weight was related to body weight (Fig. 4.28B). Microscopic examination of H&E-stained histological sections of the cranial tip of epididymal white adipose tissue from 17-week-old high-fat diet-fed *Dro1*^{-/-} males revealed no obvious pathologic changes

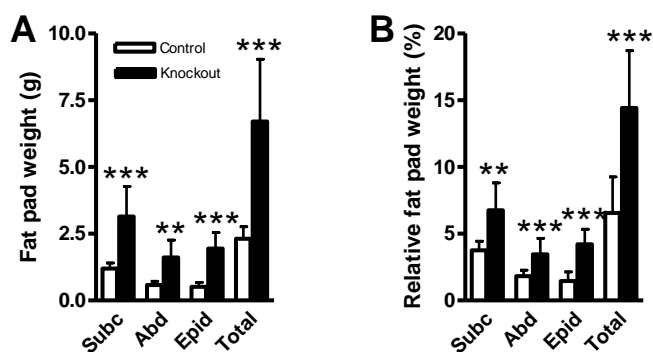


Fig. 4.28 Absolute (A) and relative (B) weight of the subcutaneous (subc), abdominal (abd) and epididymal (epid) white fat pad in *Dro1*^{-/-} (knockout) and control mice (n=9/group) after fed a high-fat diet for 16 weeks starting from the 11th day of life. Relative fat pad weight was calculated as percent of body weight. Legend displayed in (A) applies to (B). **: P ≤ 0.01; ***: P ≤ 0.001.

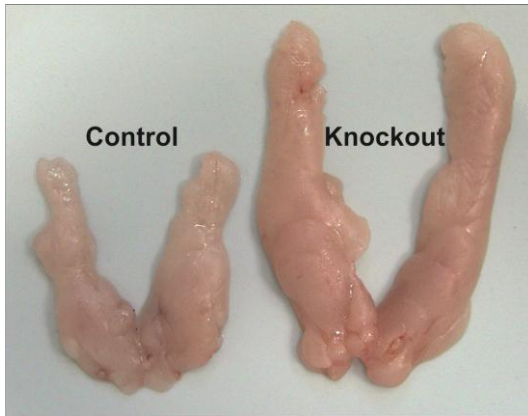


Fig. 4.29 Representative pictures of epididymal white fat pads from a control and $Dro1^{-/-}$ (knockout) mouse after fed a high-fat diet for 16 weeks starting from the 11th day of life.

4.3.2.5 Liver histology

At necropsy, livers of high-fat diet-fed $Dro1^{-/-}$ mice were substantially increased and exhibited a pale appearance. Microscopic evaluation of H&E-stained $Dro1^{-/-}$ liver sections revealed severe mixed steatosis with microvesicular and medium sized fat vacuoles in more than 80% of hepatocytes of the centrilobular region in 4 of 9 $Dro1^{-/-}$ mice (Fig. 4.30A). The remaining cases exhibited macrovesicular or mixed steatosis with fat vacuoles in 20 to 40% of hepatocytes. In contrast, hepatocellular steatosis was not observed in liver sections from control animals (Fig. 4.30A). Colorimetric quantification of triglycerides in homogenized liver samples confirmed significantly elevated triglyceride levels in $Dro1^{-/-}$ mice as compared to controls (Fig. 4.30B). Noteworthy, a slight pericellular and perisinusoidal fibrosis with chicken wire pattern could be demonstrated by EvG staining (Fig. 4.30A). Furthermore, a minor Kupffer cell aggregation was observed.

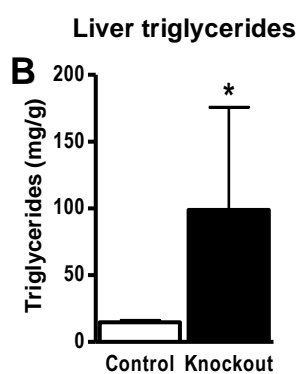
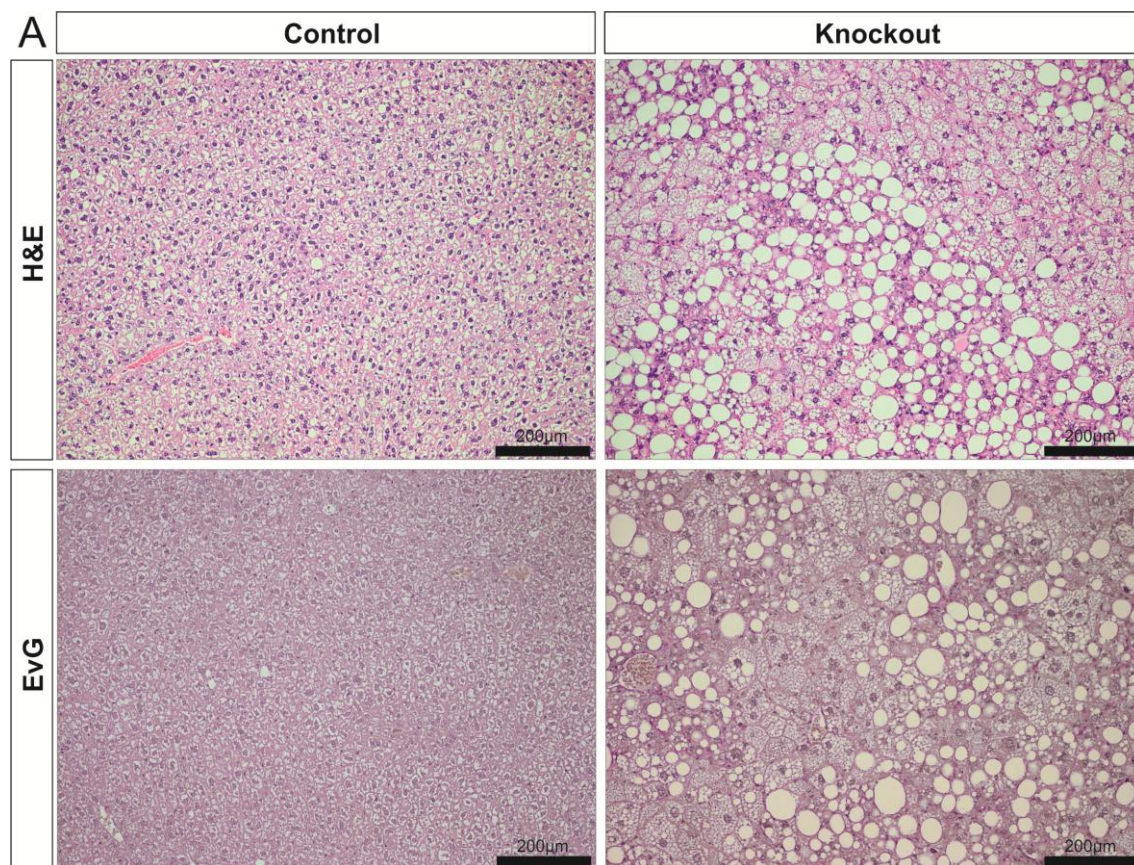


Fig. 4.30 (A) H&E- and EvG-stained liver sections from a control and $Dro1^{-/-}$ (knockout) mouse at 17 weeks of age after maintained on a high-fat diet for 16 weeks starting from the 11th day of age. (B) Mean triglyceride content in livers of control and $Dro1^{-/-}$ mice (n=9/ group). *: $P \leq 0.05$.

4.3.2.6 Serum triglycerides and free fatty acids

To investigate changes in circulating triglycerides and free fatty acids, blood of high-fat diet-fed *Dro1*^{-/-} and control mice was collected after they had been exposed to a high-fat diet for 16 weeks and the serum was isolated. No significant differences were recorded between *Dro1*^{-/-} and control mice in serum triglycerides (Fig. 4.31A) and free fatty acids (Fig. 4.31B).

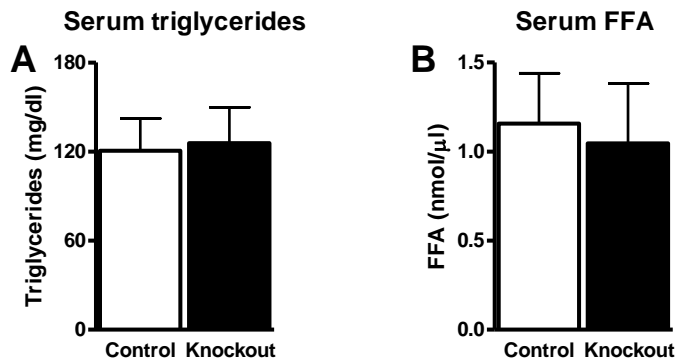


Fig. 4.31 Serum triglycerides (A) and free fatty acids (FFA) (B) in *Dro1*^{-/-} and control mice (n=7/ group) at the age of 17 weeks after exposed to a high-fat diet for 16 weeks.

4.3.3 Analysis of adipogenesis in SV cells

Since down-regulation of *Dro1* in 3T3-L1 cells was demonstrated to impair adipocyte differentiation (Tremblay *et al.*, 2009), a possible impact of *Dro1* loss on adipogenesis in white adipose tissue SV cells containing primary preadipocytes (Hausman *et al.*, 2008; Poulos *et al.*, 2010) was investigated *in vitro*. For this purpose, *Dro1*^{-/-} and control mice were sacrificed at the age of 21 days and SV cells were isolated from the inguinal white fat pads, grown confluent and differentiated. Confluence was reached at day 14 after isolation independently of the *Dro1* status and SV cells were differentiated for additional 14 days. Oil red O staining revealed that the accumulation of lipids was severely increased in differentiated *Dro1*^{-/-} SV cells as compared to control SV cells (Fig. 4.32A), with a significant increase in the mean number (Fig. 4.32B) and size (Fig. 4.32C) of lipid droplets.

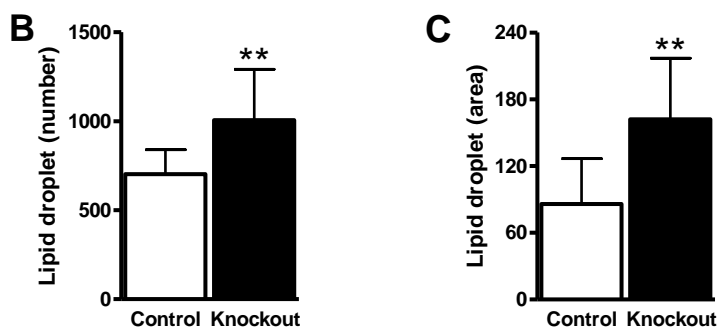
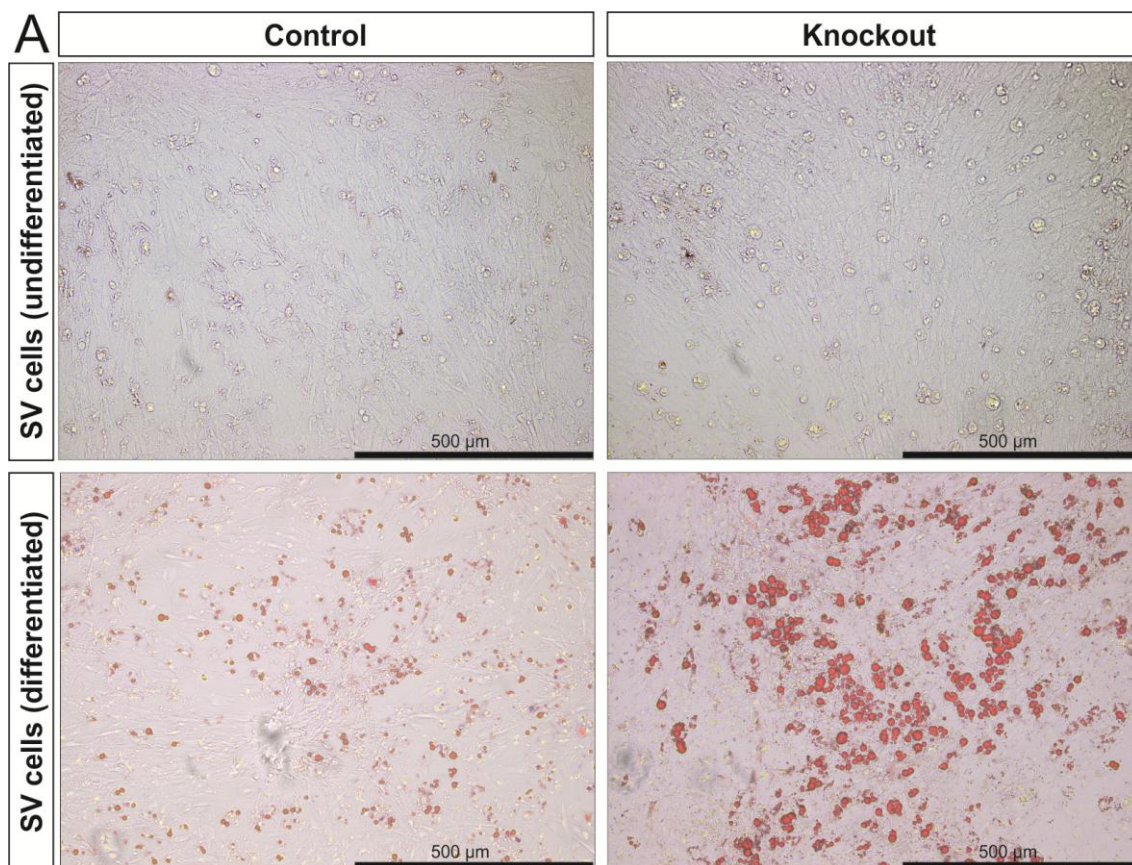


Fig. 4.32 (A) Representative pictures of undifferentiated and differentiated oil red O-stained control and $Dro1^{-/-}$ (knockout) white adipose tissue SV cells. Mean number (B) and mean size (C) of lipid droplets in control and $Dro1^{-/-}$ (knockout) white adipose tissue SV cells. Multiplicity and size of lipid droplets were investigated for areas showing a high grade of differentiated cells ($n=10$ areas for $Dro1^{-/-}$ and $n=8$ areas for control SV cells). **: $P \leq 0.01$.

5. Discussion

Previous *in vitro* studies suggested *DRO1* to be a putative tumor suppressor (Bommer *et al.*, 2005) and modulator of adipogenesis (Tremblay *et al.*, 2009). Until today, investigation of *Dro1* function *in vivo* was restricted to expression analysis, offering evidence for involvement in colorectal, mammary and thyroid carcinogenesis (Marcantonio *et al.*, 2001; Visconti *et al.*, 2003; Bommer *et al.*, 2005), obesity (Aoki *et al.*, 2002; Okada *et al.*, 2008), eye development (Mu *et al.*, 2003) and skeletogenesis (Liu *et al.*, 2004; Wilson *et al.*, 2011). The aim of the present study was to elucidate the function of *Dro1* in colorectal carcinogenesis and body growth *in vivo*. We therefore generated the first knockout mouse model in which the *Dro1* gene is constitutively inactivated using a Cre/loxP strategy.

5.1 Generation of *Dro1*^{-/-} mice

In *Dro1*^{-/-} mice, genetic deletion of *Dro1* by Cre-recombinase was demonstrated by Southern blot analysis with liver genomic DNA from 8-week-old animals. Loss of the targeted exon 2 was further confirmed by PCR analysis from genomic tail tip DNA. As expected from the ubiquitous expression of Cre-recombinase under control of the CMV promoter, no significant *Dro1* expression was detected in various tissues of *Dro1*^{-/-} mice, including white adipose tissue and intestinal epithelium, suggesting a high efficiency of *Dro1* depletion. In accordance with previous findings (Aoki *et al.*, 2002; Liu *et al.*, 2004; Bommer *et al.*, 2005; Okada *et al.*, 2008; Tremblay *et al.*, 2009), control mice expressed *Dro1* in all tissues tested. Unfortunately, it was not possible to investigate *Dro1* expression by Western blot analysis since antibodies raised against human DRO1 were inappropriate to detect the mouse DRO1 protein. This observation is rather surprising considering the high sequence homology between human and mouse *DRO1/Dro1* (Mu *et al.*, 2003; Liu *et al.*, 2004; Bommer *et al.*, 2005).

Dro1^{-/-} mice were viable and fertile and showed no changes in mortality as compared to controls, indicating that *Dro1* expression is dispensable for survival. Depletion of *Dro1* was not observed to cause embryonic lethality since the litter size from *Dro1*^{-/-} parents was unchanged as compared to litters from control animals.

5.2 Effects of *Dro1* loss on intestinal tumor formation

Quantitative analysis of length and wet weight of small intestine and colon revealed no changes in 2-month-old *Dro1*^{-/-} mice, indicating normal intestinal growth. Microscopic evaluation of H&E-stained histologic sections of the intestine from 4-month-old *Dro1*^{-/-} mice revealed no obvious pathologic alterations in the architecture of the intestinal epithelium. As demonstrated by PAS staining, the number and distribution of goblet cells along the crypt-villus-axis was unchanged. In addition, a normal localization of Paneth cells at the bottom of the crypt was observed. These findings offer strong evidence that *Dro1* expression is dispensable for cell maturation and positioning in the intestinal epithelium.

To investigate cell proliferation in the intestinal epithelium, 4-month-old *Dro1*^{-/-} and control mice were injected with BrdU 1 h prior to sacrifice. Immunohistochemical detection of BrdU incorporation revealed no effect on the number of BrdU-positive cells per crypt, suggesting an unchanged proliferative activity. Furthermore, a normal distribution of proliferating cells was observed, with BrdU-positive cells being localized close to the crypt base. As demonstrated by immunohistochemical staining for cleaved caspase-3, the number of apoptotic cells in the intestinal epithelium was also unaffected. Restoration of *DRO1* expression in cancer cell lines has been described to result in sensitization to various apoptotic stimuli (Bommer *et al.*, 2005; Ferragud *et al.*, 2011), however, no pro-apoptotic effect of *DRO1* was observed under standard adherent growth conditions (Bommer *et al.*, 2005). In summary, our data suggest that *Dro1* gene expression is dispensable for the maintenance of the intestinal epithelium.

In vitro studies have implicated *DRO1* to be a candidate tumor suppressor gene (Bommer *et al.*, 2005). To investigate a possible effect of *Dro1* deficiency on spontaneous tumor formation in the intestinal tract, *Dro1*^{-/-} and control mice were sacrificed at the age of 18 months and the intestines were examined. Regardless of the *Dro1* status, no spontaneous tumors of the intestine were observed. It is known that inactivation of a tumor suppressor gene alone is often not sufficient to cause tumorigenesis, and additional mutation events that result in perturbation of other critical signaling pathways are necessary (Berger *et al.*, 2011).

To study the consequences of *Dro1* deficiency on intestinal tumorigenesis in a tumor-prone background, *Dro1*^{-/-} mice were intercrossed with *Apc*^{+/^{Min}} mice, a well-established

intestinal tumor mouse model (Moser *et al.*, 1990). Mice on the $Apc^{+/Min}$ background were monitored daily for symptoms of distress and sacrificed when moribund. Survival was significantly reduced in $Dro1^{-/-};Apc^{+/Min}$ mice as compared to $Apc^{+/Min}$ controls, demonstrating a profound effect of *Dro1* deficiency on morbidity and mortality in $Apc^{+/Min}$ mice.

Microscopic examination of whole-mount colon preparations from moribund and 10-week-old mice revealed that $Dro1^{-/-};Apc^{+/Min}$ mice were characterized by a striking increase in mean colonic tumor multiplicity as compared to $Apc^{+/Min}$ controls, suggesting a critical role for *Dro1* in suppressing tumor initiation in the colon of $Apc^{+/Min}$ mice. The dramatically reduced survival observed in $Dro1^{-/-};Apc^{+/Min}$ mice is most probably due to the severe rise in mean colonic polyp frequency implicating an early onset of morbidity. In cancer cell lines, *DRO1* expression has been shown to impair growth (Bommer *et al.*, 2005) and induce sensitization to various apoptotic stimuli (Bommer *et al.*, 2005; Ferragud *et al.*, 2011). Moreover, overexpression of *DRO1* in mammary cancer cells has been shown to result in up-regulation of B-cell lymphoma 2-associated transcription factor 1 (*BCLAF1*), a death-promoting transcriptional repressor (Ferragud *et al.*, 2011). Resistance to cell death by apoptosis-avoiding mechanisms constitutes one of the hallmarks of cancer cells (Hanahn and Weinberg, 2011). It is therefore tempting to suggest that loss of *Dro1* function supports the survival of nascent tumors in $Apc^{+/Min}$ mice, resulting in an increase in the final number of polyps. The hypothesis that *Dro1* deficiency may promote tumor establishment by providing a survival benefit for adenomas with *Apc* inactivation is further supported by the fact that the primary localization of colonic polyps was unchanged in $Dro1^{-/-};Apc^{+/Min}$ mice as compared to $Apc^{+/Min}$ controls, indicating that tumorigenesis is primarily initiated by loss of *Apc* function. Although $Dro1^{-/-};Apc^{+/Min}$ mice showed a profound increase in mean tumor multiplicity throughout the colon, the percentage distribution of polyps between the proximal and distal colon was unchanged when compared to $Apc^{+/Min}$ control mice. Interestingly, *Dro1* loss did not change the mean size of colonic polyps in $Apc^{+/Min}$ mice.

Histopathologic analysis of tumors isolated from the colon of moribund and 10-week-old animals revealed that $Dro1^{-/-};Apc^{+/Min}$ mice developed adenomas, intramucosal adenocarcinomas and invasive adenocarcinomas, whereas tumors from $Apc^{+/Min}$ controls overall resembled tubular adenomas (a single adenocarcinoma was observed in

the colon of a 10-week-old $Apc^{+/Min}$ control animal). Approximately one third of colonic tumors from moribund $Dro1^{-/-};Apc^{+/Min}$ mice had progressed to malignancy and adenocarcinomas arose in about 50% of $Dro1$ knockout mice. Although local invasion of colonic adenocarcinomas through the lamina muscularis mucosae into the tela submucosa was regularly observed in moribund $Dro1^{-/-};Apc^{+/Min}$ mice, no visible metastatic tumors were recorded at necropsy. This may be explained by the rather early onset of morbidity in $Dro1^{-/-};Apc^{+/Min}$ mice at an average of 94 d, with insufficient time for tumors to generate detectable metastases. Our results also demonstrate that ablation of *Dro1* in $Apc^{+/Min}$ mice leads to the regular formation of colonic adenocarcinomas in young animals, suggesting a critical role for *Dro1* as negative regulator of malignant progression in adenomas with *Apc* inactivation. In accordance, *DRO1* expression has been shown to reduce malignant growth properties (colony formation and anchorage independent growth) in various cancer cell lines (Bommer *et al.*, 2005).

Interestingly, analysis of colonic adenocarcinoma distribution between the proximal and distal colon in moribund $Dro1^{-/-};Apc^{+/Min}$ mice revealed that only a single malignant lesion located to the proximal colon. This asymmetric distribution pattern may be due to differences in the timing of tumor development between the proximal and distal colon. $Dro1^{-/-};Apc^{+/Min}$ mice at the age of 10 weeks had developed no tumors of the proximal colon, but exhibited plenty of lesions in the distal segment. In moribund $Dro1^{-/-};Apc^{+/Min}$ mice, a small number of tumors located to the proximal colon and tumor multiplicity in the distal colon was strongly increased as compared to 10-week-old mice. One can conclude from this that polyps in $Dro1^{-/-};Apc^{+/Min}$ mice arise first in the distal colon before extending to the proximal segment. Therefore, tumors of the distal colon have more time to progress to malignancy than tumors in the proximal segment. Another possibility is a non-requirement of *Dro1* expression for prevention of tumor progression specifically in the proximal colon. Previous studies on human colorectal cancer have shown major genetic differences between tumors of the proximal and distal colon (Distler and Holt, 1997; Iacopetta, 2002; Nawa *et al.*, 2008). It was suggested that differences in gene expression patterns between the proximal and distal colon may underlie site-specific differences in carcinogenesis (Glebov *et al.*, 2003), however, the molecular mechanisms underlying this observation are poorly understood. The development of tumors along different tumorigenic pathways may partly be due to differences between the normal proximal and distal colon, e.g. in the embryonic origin,

vascularization, crypt length, apoptosis rate and metabolism (Iacopetta, 2002). The $Dro1^{-/-};Apc^{+/Min}$ mouse model may provide further evidence that cancers of the proximal and distal colon are under the influence of different molecular pathways.

To investigate a possible effect of *Dro1* loss on Wnt signaling activation and proliferation in tumors from $Apc^{+/Min}$ mice, immunohistochemical staining for β -catenin and Ki-67 were performed on a subset of tumors from moribund $Dro1^{-/-};Apc^{+/Min}$ and $Apc^{+/Min}$ control mice. As expected from *Apc* inactivation in tumors from $Apc^{+/Min}$ mice (Luongo *et al.*, 1994; Shoemaker *et al.*, 1997), pronounced nuclear β -catenin staining was observed in all tumors analyzed, independently of the *Dro1* status. *Dro1* loss did not impact the mean percentage and distribution of cells with nuclear β -catenin accumulation within the neoplastic tissue. In addition, β -catenin localization in adjacent normal intestinal epithelium was unaffected by *Dro1* deficiency. As nuclear β -catenin accumulation is viewed as a hallmark of canonical Wnt signaling activation (MacDonald *et al.*, 2009), these results offer strong evidence that changes in colonic tumor multiplicity and neoplastic progression in $Dro1^{-/-};Apc^{+/Min}$ mice are most probably mediated by pathways other than Wnt/ β -catenin signaling.

Ki-67 immunohistochemical staining showed that cellular proliferation indices were not significantly different between colonic tumors from moribund $Dro1^{-/-};Apc^{+/Min}$ and $Apc^{+/Min}$ control mice, indicating that alterations in cellular proliferation are likely to play only a minor role, if any, in the observed phenotypic alterations.

Elimination of *Dro1* was not found to impact ACF formation in $Apc^{+/Min}$ mice. ACF, putative precursors of adenomas (McLellan and Bird, 1988a; Fenoglio-Preiser and Noffsinger, 1999; Boivin *et al.*, 2003), have been observed in some mouse models of intestinal cancer (Reitmair *et al.*, 1996; Pretlow *et al.*, 2003) and have been demonstrated to be a regular event after treatment with colon carcinogens (McLellan and Bird, 1988a; McLellan and Bird, 1988b). In the untreated $Apc^{+/Min}$ mouse ACF are known to be rare or absent (Reitmair *et al.*, 1996; Song *et al.*, 2000; Boivin *et al.*, 2003).

The *Mom1* allele is known to exert a strong influence on tumor burden in $Apc^{+/Min}$ mice (Gould *et al.*, 1996; McCart *et al.*, 2008). It has been previously shown that $Apc^{+/Min}$ mice carrying the *Mom^R* allele exhibit a significant decrease in tumor multiplicity compared to animals on the *Mom^{S/S}* background (Gould *et al.*, 1996). Analysis of the

Mom1 allelic status in *Dro1*^{-/-};*Apc*^{+/*Min*} and *Apc*^{+/*Min*} control mice revealed that both lines carried the *Mom*^S allele homozygously. This finding clearly demonstrates that differences in colonic polyp numbers between *Dro1*^{-/-};*Apc*^{+/*Min*} and *Apc*^{+/*Min*} control mice are not modulated by differences in the *Mom1* allelic status.

Another important observation is that *Dro1* deficiency did not result in obvious effects on number, size or histopathologic quality of polyps in the small intestine of *Apc*^{+/*Min*} mice, indicating that the *Dro1* tumor suppressor gene function in the intestinal tract is confined to the colon. Recent investigations on the gene expression in the murine intestinal tract have uncovered site-specific differences between the small intestine and colon (Klostermeier *et al.*, 2011). It is therefore conceivable that differences in gene expression pattern between small and large intestine are responsible for the restriction of the tumor suppressor activity of *Dro1* to one compartment.

In summary, the analysis of the first *Dro1* knockout mouse model clearly demonstrates *Dro1* to be an important colonic tumor suppressor gene that suppresses polyp initiation and particularly prevents tumor progression towards malignancy in *Apc*^{+/*Min*} mice. Further studies are needed to clarify the underlying mechanisms for the phenotypic alterations observed in *Dro1*^{-/-};*Apc*^{+/*Min*} mice.

Human colorectal cancer is assumed to develop from adenomatous precursor lesions by the accumulation of multiple independent somatic alterations in oncogenes and tumor suppressor genes (Fearon, 2011). Inactivating mutations of the *APC* tumor suppressor gene are viewed as an early if not initiating event in up to 80% of human sporadic colorectal cancers and implicate the development of a multitude of adenomas in the colon and rectum of FAP patients (Giles *et al.*, 2003; Fearon, 2011). Our findings strongly suggest that loss of *DRO1* may be a critical step in colorectal cancer development by promoting progression to malignancy in adenomas with *APC* inactivation. This role of *DRO1* is supported by the fact that *DRO1* expression has been shown to be highly reduced in the majority of primary colorectal cancer specimens and in numerous colorectal cancer cell lines (Bommer *et al.*, 2005).

5.3 Effects of *Dro1* loss on body growth

Under standard feeding conditions, *Dro1*^{-/-} mice showed normal development until 10 (males) and 12 (females) weeks of age, after which a significant increase in body weight

was observed as compared to gender-matched controls. Analysis of body composition in young males from weeks 4 to 15 by MRI showed that *Dro1* loss causes a mild increase in total body fat by week 14. At the age of 6 months, the observed differences in body weight primarily originated in substantially enlarged epididymal, subcutaneous, and abdominal white fat pads. Our findings demonstrate that loss of *Dro1* causes spontaneous, widespread late-onset obesity, indicating a crucial role for *Dro1* in energy homeostasis and body weight regulation.

When exposed to a high-fat diet for 16 weeks (starting from the 11th day of age), increases in body weight and body fat developed earlier, and remained significantly higher after week 8 as compared to diet-matched controls. Moreover, high-fat diet-fed *Dro1*^{-/-} mice exhibited a significant increase in body mass and body fat when compared to age-matched, normal-fed counterparts. These findings show that the overweight phenotype under standard feeding conditions was not maximal but can further be enhanced by diet.

Femur and nose-rump-length were unchanged in 6-month-old *Dro1*^{-/-} mice, demonstrating that longitudinal growth was not affected by disruption of the *Dro1* gene. This finding offers clear evidence that the observed changes in body mass do not result from alterations in body length. The overweight in *Dro1*^{-/-} mice was further confirmed by a significant increase in relative nose-rump-length, calculated as body weight per cm body length.

Six-month-old normal-fed and 17-week-old high-fat diet-fed *Dro1*^{-/-} mice exhibited a significant increase in the absolute and relative weight of the major white fat pads. Examination of H&E-stained tissue sections from the cranial tip of epididymal white adipose tissue revealed no pathologic alterations, regardless of the feeding condition. During the development of obesity, white adipose tissue expansion can be accomplished by an increase in adipocyte size as well as by the addition of new adipocytes by adipogenesis (Hausman *et al.*, 2001; Vazquez-Vela *et al.*, 2008). White adipose tissue stromal vascular (SV) cells, a fraction enriched for preadipocytes, are often used as a model system to investigate adipogenesis (Gregoire *et al.*, 1998; Hausman *et al.*, 2008; Poulos *et al.*, 2010). SV cells were isolated from inguinal white fat pads from 3-week-old *Dro1*^{-/-} and control mice, grown confluent and differentiated into mature adipocytes.

The differentiated *Dro1*^{-/-} SV culture exhibited a significant increase in multiplicity and size of accumulated oil red O-stained lipid droplets, demonstrating that *Dro1* loss promotes lipid accumulation in SV cells after the induction of adipocyte differentiation. As the number of preadipocytes was not investigated in the freshly isolated SV cell fraction, it cannot be excluded that the observed rise in lipid droplet frequency may partly be due to an increase in the initial number of adipocyte progenitor cells. Lipid accumulation represents one of the hallmarks of adipocyte differentiation (Gregoire *et al.*, 1998; Hausman *et al.*, 2001). It is therefore probable that *Dro1* loss enhances the differentiation potential in SV cells, offering evidence that *Dro1* exerts an inhibitory effect on the maturation of preadipocytes to adipocytes. It is also tempting to suggest that excess body fat in *Dro1*^{-/-} mice may partly result from deregulated adipogenesis, increasing the total number of adipocytes in white adipose tissue. The enhanced adipocyte quantity would be available for additional lipid deposition resulting in obesity. This hypothesis is supported by the fact that 6-month-old normal-fed *Dro1*^{-/-} mice showed a significant decrease in the level of serum triglycerides. White adipose tissue is the primary site for the metabolism of circulating triglyceride-rich lipoproteins by releasing non-esterified fatty acids by the action of the adipocyte-derived lipoprotein lipase (Bamba and Rader, 2007). It can also be speculated that an increase in adipocyte multiplicity would imply more cells for lipoprotein lipase synthesis and triglyceride uptake, leading to a decrease in the level of circulating triglycerides. Future work is needed to investigate the effect of *Dro1* loss on adipose tissue cellularity and triglyceride turnover in detail.

Our results are in sharp contrast to previous findings that noted impaired adipogenesis and lipid accumulation in 3T3-L1 cells following down-regulation of *Dro1* by siRNA (Tremblay *et al.*, 2009). The 3T3-L1 preadipocyte cell line was isolated from Swiss 3T3 mouse cells derived from disaggregated 17- to 19- day embryos and contains a single cell type (Gregoire *et al.*, 1998; Poulos *et al.*, 2010). In contrast, primary SV cells include mesenchymal stem cells, T regulatory cells, endothelial precursor cells, preadipocytes and macrophages (Hausman *et al.*, 2008; Poulos *et al.*, 2010). It has been noted that the patterns and models of adipogenesis derived from established cell lines can dramatically differ from those seen with primary cells (Gregoire *et al.*, 1998; Poulos *et al.*, 2010). It is therefore most probable that the contrasting results obtained from 3T3-L1 and SV cells upon down-regulation/loss of *Dro1* may be due to metabolic and

physiologic differences between the adipogenic cell models employed. As SV fractions contain various cell types, the *in vitro* conditions may mimic *in vivo* conditions of adipose tissue complexity more closely than cultures of a single cell type (Poulos *et al.*, 2010).

An important finding is that loss of *Dro1* function causes a profound rise in lean mass from week 9 onwards, demonstrating the contribution of non-adipose tissue mass to the overweight phenotype. In *Dro1*^{-/-} mice, maintenance on a high-fat diet for 16 weeks starting from the 11th day of age caused a substantial increase in lean mass as compared to age-matched, normal-fed counterparts. In accordance to previous data on diet-induced obesity in C57BL/6 mice (Park *et al.*; 2005; Matyskova *et al.*, 2008), high-fat diet feeding had no effect on lean mass in control mice.

At the age of 2 months, when body weight of *Dro1*^{-/-} mice was not significantly different from that of control mice, absolute and relative spleen weight was significantly increased in *Dro1*^{-/-} males. At the age of 6 months a significant rise in liver, spleen and carcass weight was detected in both genders of *Dro1*^{-/-} mice as compared to age- and gender-matched controls. Moreover, the weight of lungs and kidneys was profoundly increased in 6-month-old *Dro1*^{-/-} males. In 17-week-old high-fat diet-fed *Dro1*^{-/-} mice, the absolute weight of lungs, liver, spleen and kidneys was significantly increased. These findings indicate an important role for *Dro1* in the growth of these organs. Changes in absolute weight did not persist when related to body weight, demonstrating that increases in organ weight were proportional to the rise in body mass. In 6-month-old normal-fed females, the relative weight of heart and kidneys was significantly decreased. The same was true for heart, lungs and kidneys under high-fat diet feeding, demonstrating that increases in absolute weight were insufficient to follow the increase in body weight. Furthermore, 6-month-old normal-fed and 17-week-old high-fat diet-fed *Dro1*^{-/-} mice exhibited a significant rise in the absolute weight of carcass. Under high-fat diet feeding conditions, the increase was disproportional to the increase in body weight. The carcass is a complex structure composed of muscle, bone, connective tissue and fat. Thus, further studies are needed to clarify the effects of *Dro1* loss on carcass composition.

Examination of H&E-stained tissue sections of various organs from normal-fed 2- and 6-month-old *Dro1*^{-/-} mice showed no histopathologic changes. When exposed to a high-fat diet for 16 weeks *Dro1*^{-/-} mice exhibited severe hepatosteatorosis that was

accompanied by a minor Kupffer cell aggregation and a slight pericellular and perisinusoidal fibrosis. Hepatosteatosis did not progress to steatohepatitis. No histopathologic changes were observed in the livers from diet-matched controls. Increased lipid deposition was further confirmed by a significant rise in the level of triglycerides in homogenized liver samples. In *Dro1*^{-/-} mice, maintenance on a high-fat diet implicated a profound rise in total body fat compared to normal-fed counterparts and high-fat diet-fed controls. As excess body fat is known to be a major risk factor for the development of fatty liver disease (Hebbard and George, 2010; Cohen *et al.*, 2011), it is reasonable to suggest that lipid deposition in livers from high-fat diet-fed *Dro1*^{-/-} mice develops secondary to the severe obesity caused by *Dro1* loss.

As demonstrated by intraperitoneal glucose tolerance test, 14-week-old standard-fed *Dro1*^{-/-} mice showed normal fasted blood glucose and cleared glucose from the blood as efficiently as controls, offering strong evidence that glucose metabolism is unaffected by *Dro1* loss. However, 14-week-old high-fat diet-fed *Dro1*^{-/-} mice exhibited glucose intolerance characterized by a significant increase in fasted blood glucose and a substantially decreased ability to eliminate glucose from the blood as compared to diet-matched controls. The impaired glucose tolerance was associated with insulin resistance, characterized by a significantly decreased glucose lowering rate after insulin injection as compared to controls. Excess body fat accumulation is known to be a major risk factor for the development of type 2 diabetes (Bays *et al.*, 2008). It is therefore likely that changes in glucose metabolism in high-fat diet-fed *Dro1*^{-/-} mice are secondary to obesity.

Free fatty acid serum levels were unchanged in 2- and 6-month-old normal-fed *Dro1*^{-/-} mice as compared to diet-matched controls. The same was true after maintenance on a high-fat diet for 16 weeks. In general, circulating free fatty acids are a net result of the amount of free fatty acids released from adipose tissue and free fatty acids taken up by liver, skeletal and cardiac muscle (Karpe *et al.*, 2011). These results therefore indicate that *Dro1* is most probably not involved in the turnover of free fatty acids.

In summary, our results demonstrate that *Dro1* plays a crucial role in body growth as *Dro1* loss causes the development of general late-onset obesity and stimulates the growth of lungs, liver, spleen, kidneys and carcass. Moreover, we identified *Dro1* as a

putative inhibitor of adipogenesis *in vitro*, suggesting that *Dro1* might control fat cell multiplicity in white adipose tissue depots. In the development of obesity, excess energy is initially stored by an increase in fat cell size, however, once a critical cell size has been reached, further energy storage is accomplished by the addition of new adipocytes by adipogenesis (Hausman *et al.*, 2001; Guilherme *et al.*, 2008). Impaired adipogenesis implicates excessive adipocyte hypertrophy which is thought to be one of the major risk factors for the development of metabolic disease (Bays *et al.*, 2008). As *Dro1* expression impairs the maturation of preadipocytes to adipocytes in SV cells, our findings suggest that down-regulation of *Dro1* in adipose tissue might be a critical step to allow an increase in the number of adipocytes for further energy storage. This suggestion is supported by the fact that *Dro1* was shown to be down-regulated in epididymal white adipose tissue of several obese mouse models (Okada *et al.*, 2008).

Previously, DRO1 was demonstrated to be secreted from 3T3-L1 mature adipocytes and was therefore supposed to be a novel adipokine that might influence whole body energy homeostasis (Tremblay *et al.*, 2009). In the future, a detailed analysis of energy homeostasis in *Dro1*^{-/-} mice could improve our understanding of *Dro1* functions in the development of obesity and provide valuable information on potentially involved signaling pathways.

5.4 Final considerations

The *Apc*^{+/*Min*} mouse represents a widely used, well-characterized mouse model of intestinal neoplasia. However, the usefulness of *Apc*^{+/*Min*} mice for the study of colorectal carcinogenesis is limited since *Apc*^{+/*Min*} mice mainly develop adenomas of the small intestine and only few lesions in the colon. Moreover, progression to malignancy is rare, a fact that is probably due to the short lifespan of *Apc*^{+/*Min*} mice (Shoemaker *et al.*, 1997; McCart *et al.*, 2008). In the present study, we demonstrate that inactivation of *Dro1* on the *Apc*^{+/*Min*} background strongly enhances tumor multiplicity in the colon and frequently leads to the development of colonic adenocarcinomas. Thus, *Dro1*^{-/-};*Apc*^{+/*Min*} mice recapitulate the characteristics of human sporadic colorectal cancer and inherited FAP more closely than *Apc*^{+/*Min*} animals. The *Dro1*^{-/-};*Apc*^{+/*Min*} mouse model described here may therefore facilitate the study of colorectal tumorigenesis, the role of other genes in adenoma-carcinoma transition, and potential cancer prevention and treatment strategies.

There is accumulating evidence suggesting that greater body fatness and greater abdominal fatness are associated with an increased risk to develop cancer of the colorectum (World Cancer Research Fund, 2007). However, until today, the mechanisms underlying this observation remain widely unknown. As *Dro1* loss results in the development of general late-onset obesity characterized by significantly enlarged epididymal, abdominal and subcutaneous white fat pads, the *Dro1*^{-/-} mouse model could provide a valuable tool to investigate the correlation between obesity and colorectal cancer.

6. Summary

Effects of *Dro1* loss on colorectal carcinogenesis and body growth in a constitutive knockout mouse model

Previous studies suggested *DRO1* to be a putative tumor suppressor gene that is down-regulated in various colorectal and pancreatic cancer cell lines, in the majority of colorectal cancer specimens (Bommer *et al.*, 2005) and in thyroid neoplastic cell lines and carcinomas (Visconti *et al.*, 2003). Re-expression of *DRO1* in several cancer cell lines reduced their malignant growth properties (Bommer *et al.*, 2005) and induced their sensitization to pro-apoptotic stimuli (Bommer *et al.*, 2005; Ferragud *et al.*, 2011).

DRO1/Dro1 is a gene predominantly expressed in white adipose tissue with considerably lower expression levels in other tissues (Aoki *et al.*, 2002; Liu *et al.*, 2004; Bommer *et al.*, 2005; Okada *et al.*, 2008; Tremblay *et al.*, 2009). *Dro1* was demonstrated to be profoundly decreased in epididymal white adipose tissue of several obese mouse models (Okada *et al.*, 2008). In 3T3-L1 cells, *Dro1* was implicated as a bidirectional modulator of adipogenesis (Tremblay *et al.*, 2009). Moreover, *DRO1* was found to be a secreted protein from 3T3-L1 adipocytes, indicating a role as novel adipokine that might influence adipose tissue homeostasis and whole body energy metabolism and might be involved in the development of obesity (Tremblay *et al.*, 2009).

The aim of the present study was to investigate the effects of *Dro1* loss on colorectal carcinogenesis and body growth *in vivo*. We therefore generated the first knockout mouse model in which the *Dro1* gene is constitutively inactivated (*Dro1*^{-/-}) using a Cre/lox-P strategy. Genetic deletion of *Dro1* by Cre-recombinase was demonstrated by Southern blot and further confirmed by PCR analysis. RT-PCR demonstrated no significant *Dro1* expression in various organs from *Dro1*^{-/-} mice, suggesting a high efficiency of *Dro1* depletion. *Dro1*^{-/-} mice were viable and fertile and showed no changes in lifespan.

Loss of *Dro1* had no effects on length and wet weight of the intestine. Moreover, no changes in cell maturation, positioning and the rate of proliferation and apoptosis were observed in the intestinal epithelium. *Dro1*^{-/-} mice did not develop intestinal tumors spontaneously. To investigate the effects of *Dro1* loss on intestinal tumor formation, *Dro1*^{-/-} mice were crossed into the *Apc*^{+/^{Min}} background, a widely used intestinal tumor

mouse model (Moser *et al.*, 1990). $Dro1^{-/-};Apc^{+/Min}$ mice were characterized by significantly reduced survival and a striking increase in colonic tumor multiplicity as compared to $Apc^{+/Min}$ controls. Specifically, *Dro1* loss promoted progression to malignancy in colonic tumors from $Apc^{+/Min}$ mice. Approximately one third of colonic tumors from moribund $Dro1^{-/-};Apc^{+/Min}$ mice had progressed to malignancy whereas colonic lesions from $Apc^{+/Min}$ controls resembled tubular adenomas.

Changes in colonic tumor multiplicity and neoplastic progression in $Dro1^{-/-};Apc^{+/Min}$ mice are most probably mediated by pathways other than Wnt/ β -catenin signaling and alterations in cellular proliferation are likely to play only a minor role, if any, in the observed phenotypic alterations. *Dro1* deficiency did not result in obvious effects on number, size or histopathologic quality of polyps in the small intestine of $Apc^{+/Min}$ mice, suggesting a site-specific tumor suppressor role in the colon. Our findings clearly demonstrate *Dro1* to be an important colonic tumor suppressor gene that suppresses polyp initiation and particularly prevents tumor progression towards malignancy in $Apc^{+/Min}$ mice.

$Dro1^{-/-}$ mice showed normal development until 10 (males) and 12 (females) weeks of age, after which a significant increase in body weight was observed that was not mediated by changes in longitudinal growth. At the age of 6 months, $Dro1^{-/-}$ mice exhibited substantially enlarged major white fat pads and a significant rise in the weight of lungs, liver, spleen, kidneys and carcass. The effects of *Dro1* loss on body, organ and fat pad growth could further be enhanced by high-fat diet feeding conditions. Isolation and differentiation of white adipose tissue stromal vascular (SV) cells revealed that ablation of *Dro1* significantly enhances the differentiation potential of these cells. Our results demonstrate a significant role for *Dro1* in whole body growth. Moreover, we identified *Dro1* to be a putative inhibitor of adipogenesis in primary SV culture, indicating a probable role in controlling fat cell multiplicity in white adipose tissue depots.

The $Dro1^{-/-};Apc^{+/Min}$ mouse model described here is likely to facilitate efforts to study colorectal tumorigenesis mechanisms, the role of other genes in adenoma-carcinoma transition and potential cancer prevention and treatment strategies. In addition, the $Dro1^{-/-}$ mouse model may provide a valuable tool to investigate the correlation between obesity and colorectal cancer.

7. Zusammenfassung

Auswirkungen des Verlustes von *Dro1* auf die kolorektale Karzinogenese und das Körperwachstum in einem konstitutiven Knockout-Mausmodell

Vorangehende Untersuchungen konnten zeigen, dass die *DRO1* Expression in verschiedenen Kolonkarzinom- und Pankreaskrebszelllinien und in der Mehrzahl kolorektaler Primärkarzinome stark vermindert ist (Bommer *et al.*, 2005). Entsprechendes wurde für Schilddrüsenkrebszelllinien und -karzinome berichtet (Visconti *et al.*, 2003). Eine Reexpression von *DRO1* in verschiedenen Krebszelllinien reduziert deren maligne Wachstumseigenschaften (Bommer *et al.*, 2005) und erhöht deren Sensitivität gegenüber pro-apoptischen Stimuli (Bommer *et al.*, 2005; Ferragud *et al.*, 2011). Ausgehend von diesen Befunden, wurde vermutet, dass *DRO1* ein potentielles Tumorsuppressorgen ist (Bommer *et al.*, 2005).

Es ist bekannt, dass *DRO1/Dro1* ubiquitär, vor allem jedoch im weißen Fettgewebe exprimiert wird (Aoki *et al.*, 2002; Liu *et al.*, 2004; Bommer *et al.*, 2005; Okada *et al.*, 2008; Tremblay *et al.*, 2009). Eine starke Verminderung der *Dro1* Expression wurde im epididymalen weißen Fettgewebe verschiedener Adipositas-Mausmodelle nachgewiesen (Okada *et al.*, 2008). Untersuchungen in 3T3-L1 Zellen weisen darauf hin, dass *Dro1* ein bidirektionaler Modulator der Adipogenese ist (Tremblay *et al.*, 2009). Es konnte gezeigt werden, dass *DRO1* von 3T3-L1 Adipozyten sezerniert wird (Tremblay *et al.*, 2009). Dies lässt vermuten, dass *DRO1* ein neues Adipokin sein könnte, das eine wichtige Funktion in der Homöostase des weißen Fettgewebes, in der Regulation des Energiehaushaltes und in der Entwicklung von Adipositas übernimmt (Tremblay *et al.*, 2009).

Das Ziel der vorliegenden Studie war es, die Folgen eines Verlustes von *Dro1* auf die kolorektale Karzinogenese und des Körperwachstums *in vivo* zu untersuchen. Aus diesem Grund haben wir unter Verwendung des Cre/lox-P-Systems das erste Mausmodell generiert, in welchem *Dro1* konstitutiv inaktiviert ist. Southern blot und weiterführende PCR Analysen bestätigten die korrekte Rekombination durch die Cre-Rekombinase im *Dro1* Gen. Zudem konnte mit RT-PCR keine signifikante *Dro1* Expression in verschiedenen Organen der *Dro1*^{-/-} Maus nachgewiesen werden. *Dro1*^{-/-} Mäuse waren lebensfähig, fertil und zeigten keine Veränderung in der Lebenserwartung.

Der Verlust von *Dro1* hatte keinen Einfluss auf die Länge und das Nassgewicht des Darms. Im intestinalen Epithel konnten keine Veränderungen in der Zellausreifung und -positionierung sowie in der Proliferations- und Apoptoserate beobachtet werden. Da *Dro1*^{-/-} Mäuse keine spontanen Darmtumoren bilden, wurden sie in den *Apc*^{+/^{Min} Hintergrund eingekreuzt, ein gut etabliertes intestinales Tumormausmodell (Moser *et al.*, 1990). Im Vergleich zu *Apc*^{+/^{Min} Kontrolltieren zeigten *Dro1*^{-/-};*Apc*^{+/^{Min} Mäuse eine signifikant reduzierte Lebenserwartung und eine bedeutende Erhöhung der Tumorlast im Kolon. Im Besonderen fördert der Verlust von *Dro1* die Progression vom Adenom zum Karzinom im Kolon von *Apc*^{+/^{Min} Mäusen. Ungefähr ein Drittel der untersuchten Kolontumoren aus moribunden *Dro1*^{-/-};*Apc*^{+/^{Min} Mäusen wurden als Adenokarzinome identifiziert, wohingegen alle Tumoren aus dem Kolon der *Apc*^{+/^{Min} Kontrollmäuse Adenome waren.}}}}}}

Die beobachteten Veränderungen in der Tumorzahl und Tumorprogression in *Dro1*^{-/-};*Apc*^{+/^{Min} Mäusen werden höchstwahrscheinlich durch andere Signalwege als den kanonischen Wnt/ β -catenin Signalweg vermittelt. Auch spielen Veränderungen der Proliferationsrate im Tumorgewebe keine oder nur eine untergeordnete Rolle für die Ausbildung des Darmphänotyps in *Dro1*^{-/-};*Apc*^{+/^{Min} Mäusen. Der Verlust von *Dro1* hatte keinen Einfluss auf die Anzahl, Verteilung und Histologie der Tumoren im Dünndarm von *Apc*^{+/^{Min} Mäusen. Dies weist darauf hin, dass die Tumorsuppressorfunktion von *Dro1* spezifisch für das Kolon ist. Unsere Befunde zeigen deutlich, dass *Dro1* ein wichtiges Tumorsuppressorgen im Kolon *in vivo* ist, das die Tumorinitiation unterdrückt und im Besonderen die Tumorprogression in *Apc*^{+/^{Min} Mäusen verhindert.}}}}

Dro1^{-/-} Mäuse entwickelten sich normal bis zur 10. (Männchen) bzw. 12. (Weibchen) Lebenswoche. Danach wurde eine signifikante Erhöhung des Körpergewichts beobachtet, die nicht mit Veränderungen des Längenwachstums einherging. Im Alter von 6 Monaten zeigten *Dro1*^{-/-} Mäuse stark vergrößerte weiße Fettdepots und eine signifikante Erhöhung des Gewichts von Lunge, Leber, Milz, Niere und Karkasse. Das Füttern einer fettreichen Diät verstärkte die Auswirkungen des Verlusts von *Dro1* auf die Körpergewichtsentwicklung und das Wachstum der Organe und Fettdepots. Isolierung und Differenzierung von primären Stromazellen (stromal vascular (SV) cells) aus weißem Fettgewebe zeigten, dass der Verlust von *Dro1* zu einer Steigerung des Differenzierungspotentials in diesen Zellen führt. Unsere Ergebnisse demonstrieren, dass *Dro1* eine bedeutsame Rolle im Körperwachstum spielt. Des Weiteren wurde *Dro1*

in primären SV Zellen als potentieller Inhibitor der Adipogenese identifiziert. Dies weist darauf hin, dass *Dro1* die Anzahl der Adipozyten im weißen Fettgewebe kontrollieren könnte.

Das hier beschriebene *Dro1*^{-/-};*Apc*^{+/^{Min} Mausmodell sollte die zukünftige Erforschung der kolorektalen Karzinogenese, der Funktion weiterer Gene in der Adenom-Karzinom-Sequenz sowie potentieller Krebsvorsorge und -behandlungsmethoden vorantreiben. Des Weiteren könnte die *Dro1*^{-/-} Maus ein wertvolles Modell sein, um den Zusammenhang zwischen Adipositas und der Entstehung des Kolonkarzinoms aufzuklären.}

8. Bibliography

Ahima RS, Osei SY: Adipokines in obesity. *Front Horm Res.* 2008;36:182-97.

Ailhaud G: Adipose tissue as a secretory organ: from adipogenesis to the metabolic syndrome. *C R Biol.* 2006 Aug;329(8):570-7; discussion 653-5.

Andreu P, Colnot S, Godard C, Gad S, Chafey P, Niwa-Kawakita M, Laurent-Puig P, Kahn A, Robine S, Perret C, Romagnolo B: Crypt-restricted proliferation and commitment to the Paneth cell lineage following Apc loss in the mouse intestine. *Development.* 2005 Mar;132(6):1443-51.

Aoki K, Sun YJ, Aoki S, Wada K, Wada E: Cloning, expression, and mapping of a gene that is upregulated in adipose tissue of mice deficient in bombesin receptor subtype-3. *Biochem Biophys Res Commun.* 2002 Feb 1;290(4):1282-8.

Arnold CN, Goel A, Blum HE, Boland CR: Molecular pathogenesis of colorectal cancer: implications for molecular diagnosis. *Cancer.* 2005 Nov 15;104(10):2035-47.

Bamba V, Rader DJ: Obesity and atherogenic dyslipidemia. *Gastroenterology.* 2007 May;132(6):2181-90.

Bays HE, González-Campoy JM, Bray GA, Kitabchi AE, Bergman DA, Schorr AB, Rodbard HW, Henry RR: Pathogenic potential of adipose tissue and metabolic consequences of adipocyte hypertrophy and increased visceral adiposity. *Expert Rev Cardiovasc Ther.* 2008 Mar;6(3):343-68.

Bennett CN, Ross SE, Longo KA, Bajnok L, Hemati N, Johnson KW, Harrison SD, MacDougald OA: Regulation of Wnt signaling during adipogenesis. *J Biol Chem.* 2002 Aug 23;277(34):30998-1004.

Berger AH, Knudson AG, Pandolfi PP: A continuum model for tumour suppression. *Nature.* 2011 Aug 10;476(7359):163-9.

Bienz M, Clevers H: Linking colorectal cancer to Wnt signaling. *Cell.* 2000 Oct 13;103(2):311-20.

Bird RP: Observation and quantification of aberrant crypts in the murine colon treated with a colon carcinogen: preliminary findings. *Cancer Lett.* 1987 Oct 30;37(2):147-51.

Boden G: Obesity and free fatty acids. *Endocrinol Metab Clin North Am.* 2008 Sep;37(3):635-46, VIII-IX.

Boivin GP, Washington K, Yang K, Ward JM, Pretlow TP, Russell R, Besselsen DG, Godfrey VL, Doetschman T, Dove WF, Pitot HC, Halberg RB, Itzkowitz SH, Groden J, Coffey RJ: Pathology of mouse models of intestinal cancer: consensus report and recommendations. *Gastroenterology.* 2003 Mar;124(3):762-77.

Bommer GT, Jäger C, Dürr EM, Baehs S, Eichhorst ST, Brabletz T, Hu G, Fröhlich T, Arnold G, Kress DC, Göke B, Kolligs FT: DRO1, a gene down-regulated by oncogenes, mediates growth inhibition in colon and pancreatic cancer cells. *J Biol Chem.* 2005 Mar 4;280(9):7962-75.

Brunt EM, Tiniakos DG: Histopathology of nonalcoholic fatty liver disease. *World J Gastroenterol.* 2010 Nov 14;16(42):5286-96.

Buettner R, Schölmerich J, Bollheimer LC: High-fat diets: modeling the metabolic disorders of human obesity in rodents. *Obesity (Silver Spring).* 2007 Apr;15(4):798-808.

Buske P, Galle J, Barker N, Aust G, Clevers H, Loeffler M: A comprehensive model of the spatio-temporal stem cell and tissue organisation in the intestinal crypt. *PLoS Comput Biol.* 2011 Jan 6;7(1):e1001045.

Cannon B, Nedergaard J: Brown adipose tissue: function and physiological significance. *Physiol Rev.* 2004 Jan;84(1):277-359.

Carobbio S, Rodriguez-Cuenca S, Vidal-Puig A: Origins of metabolic complications in obesity: ectopic fat accumulation. The importance of the qualitative aspect of lipotoxicity. *Curr Opin Clin Nutr Metab Care.* 2011 Nov;14(6):520-6.

Cha SY, Sung YK, Im S, Kwack MH, Kim MK, Kim JC: URB expression in human dermal papilla cells. *J Dermatol Sci.* 2005 Aug;39(2):128-30.

Cheung KJ, Tzamelis I, Pissios P, Rovira I, Gavrilova O, Ohtsubo T, Chen Z, Finkel T, Flier JS, Friedman JM: Xanthine oxidoreductase is a regulator of adipogenesis and PPARgamma activity. *Cell Metab.* 2007 Feb;5(2):115-28

Christodoulides C, Scarda A, Granzotto M, Milan G, Dalla Nora E, Keogh J, De Pergola G, Stirling H, Pannacciulli N, Sethi JK, Federspil G, Vidal-Puig A, Farooqi IS, O'Rahilly S, Vettor R: WNT10B mutations in human obesity. *Diabetologia.* 2006 Apr;49(4):678-84.

Cinti S: The adipose organ. *Prostaglandins Leukot Essent Fatty Acids.* 2005 Jul;73(1):9-15.

Cinti S, Mitchell G, Barbatelli G, Murano I, Ceresi E, Faloia E, Wang S, Fortier M, Greenberg AS, Obin MS: Adipocyte death defines macrophage localization and function in adipose tissue of obese mice and humans. *J Lipid Res.* 2005 Nov;46(11):2347-55.

Cinti S: Transdifferentiation properties of adipocytes in the Adipose Organ. *Am J Physiol Endocrinol Metab.* 2009 Nov;297(5):E977-86.

Clevers H: Wnt/beta-catenin signaling in development and disease. *Cell.* 2006 Nov 3;127(3):469-80.

Cohen JC, Horton JD, Hobbs HH: Human fatty liver disease: old questions and new insights. *Science.* 2011 Jun 24;332(6037):1519-23.

Conrad M, Brielmeier M, Wurst W, Bornkamm GW: Optimized vector for conditional gene targeting in mouse embryonic stem cells. *Biotechniques.* 2003 Jun;34(6):1136-8, 1140.

Curtin K, Slattery ML, Samowitz WS: CpG island methylation in colorectal cancer: past, present and future. *Patholog Res Int.* 2011 Apr 12;2011:902674.

DiGirolamo M, Fine JB, Tagra K, Rossmanith R: Qualitative regional differences in adipose tissue growth and cellularity in male Wistar rats fed ad libitum. *Am J Physiol.* 1998 May;274(5 Pt 2):R1460-7.

Distler P, Holt PR: Are right- and left-sided colon neoplasms distinct tumors? *Dig Dis.* 1997 Jul-Oct;15(4-5):302-11.

Fearon ER, Vogelstein B: A genetic model for colorectal tumorigenesis. *Cell.* 1990 Jun 1;61(5):759-67.

Fearon ER: Molecular genetics of colorectal cancer. *Annu Rev Pathol.* 2011 Feb 28;6:479-507.

Fenoglio-Preiser CM, Noffsinger A: Aberrant crypt foci: A review. *Toxicol Pathol.* 1999 Nov-Dec;27(6):632-42.

Ferragud J, Avivar-Valderas A, Pla A, De Las Rivas J, de Mora JF: Transcriptional repression of the tumor suppressor DRO1 by AIB1. *FEBS Lett.* 2011 Oct 3;585(19):3041-6.

Fodde R, Brabletz T: Wnt/beta-catenin signaling in cancer stemness and malignant behavior. *Curr Opin Cell Biol.* 2007 Apr;19(2):150-8.

Gesta S, Tseng YH, Kahn CR: Developmental origin of fat: tracking obesity to its source. *Cell.* 2007 Oct 19;131(2):242-56.

Giles RH, van Es JH, Clevers H: Caught up in a Wnt storm: Wnt signaling in cancer. *Biochim Biophys Acta.* 2003 Jun 5;1653(1):1-24.

Glebov OK, Rodriguez LM, Nakahara K, Jenkins J, Cliatt J, Humbyrd CJ, DeNobile J, Soballe P, Simon R, Wright G, Lynch P, Patterson S, Lynch H, Gallinger S, Buchbinder A, Gordon G, Hawk E, Kirsch IR: Distinguishing right from left colon by the pattern of gene expression. *Cancer Epidemiol Biomarkers Prev.* 2003 Aug;12(8):755-62.

Gojis O, Rudraraju B, Alifrangis C, Krell J, Libalova P, Palmieri C: The role of steroid receptor coactivator-3 (SRC-3) in human malignant disease. *Eur J Surg Oncol.* 2010 Mar;36(3):224-9.

Gould KA, Dietrich WF, Borenstein N, Lander ES, Dove WF: Mom1 is a semi-dominant modifier of intestinal adenoma size and multiplicity in Min/+ mice. *Genetics*. 1996 Dec;144(4):1769-76.

Gregoire FM, Smas CM, Sul HS: Understanding adipocyte differentiation. *Physiol Rev*. 1998 Jul;78(3):783-809.

Grossmann J, Walther K, Artinger M, Rümmele P, Woenckhaus M, Schölmerich J: Induction of apoptosis before shedding of human intestinal epithelial cells. *Am J Gastroenterol*. 2002 Jun;97(6):1421-8.

Guilherme A, Virbasius JV, Puri V, Czech MP: Adipocyte dysfunctions linking obesity to insulin resistance and type 2 diabetes. *Nat Rev Mol Cell Biol*. 2008 May;9(5):367-77.

Gupta AK, Schoen RE: Aberrant crypt foci: are they intermediate endpoints of colon carcinogenesis in humans? *Curr Opin Gastroenterol*. 2009 Jan;25(1):59-65.

Halberg RB, Katzung DS, Hoff PD, Moser AR, Cole CE, Lubet RA, Donehower LA, Jacoby RF, Dove WF: Tumorigenesis in the multiple intestinal neoplasia mouse: redundancy of negative regulators and specificity of modifiers. *Proc Natl Acad Sci U S A*. 2000 Mar 28;97(7):3461-6.

Hanahan D, Weinberg RA: Hallmarks of cancer: the next generation. *Cell*. 2011 Mar 4;144(5):646-74.

Hausman DB, DiGirolamo M, Bartness TJ, Hausman GJ, Martin RJ: The biology of white adipocyte proliferation. *Obes Rev*. 2001 Nov;2(4):239-54.

Hausman DB, Park HJ, Hausman GJ: Isolation and culture of preadipocytes from rodent white adipose tissue. *Methods Mol Biol*. 2008;456:201-19.

Hawk ET, Levin B: Colorectal cancer prevention. *J Clin Oncol*. 2005 Jan 10;23(2):378-91.

Hebbard L, George J: Animal models of nonalcoholic fatty liver disease. *Nat Rev Gastroenterol Hepatol*. 2011 Jan;8(1):35-44.

Hedrich H: The laboratory mouse. *Elsevier Academic Press*. 2004.

Hees H, Sinowatz F: Histologie: Kurzlehrbuch der Zytologie und mikroskopischen Anatomie. 3., überarb. Aufl. *Deutscher Ärzte-Verlag*. 2000. 267-276. 142-144; 245-250.

Hinoi T, Akyol A, Theisen BK, Ferguson DO, Greenson JK, Williams BO, Cho KR, Fearon ER: Mouse model of colonic adenoma-carcinoma progression based on somatic Apc inactivation. *Cancer Res*. 2007 Oct 15;67(20):9721-30.

Iacopetta B: Are there two sides to colorectal cancer? *Int J Cancer*. 2002 Oct 10;101(5):403-8.

Karpe F, Dickmann JR, Frayn KN: Fatty acids, obesity, and insulin resistance: time for a reevaluation. *Diabetes*. 2011 Oct;60(10):2441-9.

Kennell JA, MacDougald OA: Wnt signaling inhibits adipogenesis through beta-catenin-dependent and -independent mechanisms. *J Biol Chem*. 2005 Jun 24;280(25):24004-10.

Kerber RA, Neklason DW, Samowitz WS, Burt RW: Frequency of familial colon cancer and hereditary nonpolyposis colorectal cancer (Lynch syndrome) in a large population database. *Fam Cancer*. 2005;4(3):239-44.

Klostermeier UC, Barann M, Wittig M, Häsler R, Franke A, Gavrilova O, Kreck B, Sina C, Schilhabel MB, Schreiber S, Rosenstiel P: A tissue-specific landscape of sense/antisense transcription in the mouse intestine. *BMC Genomics*. 2011 Jun 10;12:305.

Lau DC, Schillabeer G, Li ZH, Wong KL, Varzaneh FE, Tough SC: Paracrine interactions in adipose tissue development and growth. *Int J Obes Relat Metab Disord*. 1996 Mar; 20 Suppl 3:S16-25.

Lemonnier D: Effect of age, sex, and sites on the cellularity of the adipose tissue in mice and rats rendered obese by a high-fat diet. *J Clin Invest.* 1972 Nov;51(11):2907-15.

Levy DB, Smith KJ, Beazer-Barclay Y, Hamilton SR, Vogelstein B, Kinzler KW: Inactivation of both APC alleles in human and mouse tumors. *Cancer Res.* 1994 Nov 15;54(22):5953-8.

Liu Y, Monticone M, Tonachini L, Mastrogiacomo M, Marigo V, Cancedda R, Castagnola P: URB expression in human bone marrow stromal cells and during mouse development. *Biochem Biophys Res Commun.* 2004 Sep 17;322(2):497-507.

Logan CY, Nusse R: The Wnt signaling pathway in development and disease. *Annu Rev Cell Dev Biol.* 2004;20:781-810.

Luongo C, Moser AR, Gledhill S, Dove WF: Loss of Apc⁺ in intestinal adenomas from Min mice. *Cancer Res.* 1994 Nov 15;54(22):5947-52.

Lynch HT, de la Chapelle A: Hereditary colorectal cancer. *N Engl J Med.* 2003 Mar 6;348(10):919-32.

MacDonald BT, Tamai K, He X: Wnt/beta-catenin signaling: components, mechanisms, and diseases. *Dev Cell.* 2009 Jul;17(1):9-26.

Manabe R, Tsutsui K, Yamada T, Kimura M, Nakano I, Shimono C, Sanzen N, Furutani Y, Fukuda T, Oguri Y, Shimamoto K, Kiyozumi D, Sato Y, Sado Y, Senoo H, Yamashina S, Fukuda S, Kawai J, Sugiura N, Kimata K, Hayashizaki Y, Sekiguchi K: Transcriptome-based systematic identification of extracellular matrix proteins. *Proc Natl Acad Sci U S A.* 2008 Sep 2;105(35):12849-54.

Marcantonio D, Chalifour LE, Alaoui-Jamali MA, Alpert L, Huynh HT: Cloning and characterization of a novel gene that is regulated by estrogen and is associated with mammary gland carcinogenesis. *Endocrinology.* 2001 Jun;142(6):2409-18.

- Matysková R, Maletínská L, Maixnerová J, Pirník Z, Kiss A, Zelezná B:** Comparison of the obesity phenotypes related to monosodium glutamate effect on arcuate nucleus and/or the high fat diet feeding in C57BL/6 and NMRI mice. *Physiol Res.* 2008;57(5):727-34.
- McCart AE, Vickaryous NK, Silver A:** Apc mice: models, modifiers and mutants. *Pathol Res Pract.* 2008;204(7):479-90.
- McLellan EA, Bird RP:** Aberrant crypts: potential preneoplastic lesions in the murine colon. *Cancer Res.* 1988a Nov 1;48(21):6187-92.
- McLellan EA, Bird RP:** Specificity study to evaluate induction of aberrant crypts in murine colons. *Cancer Res.* 1988b Nov 1;48(21):6183-6.
- Montague CT, O'Rahilly S:** The perils of portliness: causes and consequences of visceral adiposity. *Diabetes.* 2000 Jun;49(6):883-8.
- Morris DL, Rui L:** Recent advances in understanding leptin signaling and leptin resistance. *Am J Physiol Endocrinol Metab.* 2009 Dec;297(6):E1247-59.
- Moser AR, Dove WF, Roth KA, Gordon JI:** The Min (multiple intestinal neoplasia) mutation: its effect on gut epithelial cell differentiation and interaction with a modifier system. *J Cell Biol.* 1992 Mar;116(6):1517-26.
- Moser AR, Pitot HC, Dove WF:** A dominant mutation that predisposes to multiple intestinal neoplasia in the mouse. *Science.* 1990 Jan 19;247(4940):322-4.
- Moser AR, Shoemaker AR, Connelly CS, Clipson L, Gould KA, Luongo C, Dove WF, Siggers PH, Gardner RL:** Homozygosity for the Min allele of Apc results in disruption of mouse development prior to gastrulation. *Dev Dyn.* 1995 Aug;203(4):422-33.
- Mu H, Ohta K, Kuriyama S, Shimada N, Tanihara H, Yasuda K, Tanaka H:** Equarin, a novel soluble molecule expressed with polarity at chick embryonic lens equator, is involved in eye formation. *Mech Dev.* 2003 Feb;120(2):143-55.

Nawa T, Kato J, Kawamoto H, Okada H, Yamamoto H, Kohno H, Endo H, Shiratori Y: Differences between right- and left-sided colon cancer in patient characteristics, cancer morphology and histology. *J Gastroenterol Hepatol.* 2008 Mar;23(3):418-23.

Nishimura S, Manabe I, Nagasaki M, Hosoya Y, Yamashita H, Fujita H, Ohsugi M, Tobe K, Kadowaki T, Nagai R, Sugiura S: Adipogenesis in obesity requires close interplay between differentiating adipocytes, stromal cells, and blood vessels. *Diabetes.* 2007 Jun;56(6):1517-26.

Nishisho I, Nakamura Y, Miyoshi Y, Miki Y, Ando H, Horii A, Koyama K, Utsunomiya J, Baba S, Hedge P: Mutations of chromosome 5q21 genes in FAP and colorectal cancer patients. *Science.* 1991 Aug 9;253(5020):665-9.

Okada T, Nishizawa H, Kurata A, Tamba S, Sonoda M, Yasui A, Kuroda Y, Hibuse T, Maeda N, Kihara S, Hadama T, Tobita K, Akamatsu S, Maeda K, Shimomura I, Funahashi T: URB is abundantly expressed in adipose tissue and dysregulated in obesity. *Biochem Biophys Res Commun.* 2008 Mar 7;367(2):370-6.

Park SY, Cho YR, Kim HJ, Higashimori T, Danton C, Lee MK, Dey A, Rothermel B, Kim YB, Kalinowski A, Russell KS, Kim JK: Unraveling the temporal pattern of diet-induced insulin resistance in individual organs and cardiac dysfunction in C57BL/6 mice. *Diabetes.* 2005 Dec;54(12):3530-40.

Parkin DM, Bray F, Ferlay J, Pisani P: Global cancer statistics, 2002. *CA Cancer J Clin.* 2005 Mar-Apr;55(2):74-108.

Polakis P: The oncogenic activation of beta-catenin. *Curr Opin Genet Dev.* 1999 Feb;9(1):15-21.

Porter EM, Bevins CL, Ghosh D, Ganz T: The multifaceted Paneth cell. *Cell Mol Life Sci.* 2002 Jan;59(1):156-70.

Potten CS, Loeffler M: Stem cells: attributes, cycles, spirals, pitfalls and uncertainties. Lessons for and from the crypt. *Development.* 1990 Dec;110(4):1001-20.

Poulos SP, Dodson MV, Hausman GJ: Cell line models for differentiation: preadipocytes and adipocytes. *Exp Biol Med (Maywood)*. 2010 Oct;235(10):1185-93.

Powell SM, Zilz N, Beazer-Barclay Y, Bryan TM, Hamilton SR, Thibodeau SN, Vogelstein B, Kinzler KW: APC mutations occur early during colorectal tumorigenesis. *Nature*. 1992 Sep 17;359(6392):235-7.

Pretlow TP, Edelmann W, Kucherlapati R, Pretlow TG, Augenlicht LH: Spontaneous aberrant crypt foci in Apc1638N mice with a mutant Apc allele. *Am J Pathol*. 2003 Nov;163(5):1757-63.

Radtke F, Clevers H: Self-renewal and cancer of the gut: two sides of a coin. *Science*. 2005 Mar 25;307(5717):1904-9.

Ramírez-Zacarías JL, Castro-Muñozledo F, Kuri-Harcuch W: Quantitation of adipose conversion and triglycerides by staining intracytoplasmic lipids with Oil red O. *Histochemistry*. 1992 Jul;97(6):493-7.

Ravussin E, Galgani JE: The Implication of Brown Adipose Tissue for Humans. *Annu Rev Nutr*. 2011 Aug 21;31:33-47.

Ravussin E, Smith SR: Increased fat intake, impaired fat oxidation, and failure of fat cell proliferation result in ectopic fat storage, insulin resistance, and type 2 diabetes mellitus. *Ann N Y Acad Sci*. 2002 Jun;967:363-78.

Reitmair AH, Cai JC, Bjerknes M, Redston M, Cheng H, Pind MT, Hay K, Mitri A, Bapat BV, Mak TW, Gallinger S: MSH2 deficiency contributes to accelerated APC-mediated intestinal tumorigenesis. *Cancer Res*. 1996 Jul 1;56(13):2922-6.

Ross SE, Hemati N, Longo KA, Bennett CN, Lucas PC, Erickson RL, MacDougald OA: Inhibition of adipogenesis by Wnt signaling. *Science*. 2000 Aug 11;289(5481):950-3.

Sancho E, Batlle E, Clevers H: Live and let die in the intestinal epithelium. *Curr Opin Cell Biol*. 2003 Dec;15(6):763-70.

Sansom OJ, Reed KR, Hayes AJ, Ireland H, Brinkmann H, Newton IP, Batlle E, Simon-Assmann P, Clevers H, Nathke IS, Clarke AR, Winton DJ: Loss of Apc in vivo immediately perturbs Wnt signaling, differentiation, and migration. *Genes Dev.* 2004 Jun 15;18(12):1385-90.

Schonhoff SE, Giel-Moloney M, Leiter AB: Minireview: Development and differentiation of gut endocrine cells. *Endocrinology.* 2004 Jun;145(6):2639-44.

Schwenk F, Baron U, Rajewsky K: A cre-transgenic mouse strain for the ubiquitous deletion of loxP-flanked gene segments including deletion in germ cells. *Nucleic Acids Res.* 1995 Dec 25;23(24):5080-1.

Serrero G, Lepak N: Endocrine and paracrine negative regulators of adipose differentiation. *Int J Obes Relat Metab Disord.* 1996 Mar; 20 Suppl 3:S58-64.

Shoemaker AR, Gould KA, Luongo C, Moser AR, Dove WF: Studies of neoplasia in the Min mouse. *Biochim Biophys Acta.* 1997 Apr 18;1332(2):F25-48.

Simons BD, Clevers H: Stem cell self-renewal in intestinal crypt. *Exp Cell Res.* 2011 Nov 15;317(19):2719-24.

Singla P, Bardoloi A, Parkash AA: Metabolic effects of obesity: A review. *World J Diabetes.* 2010 Jul 15;1(3):76-88.

Song J, Medline A, Mason JB, Gallinger S, Kim YI: Effects of dietary folate on intestinal tumorigenesis in the apcMin mouse. *Cancer Res.* 2000 Oct 1;60(19):5434-40.

Specian RD, Oliver MG: Functional biology of intestinal goblet cells. *Am J Physiol.* 1991 Feb;260(2 Pt 1):C183-93.

Stappenbeck TS, Wong MH, Saam JR, Mysorekar IU, Gordon JI: Notes from some crypt watchers: regulation of renewal in the mouse intestinal epithelium. *Curr Opin Cell Biol.* 1998 Dec;10(6):702-9.

Su LK, Kinzler KW, Vogelstein B, Preisinger AC, Moser AR, Luongo C, Gould KA, Dove WF: Multiple intestinal neoplasia caused by a mutation in the murine homolog of the APC gene. *Science*. 1992 May 1;256(5057):668-70.

Tremblay F, Revett T, Huard C, Zhang Y, Tobin JF, Martinez RV, Gimeno RE: Bidirectional modulation of adipogenesis by the secreted protein Ccdc80/DRO1/URB. *J Biol Chem*. 2009 Mar 20;284(12):8136-47.

Vázquez-Vela ME, Torres N, Tovar AR: White adipose tissue as endocrine organ and its role in obesity. *Arch Med Res*. 2008 Nov;39(8):715-28.

Visconti R, Schepis F, Iuliano R, Pierantoni GM, Zhang L, Carlomagno F, Battaglia C, Martelli ML, Trapasso F, Santoro M, Fusco A: Cloning and molecular characterization of a novel gene strongly induced by the adenovirus E1A gene in rat thyroid cells. *Oncogene*. 2003 Feb 20;22(7):1087-97.

Wang J, Yin L, Lazar MA: The orphan nuclear receptor Rev-erb alpha regulates circadian expression of plasminogen activator inhibitor type 1. *J Biol Chem*. 2006 Nov 10;281(45):33842-8.

Weisberg SP, McCann D, Desai M, Rosenbaum M, Leibel RL, Ferrante AW Jr: Obesity is associated with macrophage accumulation in adipose tissue. *J Clin Invest*. 2003 Dec;112(12):1796-808.

Wellen KE, Hotamisligil GS: Obesity-induced inflammatory changes in adipose tissue. *J Clin Invest*. 2003 Dec;112(12):1785-8.

Wilson R, Norris E, Brachvogel B, Angelucci C, Zivkovic S, Gordon L, Bernardo B, Stermann J, Sekiguchi K, Gorman JJ, Bateman JF: Changes in the chondrocyte and extracellular matrix proteome during post-natal mouse cartilage development. *Mol Cell Proteomics*. 2012 Jan;11(1):M111.014159.

WHO: Obesity and overweight. <http://www.who.int/mediacentre/factsheets/fs311/en/index.html>. 2012 Mar. [zuletzt aufgerufen am 17.03.2012]

World Cancer Research Fund / American Institute for Cancer Research: Food, Nutrition, Physical Activity, and the Prevention of Cancer: a Global Perspective. Washington DC: AICR, 2007.

Yeung TM, Chia LA, Kosinski CM, Kuo CJ: Regulation of self-renewal and differentiation by the intestinal stem cell niche. *Cell Mol Life Sci.* 2011 Aug;68(15):2513-23.

9. Acknowledgements

First of all, I would like to thank with a deep sense of gratitude PD Dr. Marlon R. Schneider, my *Doktorvater*, for his constant support, encouragement and guidance through my research.

My special appreciation goes to Prof. Dr. Frank T. Kolligs, Klinikum der Universität München, for his support and for sharing his invaluable experience with me.

I am indebted to Prof. Dr. Eckhard Wolf for allowing me to carry out my research at the Institute for Molecular Animal Breeding and Biotechnology, Gene Center, and for the excellent working conditions.

I am particularly grateful to Felix Hiltwein for his consistent help and friendship, especially during my pregnancy and the time thereafter. It was a lot of fun to work with you and laboratory work would have been much more difficult without you!

Special thanks to Dr. Ingrid Renner-Müller, Petra Renner, Insa Härtel and all the present and former members of the animal maintenance crew for the excellent management of “my” mice strains and their constant help and advice with laboratory animal care.

I especially want to thank Sepp Millauer, Stefanie Rieseemann, Andrea Ofner, Max Marschall and Tamara Holy for introducing me to molecular biology and for the good time we had in the lab together. Thanks for giving me a hand with all the harmful chemicals during my pregnancy and the time thereafter.

Many thanks to Benjamin Hirschi, Dr. Maik Dahlhoff and PD Dr. Andreas Herbst for the critical discussions, their competent scientific advice and their good humor.

Of particular importance was the good and pleasant collaboration with Dr. Jens Neumann, Institute for Pathology, University of Munich.

Last but not least many thanks to my family for their support and encouragement during all the years.